

**Photoreceptor axon guidance in *Drosophila melanogaster*:
hu li tai shao and *golden goal***

Dissertation

an der Fakultät für Biologie der Ludwig-Maximilians-Universität München

angefertigt am Max-Planck-Institut für Neurobiologie in Martinsried

vorgelegt von Stephan Ohler

München, den 03. November 2011

Erstgutachter: Prof. Dr. Rüdiger Klein
Zweitgutachter: Prof. Dr. George Boyan
Tag der mündlichen Prüfung: 26. April 2012

Ehrenwörtliche Versicherung

Ich versichere hiermit ehrenwörtlich, dass die vorgelegte Dissertation von mir selbständig und ohne unerlaubte Hilfe angefertigt ist.

Erklärung

Hiermit erkläre ich, dass die Dissertation nicht ganz oder in wesentlichen Teilen einer anderen Prüfungskommission vorgelegt worden ist.

Hiermit erkläre ich, dass ich mich anderweitig einer Doktorprüfung ohne Erfolg nicht unterzogen habe.

München, den 03. November 2011

Stephan Ohler

Die in der vorliegenden Arbeit beschriebenen Experimente wurden zwischen Februar 2005 und August 2010 unter der Leitung von Dr. Takashi Suzuki am Max-Planck-Institut für Neurobiologie in Martinsried durchgeführt.

Teile der in dieser Dissertation präsentierten Arbeit gingen in folgende Publikationen ein:

- Tatiana Tomasi, Satoko Hakeda-Suzuki, Stephan Ohler, Alexander Schleiffer and Takashi Suzuki (2008).
The transmembrane protein Golden goal regulates R8 photoreceptor axon-axon and axon-target interactions.
Neuron 57, 691-704
- Stephan Ohler, Satoko Hakeda-Suzuki and Takashi Suzuki (2011).
Hts, the *Drosophila* homologue of Adducin, physically interacts with the transmembrane receptor Golden goal to guide photoreceptor axons.
Developmental Dynamics 240, 135-48

Table of contents

Index of figures	7
Index of tables.....	8
Abbreviations	9
Zusammenfassung	12
Abstract	14
1. INTRODUCTION.....	15
1.1 Axon guidance.....	15
1.2 The visual system of <i>D. melanogaster</i>	21
1.3 Pathfinding of <i>Drosophila</i> photoreceptor axons	23
1.4 A saturating screen for mutants affecting photoreceptor axon guidance in <i>Drosophila</i>	25
1.5 <i>gogo</i>	27
1.6 Hts and Adducin	29
2. MATERIALS AND METHODS.....	33
2.1 Generation of transgenic fly stocks.....	33
2.2 Generation of other fly stocks.....	35
2.3 Other fly stocks.....	37
2.4 Fly genotypes.....	38
2.5 Genetic tools	45
2.6 Molecular biology.....	51
2.7 Identification of Hts as a Gogo binding protein	57
2.8 Cell culture binding assay	59
2.9 Preparation of lysates from larval brains	61
2.10 Western blot.....	61
2.11 Immunostaining of adult brain cryosections.....	61
2.12 Whole mount immunostaining of larval and adult brains	62
2.13 Estimation of Add1 levels in photoreceptor axons in the medulla	62
2.14 Antibodies	63
3. RESULTS	65
3.1 Gogo requires its cytoplasmic part to function in photoreceptor axon guidance.....	65
3.2 Gogo physically interacts with Hts	67
3.3 Hts can be detected in larval photoreceptor axons	71
3.4 Loss of Hts severely affects axon guidance in the visual system	72
3.5 β -Spectrin mutants show defects in photoreceptor axon guidance	76
3.6 <i>swallow</i> mutants do not show defects in photoreceptor axon guidance	77
3.7 Add1 and HtsPD rescue <i>hts</i> ⁰¹¹⁰³ hemizygous flies but ShAdd does not	77

3.8 Mutating putative phosphorylation sites in Hts does not affect its interaction with Gogo	80
3.9 Add1 and HtsPD rescue <i>hts^{null}</i> mosaic flies	81
3.10 ShAdd does not localize to photoreceptor axons	84
3.11 The tail domain of Hts is required for its localization to the axon	85
3.12 Overexpression of Add1 and Gogo cause similar but different defects in the medulla	90
3.13 <i>hts</i> antagonizes <i>gogo</i> overexpression	93
3.14 Gogo reduces the level of Add1 protein in photoreceptor axons	95
3.15 Hts forms oligomers	99
4. DISCUSSION	101
4.1 Hts and Gogo: collaborators or antagonists?	101
4.2 Hypothesis I: Gogo affects the axonal cytoskeleton via Hts	101
4.3 Experimental evidence supporting hypothesis I	106
4.4 Hypothesis II: Hts recruits Gogo to the Spectrin cytoskeleton	108
4.5 Hypothesis III: a disordered Spectrin cytoskeleton causes unspecific phenotypes	110
4.6 Why is the MARCKS-related domain of Hts not required for axon guidance?	113
4.7 Outlook	113
5. LITERATURE	116
Acknowledgements	130
Curriculum vitae	131

Index of figures

Figure 1.4: A saturating screen for mutants affecting photoreceptor axon guidance in <i>Drosophila</i>	26
Figure 1.5: Schematic of Gogo's protein domain architecture and mutant alleles	28
Figure 1.6: Schematic of the different Hts proteins	31
Figure 2.5: The Flp/FRT system	47
Figure 2.6: The Gateway system	52
Figure 3.1.1: Schematic of the different artificial Gogo constructs used	65
Figure 3.1.2: Gogo requires its cytoplasmic part to function in photoreceptor axon guidance	66
Figure 3.1.3: Gogo ^{ΔC} -Myc and Gogo-Myc are present in larval photoreceptor axons	67
Figure 3.2.1: Gogo ^{cyto} -Myc is present in larval photoreceptors	68
Figure 3.2.2: Hts physically interacts with Gogo ^{cyto} -Myc	69
Figure 3.2.3: Gogo binds to all Hts isoforms independently of its YYD motif	70
Figure 3.3: Hts in optic lobes of wild type larvae	71
Figure 3.4: Loss of Hts severely affects axon guidance in the visual system	74
Figure 3.5: <i>β-Spectrin</i> mutants show defects in photoreceptor axon guidance	76
Figure 3.6 <i>swallow</i> mutants do not show defects in photoreceptor axon guidance	77
Figure 3.7.1: The <i>hts</i> rescue constructs do not cause defects in the medulla on their own	78
Figure 3.7.2: Ability of different rescue constructs to rescue <i>hts</i> ⁰¹¹⁰³ hemizygous flies	79
Figure 3.8: Mutating putative phosphorylation sites in Hts does not affect Gogo binding	81
Figure 3.9: Add1 and HtsPD rescues <i>hts</i> ^{null} mosaic flies	82
Figure 3.10: ShAdd does not localize to photoreceptor axons	84
Figure 3.11: Overexpression of different Hts constructs	86
Figure 3.12.1: Defects of photoreceptor axons in the medulla caused by excessive Gogo	91
Figure 3.12.3: <i>UAS-Add12A</i> produces more axonal Hts protein than <i>UAS-Add12A</i>	92
Figure 3.13: <i>hts</i> antagonizes <i>gogo</i> overexpression	94
Figure 3.14.1: The axonal Hts protein level is reduced by excessive Gogo	96
Figure 3.14.2: Decrease in Hts caused by different insertions of Gogo constructs	98
Figure 3.14.3: Loss of Gogo does not detectably increase the axonal Hts level	99
Figure 3.15: Hts forms oligomers	100
Figure 4.2: A speculative model of the Hts and Gogo functions	105
Figure 4.3: A possible explanation of the <i>hts</i> and <i>gogo</i> overexpression phenotypes	106
Figure 4.4: Overexpression phenotypes resulting from an ectopic function of monomeric Gogo	110

Index of tables

Table 2.1: List of transgenic fly stocks that were generated.....	34
Table 2.5: List of genetic elements that were used.....	48
Table 2.6.1: List of expression clones	53
Table 2.6.2: List of destination vectors	54
Table 2.6.3: List of entry clones	54
Table 2.6.4: List of other plasmids	55
Table 2.6.5: List of oligonucleotides	56
Table 2.14.1: List of antibodies used for western blots	63
Table 2.14.2: List of antibodies used for immunostainings.....	64
Table 3.4: Severity of the defects observed in different <i>hts</i> mutants.....	73
Table 3.7: Ability of different rescue constructs to rescue <i>hts</i> ⁰¹¹⁰³ hemizygous flies	80
Table 3.9: Ability of different rescue constructs to rescue <i>hts</i> ^{null} mosaic flies	83
Table 3.11: Effects of different transgenic <i>hts</i> constructs.....	90
Table 3.12: Penetrance of several insertions of constructs encoding Gogo	92
Table 3.13: <i>hts</i> antagonizes the effects of excessive Gogo in photoreceptor axons.....	95
Table 3.14: Decrease in Hts caused by different insertions of Gogo constructs.....	97

Abbreviations

aa.....	amino acid residue(s)
BMP	bone morphogenetic protein
bp.....	base pair(s)
BSA.....	bovine serum albumin
CAM	cell adhesion molecule
cAMP.....	cyclic adenosine monophosphate
<i>C. elegans</i>	<i>Caenorhabditis elegans</i>
CNS	central nervous system
d.....	day(s)
DCC	deleted in colorectal cancer
<i>D. melanogaster</i>	<i>Drosophila melanogaster</i>
DNA	deoxyribonucleic acid
Dscam	Down syndrome cell adhesion molecule
DTT	dithiothreitol
<i>E.coli</i>	<i>Escherichia coli</i>
EDTA.....	ethylene diamine tetraacetic acid
e.g.....	for example
EGTA	ethylene glycol tetraacetic acid
EMS	ethyl methane sulfonate
ERM.....	Ezrin, Radixin, Moesin
<i>ey</i>	<i>eyeless</i>
F-Actin.....	filamentous Actin
FCS.....	fetal calf serum
Flp.....	Flipase
FRT	Flipase recognition target
<i>g</i>	standard gravity
GABA	γ -aminobutyric acid
GAP	GTPase activating protein
GEF.....	guanine nucleotide exchange factor
GFP.....	green fluorescent protein
<i>gl</i>	<i>glass</i>
GMR.....	glass multimer reporter
<i>gogo</i>	<i>golden goal</i>
GPI.....	glycosyl phosphatidyl inositol
GTP.....	guanosine triphosphate

h.....	hour(s)
HEPES.....	4-(2-hydroxyethyl)-1-piperazineethanesulfonic acid
HRP	horseradish peroxidase
<i>hts</i>	<i>hu li tai shao</i>
Ig.....	immunoglobulin
K_d	dissociation constant
kDa	kilodaltons
KO.....	Kusabira Orange
LAR.....	leukocyte-antigen-related-like
LRR.....	Leucine-rich repeat
MAP	microtubule-associated protein
MARCKS.....	myristoylated Alanine-rich C kinase substrate
MCS.....	multiple cloning site
mRNA	messenger RNA
NGS	normal goat serum
PAGE.....	polyacrylamide gel electrophoresis
Pak.....	p21 activated kinase
PBS.....	phosphate buffered saline
PCR	polymerase chain reaction
PKA.....	protein kinase A
PKC	protein kinase C
PMSF.....	phenyl methyl sulfonyl fluoride
PTP69D.....	protein Tyrosine phosphatase 69D
RGC.....	retinal ganglion cell
RNA	ribonucleic acid
Robo	Roundabout
RTK.....	receptor Tyrosine kinase
SDS	sodium dodecyl sulfate
SEM.....	standard error of the mean
SI.....	International System of Units
STED	stimulated emission depletion
TGF.....	transforming growth factor
TSP.....	Thrombospondin
U.....	enzyme unit(s)
UAS	upstream activating sequence
UTR	untranslated region

w.....*white*

X. laevis.....*Xenopus laevis*

y.....*yellow*

Standard abbreviations were used to denote amino acid residues, nucleotides, chemical elements, and SI units. For a list of abbreviations used to denote genetic elements, see table 2.5.

Zusammenfassung

Tierisches Leben ist auf funktionierende neuronale Netze angewiesen, die sich während der Entwicklung ausbilden. Um sich mit den richtigen Zielzellen verknüpfen zu können, verfügen wachsende Axone an ihrer Spitze über Wachstumskegel, die auf die chemische Umgebung im Organismus reagieren. Jede der Ommatidien im Facettenauge von *D. melanogaster* enthält acht verschiedene Photorezeptoren, R1 bis R8, die topographisch in unterschiedliche Schichten des Gehirns projizieren. Die Axone von R1 bis R6 enden in der Lamina, und die Axone von R7 und R8 enden in zwei unterschiedlichen Schichten in der Medulla.

gogo wurde in einem groß angelegten Screen für Mutanten, die die Wegfindung der Photorezeptoraxone in *Drosophila* beeinträchtigen, gefunden. Es kodiert ein Transmembranprotein, das, je nach Kontext, unterschiedliche Funktionen ausübt. Gogo sorgt für die gegenseitige Abstoßung zwischen R8-Axonon, um deren regelmäßige Verteilung in der Medulla sicher zu stellen, es wirkt adhäsiv bei der vorübergehenden Verankerung der R8-Axonenden in ihrer intermediären Zielschicht an der Oberfläche der Medulla und kooperiert mit Flamingo in der finalen Phase der R8-Zielerkennung. Um die molekulare Funktion von Gogo aufzuklären, war es Ziel der vorliegenden Arbeit, ein anderes Protein zu finden, das mit Gogo physisch interagiert. Als solches identifiziert wurde Hts, das einzige Homologe von Säugetier-Adducin in *Drosophila*. Bisher konzentrierte sich die Forschung über Hts auf seine Rolle während der Oogenese. Über seine Rolle in der Neuralentwicklung war noch nichts bekannt.

Die physische Interaktion erfolgt zwischen dem zytoplasmatischen Teil Gogos und den N-terminalen 472 Aminosäureresten von Hts, die in allen bekannten Isoformen gleich sind, und ist unabhängig vom konservierten YYD-Motif im zytoplasmatischen Teil Gogos.

Hts kann in larvalen Photorezeptoraxonen nachgewiesen werden, und sein Verlust verursacht Defekte in der Wegfindung der Photorezeptoraxone ähnlich denen in *gogo* Mutanten. Die Gesamtstruktur der Medulla ist gestört, die regelmäßige Anordnung der R7- und R8-Axone geht verloren, Axone verklumpen, R8-Axone überwachsen häufig ihre eigentliche Zielschicht M3, und es zeigen sich auffällig dicke Schwellungen an den Axonenden und in der Schicht M1. β -Spectrin-, nicht aber *swallow*-Mutanten, weisen ähnlich Defekte auf.

Die durch den Verlust von Hts verursachten Defekte werden durch die Expression von Add1 oder HtsPD, Hts-Isoformen, die über seine Schweifdomäne verfügen, in Photorezeptoren abgemildert. Hts benötigt seine Schweifdomäne für die Lokalisation im Axon, und ShAdd, eine Hts Isoform ohne Schweifdomäne, kann *hts*-Mutanten nicht retten.

Übermäßiges Add1 im Photorezeptor verursacht dicke Schwellungen der R8-Axone an der M1-Schicht, ähnlich übermäßigem Gogo, das dicke Schwellungen der R8-Axone an M1 und M3 verursacht. Überraschenderweise erscheinen die R8-Axone normal, wenn *hts* und *gogo* gemeinsam überexprimiert werden. Einen direkten Hinweis auf eine antagonistische Interaktion

zwischen Gogo und Hts liefert die Beobachtung, dass ein erhöhtes Gogo-Niveau zu einer Verminderung von Hts im Axon führt.

Weder für Hts noch für Adducin wurde bisher eine Rolle in axonaler Wegfindung beschrieben. Adducin ist aber ein wichtiger Faktor für den korrekten Aufbau des Actin-Spectrin-Zytoskeletts, und so könnte die Funktion von Hts in der axonalen Wegfindung mit einer Beeinflussung des Zytoskeletts einhergehen.

Abstract

Animal life relies on functional neuronal networks that are established during development. To connect to their correct target cells, the tips of growing axons are equipped with growth cones that respond to the chemical environment in the organism. Each of the ommatids in the compound eye of *D. melanogaster* contains eight different photoreceptors, R1 to R8, that project in a topographic manner to distinct target layers in the brain. The axons from R1 to R6 terminate in the lamina, and the axons from R7 and R8 terminate in two distinct layers in the medulla.

gogo was identified in a large-scale screen for mutants that affect photoreceptor axon guidance in *Drosophila*. It encodes a transmembrane protein that serves distinct functions in different contexts. Gogo repels R8 axons from each other to assure their even spacing in the medulla, serves an adhesive function by transiently anchoring R8 termini to their intermediate target layer at the surface of the medulla, and co-operates with Flamingo in the final phase of R8 target selection. To elucidate the function of Gogo at the molecular level, this work aimed to detect another protein that physically interacts with Gogo and led to the identification of Hts, the single homolog of mammalian Adducin in *Drosophila*. As yet, research on Hts focused on its role during oogenesis and nothing was known about its role in neural development.

The physical interaction occurs between the cytoplasmic part of Gogo and the N-terminal 472 aa of Hts that are shared among all known isoforms, and it does not depend on the conserved YYD motif in the cytoplasmic tail of Gogo.

Hts can be detected in larval photoreceptor axons and its loss causes defects in photoreceptor axon guidance that are similar to those observed in *gogo* mutants: The overall structure of the medulla is disrupted, the regular array of R7 and R8 axons is lost, axons clump together, R8 axons often overshoot their correct target layer M3, and abnormally thick swellings at the axon termini and at the M1 layer can be observed. β -Spectrin mutant flies show comparable defects, *swallow* mutant flies do not.

The expression of Add1 or HtsPD, Hts isoforms containing its tail domain, in photoreceptors restores the defects caused by the loss of Hts. The tail domain of Hts is required for its localization to the axon, and ShAdd, an Hts isoform lacking the tail domain, does not rescue *hts* mutant flies.

Excessive Add1 in photoreceptors causes abnormally thick swellings of R8 axons at the M1 layer, similar to excessive Gogo that causes thick swellings of R8 axons at M1 and M3. Surprisingly, R8 axons appear normal when both *hts* and *gogo* are co-overexpressed. Direct evidence for an antagonistic interaction between Gogo and Hts comes from the observation that an increase in the level of Gogo reduces the axonal level of Hts.

Neither for Hts nor for Adducin has a role in axon guidance been reported yet. However, Adducin is an important factor in the proper assembly of the Actin-Spectrin cytoskeleton, and the function of Hts in axon guidance is therefore likely to involve interactions with the cytoskeleton.

1. INTRODUCTION

1.1 Axon guidance

All manifestations of animal life, from the reflexes of *Aplysia* to the most sophisticated achievements of the human mind, rely on functional neuronal networks. These are established during development, when neurons send out axons and dendrites to connect to their target cells. How a certain axon is directed to its correct target cell became subject to scientific investigation more than a century ago, when the Spanish histologist Santiago Ramón y Cajal discovered “a concentration of protoplasm of conical form, endowed with amoeboid movements” at the tip of growing axons, which he named “growth cone” (Cajal 1966). The growth cone, he correctly assumed, leads the axon on the right track through the developing organism to its proper destination. However, for many decades it was completely unclear how the growth cone would fulfill this task.

Several alternative concepts were discussed in the first half of the 20th century before increasing experimental evidence approved the “chemoaffinity theory” by Roger Wolcott Sperry. The chemoaffinity theory proposed that axons are guided by chemical means, and that a certain neuron differs from other neurons in its cytochemical configuration, which makes it respond in a specific way to its chemical environment in the organism (Sperry 1963). In the following decades, some of the underlying molecules and mechanisms have been identified. It turned out that axons are guided both positively by attracting and negatively by repelling cues. The molecules mediating attraction or repulsion each can be diffusible or bound to cells or the extracellular matrix, resulting in four different modes of axon guidance: chemoattraction, chemorepulsion, contact attraction, and contact repulsion, respectively (Tessier-Lavigne and Goodman 1996).

Any given organism can produce only a limited number of different molecules, and the sheer numbers of neurons and their connections to each other apparently exclude the existence of specific guidance molecules for each neuron. For example, the human brain was estimated to possess 10^{11} neurons that form 10^{14} synapses (Williams and Herrup 1988). Although the *Drosophila* axon guidance receptor gene *Dscam* that encodes 4×10^4 different potential proteins provides a prominent example for extreme molecular diversity reflecting the staggering complexity of brain wiring (Schmucker et al. 2000), this seems to be an exception. In general, it appears that specificity arises rather in a combinatorial manner from very precisely tuning the composition of a relatively moderate number of different ligand-receptor systems at the growth cone and the modulation of the received guidance information. Accordingly, the spatial, temporal, and cell-type specificity of a neuron’s responsiveness depends on the regulation of its axon guidance receptors and intracellular effectors from the transcriptional up to the posttranslational level (reviewed by

Gomez and Zheng 2006; Polleux et al. 2007; O'Donnell et al. 2009). The major classes of known ligand-receptor systems are described below.

CAMs

Three of the four major CAM families, Ig superfamily CAMs, cadherins, and integrins, are abundantly expressed in neural tissue (Rutishauser 1993). Many CAMs were among the earliest candidates for axon guidance molecules, but they were thought to act in a permissive manner rather than by actively inducing growth cone turning (Chilton 2006). However, recent experimental evidence suggests more instructive roles for CAMs during axon guidance.

The LRR-type CAM *Capricious* has been demonstrated to be required and sufficient in the *Drosophila* visual system for the correct layer-specific targeting of R8 photoreceptor axons to the M3 layer in the medulla (Shinza-Kameda et al. 2006). *capricious* is specifically expressed in R8 photoreceptors and in M3, the correct target layer of their axons, but not in R7 photoreceptors and M6, the correct target layer of R7 axons. Loss of *capricious* causes local R8 targeting errors, including layer change, and the ectopic expression of *capricious* in R7 photoreceptors redirects R7 axon termini to M3.

Another example for a CAM that rather acts in an instructional way during axon guidance is the Ig superfamily CAM L1. The extracellular domain of L1 mediates adhesion to the matrix or to other cells through interactions with β 1-integrins in cis or homophilic binding in trans (Buhusi et al. 2008). Its cytoplasmic domain provides linkage to the cytoskeleton through ERM binding (Dickson et al. 2002) and through binding to Ankyrin (Davis and Bennett 1994). L1 has been implicated in regulating the retinotopic mapping of retinocollicular projections of RGC axons in mice (Demyanenko and Maness 2003). The axons from wild type RGCs project from the retina to the contralateral superior colliculus in a temporal to anterior, nasal to posterior, dorsal to lateral, ventral to medial way. A point mutation in the L1 cytoplasmic domain that abolishes binding to Ankyrin is sufficient to disturb the correct projection of ventral RGCs to the medial superior colliculus and induces their mistargeting to abnormally lateral sites (Buhusi et al. 2008). This is clearly an axon targeting defect that can not be explained as the mere consequence of impaired axon extension and argues for an instructive role of L1 during RGC axon guidance. The correct medial-lateral position in the superior colliculus is targeted by interstitial branches that emanate from a primary RGC axon that has grown along the anterior-posterior axis before. If this primary axon has grown medially of the correct target area, the interstitial branches are biased towards the lateral side of the superior colliculus, and, vice versa, the branches from primary axons that lie laterally of their correct target area show a medial bias. If the binding of L1 to Ankyrin is abolished, the interstitial branches from primary axons that lie laterally of their correct target zone do not only lose their medial bias but show a lateral bias (Buhusi et al. 2008). This could suggest that the affected axons

do not merely lose their ability to sense the cue directing them towards their proper target but rather misinterpret it in an inverted way and are directed away from their target. Interestingly, L1 was reported to control the directionality of a growth cone's response to asymmetric Ca^{2+} concentrations within the growth cone via the Ankyrin_B-dependent modulation of cAMP (Ooashi and Kamiguchi 2009). Growth cones on L1 or N-cadherin substrates respond attractively to asymmetric Ca^{2+} concentrations due to high levels of cAMP (Ooashi et al. 2005). The loss of Ankyrin_B reduces the level of cAMP in growth cones on an L1 but not on an N-cadherin substrate and inverts their attractive response to asymmetric Ca^{2+} concentrations into a repulsive one (Ooashi and Kamiguchi 2009).

Netrins and their receptors DCC and Unc-5

Netrins are proteins of the Laminin superfamily and include the secreted molecules Unc-6 in *C. elegans* (Ishii et al. 1992), which was the first reported Netrin, Netrin-A and Netrin-B in *D. melanogaster* (Harris et al. 1996), and Netrin-1, Netrin-3, and Netrin-4 in vertebrates (Rajasekharan and Kennedy 2009). Netrins are bifunctional guidance cues that can act either attractive or repulsive on a growing axon, depending on the receptors on its growth cone (Round and Stein 2007). Attraction towards Netrins is mediated by members of the DCC family, which includes Unc-40 in *C. elegans*, Frazzled in *D. melanogaster*, and DCC and Neogenin in vertebrates (Huber et al. 2003). Upon Netrin-1 binding, DCC forms homodimers that mediate attraction (Stein et al. 2001). In the presence of an Unc-5 receptor, however, Netrin-1 binding induces the association of DCC and Unc-5 to form a complex that mediates repulsion (Hong et al. 1999). In invertebrates, Unc-5 proteins can mediate repulsion from Netrins on their own without a requirement for DCC (Leung-Hagesteijn et al. 1992). The molecular pathways that mediate attraction towards Netrins downstream of DCC receptors are not completely understood yet. Members of the Rho family of GTPases play an important role and provide a direct link to rearrangements of the Actin cytoskeleton (Rajasekharan and Kennedy 2009). The molecular pathways that mediate Netrin induced repulsion downstream of Unc-5 are even less clear.

Semaphorins and their receptors Plexin and Neuropilin

Semaphorins are defined by having a Semaphorin and a PSI domain. They are categorized into eight classes on the basis of additional protein domains, with the five Semaphorins found in invertebrates belonging to classes 1, 2, and 5, and the 20 Semaphorins from vertebrates to classes 3 to 7. The eighth class V contains virally encoded Semaphorins. The Semaphorins of classes 2, 3, and V are secreted proteins, the remaining ones are transmembrane proteins or GPI linked (Zhou et al. 2008). Initially thought to act primarily as short-range inhibitory cues in axon guidance (Dickson 2002), Semaphorins turned out to conduct various functions by diverse

mechanisms. Semaphorins can be both repulsive and attractive, and they function not only as ligands but also as receptors (Zhou et al. 2008). They function not only in the nervous system, but also in the formation and functioning of the cardiovascular, endocrine, gastrointestinal, hepatic, immune, musculoskeletal, renal, reproductive, and respiratory systems. Accordingly, they were implicated in several human diseases like cancer, retinal degradation, decreased bone mineral density, and rheumatoid arthritis (Yazdani and Terman 2006).

Semaphorins signal through various receptors and receptor complexes consisting of diverse proteins, most notably Plexins and members of the Neuropilin family. Apparently, the effects of Semaphorins are not mediated by canonical signal transduction pathways (Yazdani and Terman 2006). The induction of changes in the cytoskeleton mediated by small GTPases plays an important role, and the cytoplasmic parts of several Plexins have GAP activity or bind GAPs or GEFs (Oinuma et al. 2004; Barberis et al. 2005; Pasterkamp 2005; Toyofuku et al. 2005).

Ephrins and their Eph Receptors

Ephrins are divided into two classes, the GPI anchored ephrinAs and the ephrinB transmembrane proteins. Alike, two classes of associated receptors, EphA receptors and EphB receptors, exist. Typically, ephrinAs bind EphA receptors, and ephrinBs bind EphB receptors, with some exceptions known. The interaction of ephrin with Eph triggers not only forward signaling in the Eph producing cell, but also reverse signaling in the ephrin bearing cell, so that ephrins also function as receptors themselves (Egea and Klein 2007). Eph receptors comprise the largest family of RTKs but signal differently from the canonical RTK pathway in view of the fact that they activate Rho GTPases to remodel the Actin cytoskeleton (Noren and Pasquale 2004; Egea and Klein 2007). Ephs and ephrins are most prominent for their role in retinotectal topographic map formation in vertebrates. In the retina, ephrinAs are expressed in a high nasal to low temporal gradient, and EphAs are expressed in a high temporal to low nasal gradient. In the optic tectum, EphAs form a high rostral to low caudal gradient, and ephrinAs form a high caudal to low rostral gradient. Accordingly, axons from the temporal part of the retina project to the rostral part of the optic tectum. Likewise, ephrinB and EphB gradients regulate topographic map formation along the dorsal-ventral axis. Axons from the dorsal part of the retina that is characterized by high ephrinB and low EphB levels project to the ventral part of the optic tectum with high EphB and low ephrinB levels. Vice versa, the axons from RGCs in the ventral part of the retina with low ephrinB and high EphB levels project to the dorsal part of the optic tectum with low EphB and high ephrinB levels (Scicolone et al. 2009).

Slit and Robo

Slit proteins serve a conserved role as midline repellents (Dickson and Gilestro 2006). In *Drosophila*, the single *slit* gene is expressed in midline glia and encodes a secreted protein (Rothberg et al. 1988; Rothberg et al. 1990). Slit prevents ipsilateral axons from crossing the midline and commissural axons from recrossing the midline through its receptor Robo that is present on the growth cones of ipsilateral axons and on the growth cones of commissural axons after they have crossed the midline (Kidd et al. 1998). In commissural axons that have not crossed the midline yet, Robo is sorted from the trans-Golgi network to endosomes by the protein Commissureless and does not reach the axonal membrane, allowing the axons to grow towards the midline (Keleman et al. 2002). Additionally, Robo and the two other Robo proteins found in *Drosophila*, Robo2 and Robo3, are involved in the lateral positioning of longitudinal fascicles (Rajagopalan et al. 2000; Simpson et al. 2000). The three Slit proteins found in mammals are secreted from the floor plate, the vertebrate equivalent to midline glial cells (Holmes et al. 1998; Itoh et al. 1998; Yuan et al. 1999b). Three Robo proteins, Robo1, Robo2 and Robo3, are expressed in the mammalian CNS, which are not the orthologues of *Drosophila* Robo, Robo2, and Robo3, respectively (Kidd et al. 1998; Yuan et al. 1999a; Dickson and Gilestro 2006). Only Robo1 and Robo2 mediate the repulsive actions of Slits, whereas mammalian Robo3 rather takes over the function of *Drosophila* Commissureless and negatively regulates Robo1 to determine whether or not an axon crosses the midline (Long et al. 2004; Sabatier et al. 2004). However, the molecular mechanisms employed by mammalian Robo3 and *Drosophila* Commissureless to regulate Slit sensitivity are different, as mammalian Robo3 does not affect the localization of Robo1 or Robo2 to the axonal membrane (Sabatier et al. 2004).

Morphogens

Most morphogens are secreted signaling molecules that form a concentration gradient and determine the developmental fate of responding cells according to the specific morphogen concentration that these cells perceive (Gurdon and Bourillot 2001). Rather recently, it turned out that morphogen gradients are also capable of directly guiding axonal growth cones (Augsburger et al. 1999; Charron et al. 2003). Since then, work in mice, chicks, worms, and flies has revealed evolutionarily conserved roles in axon guidance for members of all three known major classes of morphogen families, the Hedgehog, the BMP/TGF β , and the Wnt family (Osterfield et al. 2003; Sanchez-Camacho and Bovolenta 2009). The morphogenetic function of morphogens, imposing particular cell fates on their target cells, relies on the concentration-dependent activation of signaling cascades within the target cells that affect gene transcription (Sanchez-Camacho and Bovolenta 2009). Axon guidance, however, requires fast and local changes in the growth cone's cytoskeletal organization (Guan and Rao 2003). Morphogens of the Hedgehog and the Wnt family

apparently solve this problem by binding to receptors different from those that they use for their morphogenetic function when guiding axons. BMP/TGF β family members instead bind exclusively to their classical receptors known from their role as morphogens also when performing their axon guiding function, which nevertheless activates a divergent pathway specific for axon guidance (reviewed by Sanchez-Camacho and Bovolenta 2009).

The axonal growth cone and its cytoskeleton

The growth cone is the highly dynamic, sensory-motile structure at the end of growing axons. It is divided into several morphological regions. In the axonal shaft, microtubules are tightly bundled by MAPs and oriented with their plus-ends pointing distally. Their array becomes looser as they extend through the axonal wrist into the central domain of the growth cone. The central domain is filled with mitochondria, vesicles, and reticulum. By the transition zone, it is connected to the peripheral domain. Only few microtubules extend into the peripheral domain, and F-Actin organized into filopodia and lamellipodia is the dominant cytoskeletal component here (Geraldo and Gordon-Weeks 2009).

Within filopodia, Actin filaments are oriented with their barbed ends pointing distally and Actin polymerization takes place at the distal tips of the filopodia (Forscher and Smith 1988; Lin et al. 1996). Actin polymerization causes a force that pushes the Actin filament in the proximal direction (retrograde flow) and the membrane into the distal direction (filopodium extension). The rates of retrograde flow and filopodium extension can vary independently of each other and depend partly on the strength of the filopodium's adhesion to the substrate (Mallavarapu and Mitchison 1999; Bard et al. 2008).

Retrograde Actin flow clears the filopodium from microtubules (Schaefer et al. 2002). If retrograde Actin flow is attenuated, microtubules extend further into the filopodium (Forscher and Smith 1988; Medeiros et al. 2006; Schaefer et al. 2008). Conversely, an increase in retrograde Actin flow lets microtubules penetrate filopodia less successfully (Zhou et al. 2002; Brown and Bridgman 2003). Growth cone turning relies on this interaction between F-Actin and microtubules, as the direction of growth cone turning is determined by stable microtubules. Artificial stabilization of microtubules at one side of the growth cone induces a turn towards this side. Conversely, artificial destabilization of microtubules at one side of the growth cone induces a turn away from that side (Buck and Zheng 2002). Therefore, if the filopodial F-Actin is stabilized against retraction on one side of the growth cone by an attractive guidance cue, microtubules are able to enter these filopodia, and the growth cone will turn towards that side (Sabry et al. 1991).

1.2 The visual system of *D. melanogaster*

The compound eye of adult *Drosophila* consists of approximately 750 single ommatids (Cagan and Ready 1989). Every ommatid contains eight photoreceptor cells, R1 to R8 (Dietrich 1909). Each photoreceptor carries a stack of photosensitive microvilli, the rhabdomere (Eakin 1972). The rhabdomeres are oriented such that the R7 rhabdomere lies on top of the R8 rhabdomere in the center, surrounded by the rhabdomeres of R1 to R6. Therefore, R7 and R8 are often referred to as “inner” photoreceptors and R1 to R6 as “outer” photoreceptors, respectively (Voas and Rebay 2004). Additional components of an ommatidium are each four cone cells that are involved in secreting the corneal lens and two primary pigment cells. Every ommatid is optically insulated from its neighbors by six shared secondary and three shared tertiary pigment cells (Cagan and Ready 1989; Voas and Rebay 2004). Finally, an ommatid usually contains one mechanosensory bristle. Each bristle group is formed by four cells, the socket secreting tormogen, the bristle secreting trichogen, the sensory neuron, and the thecogen, its supporting glial cell (Cagan and Ready 1989). However, tormogen and trichogen degenerate at the pupal stage (Perry 1968).

In addition to the retina, the fly visual system comprises four optic ganglia: the lamina, the medulla, the lobula, and the lobula plate (Meinertzhagen and Hanson 1993). Unlike in vertebrates, *Drosophila* photoreceptors send their axons directly into the brain, with the eight axons from one ommatidium forming a single fascicle (Ting and Lee 2007). The axons from photoreceptors R1 to R6 defasciculate in the first optic ganglion, the lamina, and each projects in a stereotyped pattern to connect to lamina neurons, forming a synaptic unit called “cartridge” (Ting and Lee 2007). Every cartridge obtains visual input from each one of the six outer photoreceptors of six different ommatids in such a way that the six photoreceptors that project to the same cartridge see the same point in space. Thereby, a retinotopic map is formed where two adjacent points in the visual world are represented by two neighboring cartridges (Mast et al. 2006; Ting and Lee 2007).

Axons from the inner photoreceptors R7 and R8 extend through the lamina into the second optic ganglion, the medulla, where they stop in two different layers. R8 axons stop in layer M3, and R7 axons in the deeper layer M6. The medulla is organized into columns and the retinotopic map is sustained in the medulla. Every column obtains direct input from the R7 and the R8 axon of the same ommatid and indirect input from the corresponding R1 to R6 neurons via lamina neurons from the lamina cartridges (Mast et al. 2006).

Like almost all structures of the adult fly, the eye develops from an imaginal disc, specifically the eye-portion of the eye-antennal disc, which is a sac-like epithelial bilayer (Cagan 2009). The eye disc remains unpatterned throughout the first and the second larval stage (Meinertzhagen and Hanson 1993). In third instar larvae, differentiation starts at the posterior edge of the eye disc and proceeds in the anterior direction, accompanied by an apical constriction of the disc epithelium known as “morphogenetic furrow” (Ready et al. 1976; Wolff and Ready 1993; Voas and Rebay

2004). As it traverses the epithelium, the morphogenetic furrow leaves behind proneural clusters consisting of approximately 12 cells each that are marked by a high expression level of *atonal* (Jarman et al. 1993). Through Notch-mediated lateral inhibition, *atonal* expression is then restricted to a single cell in each proneural cluster, which is the future R8 photoreceptor (Voas and Rebay 2004). This newly specified R8 cell nucleates an ommatid and induces the sequential differentiation of R2 and R5, R3 and R4, R1 and R6, and finally R7 (Tomlinson and Ready 1987). Then, the four cone cells, the pigment cells, and the cells forming the mechanosensory bristle are recruited (Cagan 2009). Finally, unused cells are eliminated by apoptosis (Wolff and Ready 1991). Within every ommatid, R8 neurons are the first to differentiate, and also the first to send their axons to the posterior edge of the eye disc and through the optic stalk into the optic lobe. Here, they stop in the R8 temporary layer in the medulla region (Tayler and Garrity 2003; Mast et al. 2006; Ting and Lee 2007). To enter the optic stalk, photoreceptor axons rely on the retinal basal glia, which originate in the optic stalk, migrate into the eye disc, and follow the morphogenetic furrow (Choi and Benzer 1994; Rangarajan et al. 1999; Tayler and Garrity 2003). The axons from R1 to R6 follow the pioneering R8 axon and stop in the lamina region of the optic lobe (Ting and Lee 2007). The axon from R7 follows the R8 axon into the medulla region of the optic lobe and then projects past the R8 temporary layer to the R7 temporary layer. In a second step later in development, R7, R8, and lamina neuron axons extend to form the adult structure of the medulla (Mast et al. 2006).

Unlike the development of the retina, which takes place autonomously, the development of the lamina region of the optic lobe depends on retinal innervation (Meyerowitz and Kankel 1978; Steller et al. 1987; Halder et al. 1995). By delivering Hedgehog and Spitz in the optic lobe, photoreceptor axons induce the differentiation of the lamina neurons with which they then form lamina cartridges (Huang and Kunes 1996; Huang et al. 1998). This assures the numeral adjustment of postsynaptic lamina neurons to afferent photoreceptor axons. Also the outgrowth of scaffold axons that guide glial cell migration is dependent on photoreceptor axons, adjusting the distribution of glia to photoreceptor axons (Dearborn and Kunes 2004). As rows of R8 neurons differentiate sequentially from the posterior to the anterior part of the retina following the morphogenetic furrow, their axons enter the brain in a temporal sequence. Consequently, the development of lamina cartridges is induced row by row from the posterior to the anterior part of the lamina, as every row of R8 axons targets immediately anterior to the preceding row (Mast et al. 2006).

Compared to the lamina, the development of the more proximal parts of the visual system happens independently of innervation from the retina. The medulla and the lobular complex contain differentiated neurons and display their columnar organization also in the absence of the eye (Fischbach 1983). However, innervation by photoreceptor axons is required for the survival of

neurons, and they die after failure to establish a sufficient number of functional connections (Fischbach and Technau 1984).

During the pupal stage, the structure of the visual system is heavily reorganized. The eye disc evaginates to form the eye, and the optic lobe moves in such a way that the lamina is placed directly underneath the retina afterwards, which lets the optic stalk disappear. Instead, as the medulla rotates relative to the lamina, the optic chiasm is formed between lamina and medulla (Meinertzhagen and Hanson 1993).

1.3 Pathfinding of *Drosophila* photoreceptor axons

The navigation of *Drosophila* photoreceptor axons covers several distinct choices. First, photoreceptor axons have to choose the correct neuropil, the lamina in the case of R1 to R6 axons and the medulla in the case of R8 and R7 axons. Within the medulla, R8 and R7 axons have to choose their correct target layer M3 and M6, respectively. Moreover, photoreceptor axons have to choose their correct position along both the anterior-posterior axis and the dorsal-ventral axis to sustain their relative spatial relations to each other, establishing a retinotopic map.

Choosing the correct neuropil

On its way to the medulla, the pioneering R8 axon transits the lamina. Here, the R8 axon does not only induce the differentiation of lamina neurons, but is also responsible for the migration of glial cells into the lamina (Dearborn and Kunes 2004). These glial cells then provide a stop signal to the following axons from R1 to R6, which differentiate and send out their axons after the R8 neuron in every ommatid. Accordingly, R1 to R6 axons extend into the medulla when glial differentiation or migration is disrupted (Poeck et al. 2001; Suh et al. 2002; Mast et al. 2006). The molecular identity of the glial stop signal is not yet known (Mast et al. 2006; Ting and Lee 2007). However, several factors have been implicated in the response of R1 to R6 axons to the stop signal. These include the transcription factors Brakeless and Runt, the adaptor protein Dreadlocks, the receptor tyrosine phosphatase PTP69D, the receptor tyrosine kinase Off-track, and the serine/threonine kinase Misshapen (Garrity et al. 1996; Garrity et al. 1999; Ruan et al. 1999; Newsome et al. 2000a; Rao et al. 2000; Senti et al. 2000; Kaminker et al. 2002; Ruan et al. 2002; Cafferty et al. 2004; Ting and Lee 2007). R7 axons are apparently insensitive to the stop signal provided by the glia in the lamina and extend into the medulla.

Choosing the correct target layer in the medulla

R8 and R7 axons reach their final target layers in the medulla in a step-wise fashion. The R8 axon first stops extension in a superficial layer of the medulla, which the following R7 axon then passes to stop extension shortly underneath in the R7 temporary target layer. During the late pupal stage,

the R8 and the R7 axon progress synchronously to their final target layers M3 and M6, respectively (Ting et al. 2005).

Several proteins, including N-cadherin, PTP69D, and LAR, were implicated in R7 axon layer targeting, as mutations in the corresponding genes cause R7 axons to terminate at the R8 target layer M3 or between M3 and the correct R7 target layer M6. However, none of these proteins seems to specifically instruct R7 axons to target the M6 layer, as their presence in R8 axons does not cause them to overshoot their correct target layer M3 (Newsome et al. 2000a; Clandinin et al. 2001; Lee et al. 2001). But then, what does distinguish R8 and R7 axons and lets them terminate in different target layers in the medulla?

One protein was reported to be present exclusively in R8, but not in R7 axons, namely Capricious (Shinza-Kameda et al. 2006). In addition to R8 axons, Capricious is present at M3, but not in R7 axons or at M6. Loss of *capricious* causes R8 axons to target improper layers, and its ectopic expression in R7 redirects R7 axons to terminate in M3. Capricious is therefore required and sufficient for correct R8 target layer recognition (Shinza-Kameda et al. 2006). Flamingo is another transmembrane protein that was implicated in R8 axon layer targeting, but due to its broad expression and pleiotropic functions in other photoreceptors, its mode of action eluded a plain mechanistic explanation (Senti et al. 2003; Ting and Lee 2007). Recently, it could be shown that Flamingo is indeed responsible for the recognition of M3 as the correct target layer specifically by R8 axons. This specificity is conferred by Gogo, another transmembrane protein. Gogo and Flamingo cooperate in the M3 targeting of R8 axons, and ectopic expression of both Gogo and Flamingo in R7 photoreceptors is sufficient to redirect R7 terminals to M3 (Hakeda-Suzuki et al. 2011). In addition to confer R8 specificity to the recognition of M3 by Flamingo, Gogo has other functions in axon guidance. Gogo anchors R8 growth cones to their intermediate target layer and repels R8 axons from each other to assure their proper spacing in the medulla (Tomasi et al. 2008).

Establishing a retinotopic map

Drosophila possesses a single *ephrin* gene and a single gene encoding an Eph receptor (Mellott and Burke 2008). Ephrins and their Eph receptors are key players during the formation of the retinotopic map in vertebrates, and also the *Drosophila* Eph receptor was implicated in topographic map formation in the visual system (Dearborn et al. 2002). The *Drosophila* Eph receptor is expressed in the medulla in a symmetrical concentration gradient along the dorsal-ventral axis with a high level of Eph receptor along the midline that decreases towards the dorsal and the ventral edge of the medulla. The loss of Eph receptor function affects the correct topographic projection of photoreceptor axons along the dorsal-ventral axis. Although this could be a secondary consequence of severe disruptions in the medulla, results on DWnt4 and Dfrizzled2 make the

symmetrically graded distribution of the Eph receptor a promising candidate cue for routing photoreceptor axons along the dorsal-ventral axis. The photoreceptors of the ventral half of the retina, unlike those of the dorsal half, express *Dfrizzled2*. Their axons are able to respond to *DWnt4*, a secreted protein of the Wnt family expressed in the ventral half of the lamina through the non-canonical Wnt pathway involving the adaptor protein Dishevelled (Sato et al. 2006; Ting and Lee 2007). In the photoreceptors of the dorsal half of the retina, expression of *Dfrizzled2* is presumably suppressed by the homeobox transcription factor *Iroquois* to prevent their axons from entering the ventral half of the lamina. However, *DWnt4* does not show a graded expression in the lamina but instead a binary expression pattern, which can not explain the precise axonal intercalations that occur along the dorsal-ventral axis. Therefore, *DWnt4* may provide only rough positional information that must be combined with other cues provided by proteins expressed in a graded manner.

Other proteins that were implicated in the maintenance of the spatial relationships among photoreceptor axon bundles to establish a retinotopic map are *Dreadlocks*, *Pak*, and *Trio* that form a conserved signaling module coupled to the activation of the *Drosophila* insulin-like receptor (Garrity et al. 1996; Steven et al. 1998; Hing et al. 1999; Newsome et al. 2000b; Hakeda-Suzuki et al. 2002; Song et al. 2003; Ng and Luo 2004; Mast et al. 2006). However, mutations in *dreadlocks*, *pak* or *trio* cause complex phenotypes and do not only lead to a disordered topography, but also to axonal clumps and overshoots (Garrity et al. 1996; Hing et al. 1999; Newsome et al. 2000b; Mast et al. 2006). Therefore, they may play a more general role in axon guidance than specifically mediating the positional information to photoreceptor axons that they require to form a retinotopic map in the brain.

So far, no guidance cue is known that routes photoreceptor axons along the anterior-posterior axis. However, the sequential differentiation of photoreceptors and their concomitantly sequential innervation of the brain may enable their axons to find their correct position along the anterior-posterior axis.

1.4 A saturating screen for mutants affecting photoreceptor axon guidance in *Drosophila*

Although classical screens for genes involved in *Drosophila* photoreceptor axon guidance were successful in the past (Martin et al. 1995; Garrity et al. 1996), they always were limited by two major obstacles. First, a gene that is involved in axon guidance may have an essential function earlier in development. If a mutant animal dies before photoreceptor axon guidance takes place, that particular mutant will, of course, be missed in screens specifically aiming for defects in photoreceptor axon guidance. This is best illustrated by the classic morphogenes that appear to play a major role in axon guidance but were identified as guidance molecules only quite recently (Zou and Lyuksyutova 2007). Second, severe overall defects resulting from the lack of a certain

Expression of Flipase specifically in the eye then leads to mosaic flies that are overall heterozygous but have eyes almost completely homozygous for a certain chromosome arm (Newsome et al. 2000a).

For each of the four major autosomal arms, males with an *FRT* chromosome, the *ey-Flp* construct, and the *gl-lacZ* reporter were mutagenized with EMS (Figure 1.4 and Newsome et al. 2000a). The *ey-Flp* construct causes expression of Flipase mainly in the eye disc (Hauck et al. 1999; Newsome et al. 2000a), and the *gl-lacZ* reporter marks photoreceptor axons by β -galactosidase activity (Moses and Rubin 1991). The mutagenized males were crossed to females that carried the corresponding *FRT* chromosome arm with a cell lethal mutation, the *ey-Flp* construct, and the *gl-lacZ* reporter. As a roughening of the eye surface indicates patterning defects in the retina, rough-eyed F_1 progeny was discarded and only smooth-eyed male descendants were individually backcrossed. The F_2 progeny from more than 32 000 F_1 backcrosses was scored for defective photoreceptor projections at the 3rd instar larval stage (Newsome et al. 2000a). In the end, 122 mutant lines with correctly specified photoreceptor cell fates but abnormal photoreceptor projections were obtained (Berger et al. 2008).

Subsequent systematic analysis of the 122 mutations obtained from the screen revealed that they affected 42 different genes, 36 of which could be identified (Newsome et al. 2000a; Newsome et al. 2000b; Senti et al. 2000; Berger et al. 2001; Maurel-Zaffran et al. 2001; Senti et al. 2003; Berger et al. 2008). One complementation group consisted of three alleles that affected the previously undescribed gene CG32227, which was termed *gogo* (Berger et al. 2008; Tomasi et al. 2008).

1.5 *gogo*

All three mutant *gogo* alleles (Figure 1.5) are recessive lethal and considered as null alleles. The loss of Gogo causes defects in all photoreceptor subtypes. In the *gogo* mutant adult visual system, R1 to R6 axons correctly target the lamina, but the overall lamina structure shows mild irregularities. R7 axons cross each other and sometimes undershoot their correct target layer M6 in the medulla. R8 axons are affected most, cross and bundle each other, often overshoot their correct target layer M3 and stop in the R7 target layer M6 instead, or stall at their superficial intermediate target layer M1 and fail to innervate the medulla. In *gogo* mutants, axon pathfinding defects can already be detected at the 3rd instar larval stage. In the optic lobe, adjacent R8 axons form bundles with irregular gaps in between instead of the evenly distributed parallel tracts observed in wild type animals (Tomasi et al. 2008).

gogo encodes a 1272 aa single transmembrane protein (Figure 1.5). Its extracellular part features a TSP1 and a CUB domain, which are found in several proteins implicated in directing cell and growth cone migration. Additionally, it contains a region termed GOGO domain that is characterized by eight conserved cystein residues and dominated by beta strands. The GOGO

domain, together with the adjacent TSP1 but not the CUB domain, was also found in Gogo homologs in other insects, nematodes, and vertebrates. As shown by rescue experiments with fragments covering different parts of Gogo, the GOGO domain and the TSP1 domain are required for Gogo's function in axon guidance, whereas the CUB domain is not (Tomasi et al. 2008). In contrast to the extracellular part of Gogo, its intracellular part does not display any informative sequences. Only a short motif consisting of three aa, YYD, is conserved among species. The YYD motif is functionally important, as its deletion or mutation to DDD abolishes Gogo's axon guidance function, whereas mutating it to FFD does not (Luu 2008).

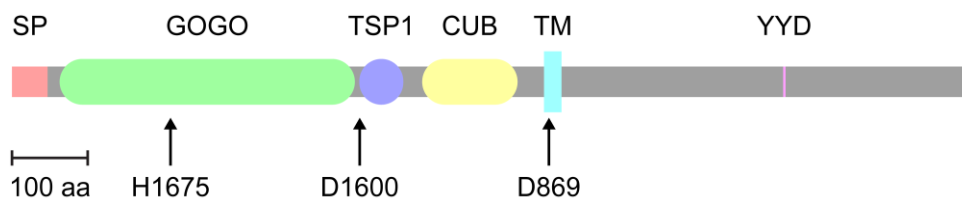


Figure 1.5: Schematic of Gogo's protein domain architecture and mutant alleles

The extracellular part of Gogo features a signal peptide (SP), the GOGO domain, a TSP1 domain, and a CUB domain. C-terminally of the transmembrane domain (TM), only the short YYD motif is conserved. In *gogo*^{H1675} mutants, the triplet normally encoding Q¹²⁵⁵ is replaced by a stop codon. In *gogo*^{D1600} and *gogo*^{D869} mutants, the splicing donor following the triplet encoding Q⁵⁷³ and L⁶⁶⁹, respectively, is defective, leading to 28 or 2 novel aa residues before translation is terminated. Scale bar: 100 aa.

Gogo is dynamically expressed in the developing visual system. In 3rd instar larvae, Gogo can be detected at the tips of R8 axons in the medulla region and in medulla neurons, but not at the termini of R1 to R6 axons. Later, during the early pupal stages, Gogo is present at the tips of all photoreceptors. From the midpupal stage onward, *gogo* expression decreases, but low protein levels persist on R7 and R8 axons (Tomasi et al. 2008). Although *gogo* is expressed in R7, it is apparently not required there for guiding R7 axons. Neither does the lack of Gogo specifically in R7 cause axon guidance defects, nor does the expression of *gogo* specifically in R7 restore the R7 axon guidance defects in *gogo* mutants. In contrast, expressing *gogo* specifically in R8 restores the axon guidance defects of both R8 and R7. Therefore, Gogo functions in R8 but not in R7 to guide axons, and the defective projections of R7 axons in *gogo* mutants are a secondary consequence of misguided R8 axons. Likewise, the expression of *gogo* in the brain is not required for photoreceptor axon guidance (Tomasi 2008; Tomasi et al. 2008). In contrast, the defects in the lamina of *gogo* mutants are directly due to the lack of Gogo in R1 to R6 and not the consequence of misguided R8 axons. In *gogo* mutants, the assembly of lamina cartridges is disturbed, leading to cartridges that contain an abnormal number of R1 to R6 termini instead of the six termini in wild

type lamina cartridges (Tomasi 2008). This defect can still be observed when the R8 pathfinding errors are restored by R8 specific expression of *gogo* (Hakeda-Suzuki et al. 2011).

Gogo appears to have distinct functions in different contexts. In the larval visual system, it was supposed to act as a heterophilic receptor that repels R8 axons from each other to assure their proper, evenly spaced array in the medulla. *gogo* mutant R8 axons entangle each other even if only small numbers of neighboring R8 axons are mutant, but neighboring wild-type axons are not affected, and also single mutant R8 axons appear normal (Tomasi et al. 2008). At the temporary R8 target layer, *Gogo* serves an adhesive function and anchors the termini of R8 axons. Excessive *Gogo* enhances the affinity for the temporary R8 target layer, which becomes manifest in enlarged swellings of R8 axons at the M1 layer in the adult medulla (Tomasi et al. 2008). This adhesive function of *Gogo* is antagonized by *Flamingo*, as the number of abnormal swellings is reduced if *flamingo* is co-overexpressed, whereas excessive *Gogo* results in a permanent stalling of many R8 axons at the M1 layer in a *flamingo* hypomorphic background (Hakeda-Suzuki et al. 2011). However, *Gogo* and *Flamingo* cooperate in the later phase of R8 target selection, when the R8 axons extend into the medulla to reach their final target layer M3. This becomes most evident in the re-targeting of R7 axon termini to the R8 target layer M3 when both *flamingo* and *gogo* are overexpressed specifically in R7 axons. Unlike *Gogo*, *Flamingo* is also required in the target area of R8 axons in the brain. In the photoreceptors, the cytoplasmic part of *Gogo* but not that of *Flamingo* is required for normal R8 axon targeting. Therefore, it was supposed that *Gogo* and *Flamingo* cooperate in R8 photoreceptor axons to detect M3 labeled by *Flamingo* as the correct target layer of R8 axons.

1.6 Hts and Adducin

The cytoplasmic part of *Gogo* is indispensable for its function. However, as it does not include any informative sequence, it was completely unclear how the cytoplasmic part of *Gogo* would act to guide photoreceptor axons. To elucidate its function at the molecular level, this work aimed to detect another protein that physically interacts with the cytoplasmic part of *Gogo* and led to the identification of *Hts*, the single homolog of mammalian *Adducin* in *Drosophila*. As yet, research on *Hts* focused on its role during oogenesis and nothing was known about its role in neural development.

Adducin

Adducin is a ubiquitously expressed protein that resides, amongst others, at the axonal growth cone (Matsuoka et al. 2000). In vitro, *Adducin* bundles Actin filaments (Mische et al. 1987; Taylor and Taylor 1994), caps the fast-growing ends of Actin filaments (Kuhlman et al. 1996) and recruits Spectrin to Actin filaments (Gardner and Bennett 1987; Bennett et al. 1988; Hughes and Bennett

1995). By linking Spectrin tetramers to short Actin filaments, it is required for the proper assembly of the Actin-Spectrin cytoskeleton underlying the plasma membrane (reviewed by Matsuoka et al. 2000). Adducin consists of a head, a neck and a tail domain (Joshi and Bennett 1990; Joshi et al. 1991). The function of the head domain is largely unclear (Matsuoka et al. 2000). It may assist in forming the proper Adducin tetramers found in vivo although it is not required for oligomerization per se (Hughes and Bennett 1995; Li et al. 1998). The neck domain self-associates to form oligomers and is necessary but not sufficient for all interactions of Adducin with Actin and Spectrin (Li et al. 1998). In addition, these interactions require the tail domain with its highly conserved 22-residue MARCKS-related domain that has homology to the MARCKS protein (Li et al. 1998; Matsuoka et al. 2000). The MARCKS-related domain is an important site for the regulation of Adducin. Both phosphorylation of Adducin within the MARCKS-related domain by PKC (Matsuoka et al. 1998) or PKA (Matsuoka et al. 1996) as well as binding of Ca²⁺-Calmodulin to the MARCKS-related domain (Gardner and Bennett 1987; Kuhlman et al. 1996) inhibit its activities.

Hts

“Hu li tai shao” is a Chinese expression that can be translated as “too little nursing”. Hts was first described as an important factor in oogenesis (Yue and Spradling 1992). The *Drosophila* ovary consists of several ovarioles, each of which contains a series of developing egg chambers. A mature egg chamber comprises a surrounding epithelium of somatic “follicle cells” and a syncytium of 16 interconnected cells, one of which is the oocyte and 15 of which are “nurse cells” that nourish the oocyte through the cytoplasmic bridges. The 16-cell cysts derive from four synchronized, incomplete divisions of a “cystoblast” in the anterior part of the ovariole, the germarium (reviewed by de Cuevas et al. 1997). The cystoblast contains a structure called “spectrosome” that grows and branches during cystoblast divisions to form the “fusome” that extends through the cytoplasmic bridges, possibly to stabilize the cleavage furrows until “ring canals” form (Lin et al. 1994; Robinson et al. 1994). Spectrosome and fusome are areas of highly condensed vesicles (de Cuevas et al. 1997; Snapp et al. 2004). The fusome membranes are associated with a cytoskeleton that includes a product of the *hts* locus, Ovhts-Fus, as well as α -Spectrin, β -Spectrin and Ankyrin (Lin et al. 1994; de Cuevas et al. 1996; Petrella et al. 2007). When proliferation stops and differentiation begins, the fusome disappears and ring canals form at the arrested cleavage furrows (Robinson et al. 1994). Ring canals contain another product of the *hts* locus, Ovhts-RC, as well as F-Actin and Filamin (Warn et al. 1985; Robinson et al. 1997; Petrella et al. 2007). *hts* mutant females are sterile due to a loss of oocyte specification, too few nurse cells, absence of fusomes, deformities of the ring canals and a defective organization of the early embryonic cytoskeleton (Yue and Spradling 1992; Ding et al. 1993; Lin et al. 1994; Zaccai and Lipshitz 1996b; Petrella et al. 2007).

The *hts* locus encodes several different proteins (Figure 1.6 and Whittaker et al. 1999; Petrella et al. 2007). They all share the first 472 N-terminal aa that correspond to the head and the neck domain of Adducin, but have unique C-termini.

ShAdd (495 aa in length) is a truncated Hts isoform that has only 23 more unique aa.

Add1 (718 aa) and Add2 (741 aa) contain the Adducin tail including the MARCKS-related domain and are the Hts isoforms most closely related to Adducin (Petrella et al. 2007).

HtsPD (668 aa) is another Hts isoform predicted by FlyBase. Its N-terminal 659 aa are identical to Add1 and it contains most of the Adducin tail but lacks the very C-terminal part including the MARCKS-related domain. HtsPD has not been found in vivo yet.

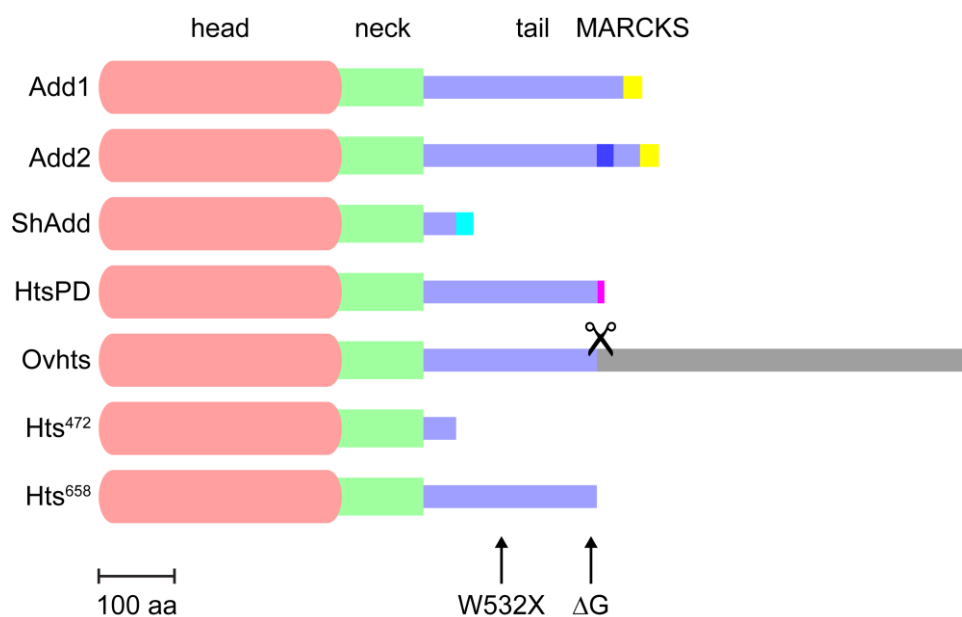


Figure 1.6: Schematic of the different Hts proteins

Add1 is the Hts isoform most similar to Adducin and comprises the head (red), the neck (green), and the tail (blue) domain including the MARCKS-related domain (yellow). Add2 resembles Add1 and differs only in 23 additional aa (dark blue). ShAdd is a truncated isoform that lacks almost the complete tail domain. HtsPD is very similar to Add1 and contains most of the tail domain, but it lacks the MARCKS-related domain. Ovhts is posttranslationally cleaved to produce the two functional proteins Ovhts-Fus that resembles Adducin and Ovhts-RC that shows a completely unrelated sequence. Hts⁴⁷² is the fragment of Hts that is shared among all isoforms. Hts⁶⁵⁸ is the fragment of Hts that is shared among all isoforms but ShAdd. In *hts*^{W532X} mutants, the triplet normally encoding W⁵³² is replaced by a stop codon. In *hts*^{ΔG} mutants, the deletion of a single G in the triplet encoding R⁶⁵⁰ causes a frameshift that leads to the replacement of R⁶⁵⁰ by 6 novel aa, followed by a premature stop codon. Same color indicates same sequence. Scale bar: 100 aa.

Ovhts (1156 aa) contains most of the Adducin tail (excluding the MARCKS-related domain) and continues after its N-terminal 658 aa that are identical to Add1 with a large novel domain designated the RC domain. Ovhts is posttranslationally cleaved to produce two distinct proteins,

Ovhts-Fus that is associated with the fusome, and Ovhts-RC that is associated with ring canals (Petrella et al. 2007). Ovhts is not expressed in the head and not at all in males (Telonis-Scott et al. 2009). Therefore, it is inconceivable to function in photoreceptor axon guidance and was excluded from the experiments presented in this work.

2. MATERIALS AND METHODS

2.1 Generation of transgenic fly stocks

Transgenic flies are usually obtained from the microinjection of a P-element based transformation vector together with a helper plasmid into preblastoderm stage embryos. The P-element is a natural transposon occurring in *Drosophila*. It features 31 bp inverted terminal repeats and 11 bp inverted subterminal repeats as the major cis-acting elements required for transposition, which flank the transposase encoding gene that consists of four exons (Castro and Carareto 2004). As not more than 138 bp at the 5' end and 216 bp at the 3' end of the P-element are required for transposition in cis (Beall and Rio 1997), the transposase gene can be removed from the P-element. Replacing it by a selectable marker, usually a w^+ allele conferring red eyes to w mutant flies that otherwise have white eyes, and an MCS to take up exogenous DNA yields a transformation vector that is able to transpose from the injected plasmid into the genome. Moreover, removing the transposase gene from the P-element prevents it from continued transpositions and allows for stable transgenic stocks. For the initial transposition from the injected plasmid into the genome, the transposase is supplied from a co-injected helper plasmid. Transformation vector and helper plasmid are injected into the posterior pole of the embryo before cellularization. The *Drosophila* embryo develops as a syncytium for the first 1.5 h after fertilization (Allis et al. 1977). Upon cellularization, the nuclei deposited at the posterior pole of the syncytium are incorporated into the pole cells, which are the precursors of the germ cells. A transgene inserted into the genome of a pole cell will therefore be passed on to gametes generated by the fly arising from the injected embryo and eventually to its progeny, which will then consist entirely of transgenic cells. These transgenic animals can be identified by means of the selectable marker included in the transformation vector.

Microinjections

In order to generate transgenic flies with *gogo* constructs, embryos homozygous for the w^{118} mutation, which causes white eye color, were collected for 30' at 25 °C on apple juice agar plates from a population cage. To dechorionate the embryos, they were treated with 50 % household bleach for 2' directly on the apple juice agar plates, then poured onto a vacuum-driven membrane filter and rinsed with plenty of tap water. The dechorionated embryos were manually lined up on the filter side by side using a fine brush. Typically, 200 embryos were used per construct. The embryos were transferred onto a coverslip that had been moistened with Scotch glue in heptane and air-dried before. Scotch glue in heptane was obtained by simply leaving Scotch Tape in n-heptane for some days with some agitation. The coverslip with the embryos was placed onto a microscope slide and the embryos were dried in a large Petri dish over silica gel for approximately

15'. Then, the embryos were covered with halocarbon oil, and a mixture of 0.6 µg/µl of the plasmid carrying the particular transgenic construct and 0.2 µg/µl of the helper plasmid in water was injected using a FemtoJet microinjector from Eppendorf (Hamburg, Germany). After injection, the coverslip with the embryos was transferred to a vial with fresh fly food.

Microinjections of plasmids with *hts* constructs into w^{1118} embryos were performed by BestGene (Chino Hills, California).

Balancing

The flies developing from the injected embryos were individually crossed to w^{1118} flies. Successful germline transformation resulted in red-eyed flies in the F1 generation. To breed stable transgenic stocks and to determine at which chromosome the transformation vector was inserted, red-eyed flies were crossed to flies from balancer stocks. If possible, the balancer chromosomes were removed from the transgenic stocks to obtain homozygous flies.

The following fly stocks were used to generate transgenic fly stocks:

w^{1118}

$w^{1118} / Y, hs-hid$

$y^* w^* / Y, hs-hid ; Pin^* / CyO$

$y^* w^* / Y, hs-hid ; sens^{Ly-1} / TM3, Sb^1$

List of transgenic fly stocks that were generated

All transgenic fly stocks that were generated and used in this work are listed below.

genotype	plasmid	chromosome	promoter	protein
$w^*, P\{GMR-gogo-Myc\}XA$	<i>pGMR-gogo-Myc</i>	X	<i>GMR</i>	Gogo-Myc
$y^* w^* ; P\{GMR-gogo-Myc\}2A$	<i>pGMR-gogo-Myc</i>	2	<i>GMR</i>	Gogo-Myc
$w^*, P\{GMR-gogo^{AC}-Myc\}XA$	<i>pGMR-gogo^{AC}-Myc</i>	X	<i>GMR</i>	Gogo ^{AC} -Myc
$y^* w^* ; P\{GMR-gogo^{AC}-Myc\}2A$	<i>pGMR-gogo^{AC}-Myc</i>	2	<i>GMR</i>	Gogo ^{AC} -Myc
$y^* w^* ; P\{GMR-gogo^{cyto}-Myc\}3B$	<i>pGMR-gogo^{cyto}-Myc</i>	3	<i>GMR</i>	Gogo ^{cyto} -Myc
$w^*, P\{GMR-Add1\}XA$	<i>pGMR-Add1</i>	X	<i>GMR</i>	Add1
$y^* w^* ; P\{GMR-Add1\}2A$	<i>pGMR-Add1</i>	2	<i>GMR</i>	Add1
$y^* w^* ; P\{GMR-Add1\}3A$	<i>pGMR-Add1</i>	3	<i>GMR</i>	Add1
$y^* w^* ; P\{GMR-Add1\}3B$	<i>pGMR-Add1</i>	3	<i>GMR</i>	Add1
$w^*, P\{GMR-ShAdd\}XA$	<i>pGMR-ShAdd</i>	X	<i>GMR</i>	ShAdd
$y^* w^* ; P\{GMR-ShAdd\}3A$	<i>pGMR-ShAdd</i>	3	<i>GMR</i>	ShAdd
$y^* w^* ; P\{GMR-ShAdd\}3B$	<i>pGMR-ShAdd</i>	3	<i>GMR</i>	ShAdd
$w^*, P\{GMR-htsPD\}XA$	<i>pGMR-htsPD</i>	X	<i>GMR</i>	HtsPD

genotype	plasmid	chromosome	promoter	protein
$y^* w^* ; P\{GMR\text{-}htsPD\}3A$	<i>pGMR-htsPD</i>	3	<i>GMR</i>	HtsPD
$y^* w^* ; P\{GMR\text{-}htsPD\}3B$	<i>pGMR-htsPD</i>	3	<i>GMR</i>	HtsPD
$y^* w^* ; P\{UAS\text{-}gogo\text{-}Myc\}2B / CyO$	<i>pUAST-gogo-Myc</i>	2	<i>UAS</i>	Gogo-Myc
$y^* w^* ; P\{UAS\text{-}gogo\text{-}Myc\}3B$	<i>pUAST-gogo-Myc</i>	3	<i>UAS</i>	Gogo-Myc
$y^* w^* ; P\{UAS\text{-}Add1\text{-}Myc\}2A / CyO$	<i>pUAST-Add1-Myc</i>	2	<i>UAS</i>	Add1-Myc
$y^* w^* ; P\{UAS\text{-}Add1\text{-}Myc\}3A$	<i>pUAST-Add1-Myc</i>	3	<i>UAS</i>	Add1-Myc
$y^* w^* ; P\{UAS\text{-}ShAdd\text{-}His\}2A$	<i>pUAST-ShAdd-His</i>	2	<i>UAS</i>	ShAdd-His
$y^* w^* ; P\{UAS\text{-}ShAdd\text{-}His\}2B / CyO$	<i>pUAST-ShAdd-His</i>	2	<i>UAS</i>	ShAdd-His
$y^* w^* ; P\{UAS\text{-}hts^{472}\text{-}His\}3A$	<i>pUAST-hts⁴⁷²-His</i>	3	<i>UAS</i>	Hts ⁴⁷² -His
$y^* w^* ; P\{UAS\text{-}hts^{472}\text{-}His\}3B$	<i>pUAST-hts⁴⁷²-His</i>	3	<i>UAS</i>	Hts ⁴⁷² -His

Table 2.1: List of transgenic fly stocks that were generated

The genotype of each stock is denoted in the first column. The second column states the plasmid that was injected and the third column the chromosome at which the transformation vector was inserted. The fourth column quotes the promoter contained in the transgenic construct to control the expression of the protein listed in the fifth column.

2.2 Generation of other fly stocks

All fly stocks that were generated in addition to the transgenic fly stocks mentioned above are listed below.

hts mutations over GFP balancers

$w^* ; nub^* b^* pr^* hts^{1G} bw^* / CyO, Kr\text{-}Gal4, UAS\text{-}GFP$

$w^* ; nub^* b^* pr^* hts^{W532X} bw^* / CyO, Kr\text{-}Gal4, UAS\text{-}GFP$

$w^* ; cn^1 P\{PZ\}hts^{01103} / CyO, Kr\text{-}Gal4, UAS\text{-}GFP ; ry^{506} / +$

$w^* ; Df(2R)BSC26 / CyO, Kr\text{-}Gal4, UAS\text{-}GFP$

The following fly stocks were used to obtain these genotypes:

$w^* ; nub^* b^* pr^* hts^{1G} bw^* / CyO, b^*$

$w^* ; nub^* b^* pr^* hts^{W532X} bw^* / CyO, b^*$

$cn^1 P\{PZ\}hts^{01103} / CyO ; ry^{506}$

$Df(2R)BSC26 / CyO$

$w^* ; L^2 Pin^1 / CyO, Kr\text{-}Gal4, UAS\text{-}GFP$

hts mutation with rescue construct

$y^* w^* ; cn^1 P\{PZ\}hts^{01103} / CyO, Kr-Gal4, UAS-GFP ; P\{GMR-htsPD\}3B$

The following fly stocks were used to obtain this genotype:

$cn^1 P\{PZ\}hts^{01103} / CyO ; ry^{506}$

$y^* w^* ; P\{GMR-htsPD\}3B$

$w^* / + ; m\delta-lacZ / CyO, Kr-Gal4, UAS-GFP ; gogo^{D1600} FRT80B / TM6B, y^+$

$y^* w^* ; wg^{Sp-1} / CyO ; MKRS / TM3, Sb^1 Ser^1, y^+$

hts mutations with R8 axon marker

$y^* w^* ey-Flp, Rh6-mCD8-GFP ; nub^* b^* pr^* hts^{\Delta G} bw^* / CyO, y^+$

$y^* w^* ey-Flp, Rh6-mCD8-GFP ; nub^* b^* pr^* hts^{W532X} bw^* / CyO, y^+$

$y^* w^* ey-Flp, Rh6-mCD8-GFP ; cn^1 P\{PZ\}hts^{01103} / CyO, y^+ ; ry^{506} / +$

$y^* w^* ey-Flp, Rh6-mCD8-GFP ; Df(2R)BSC26 / CyO, y^+$

The following fly stocks were used to obtain these genotypes:

$w^* ; nub^* b^* pr^* hts^{\Delta G} bw^* / CyO, Kr-Gal4, UAS-GFP$

$w^* ; nub^* b^* pr^* hts^{W532X} bw^* / CyO, Kr-Gal4, UAS-GFP$

$w^* ; cn^1 P\{PZ\}hts^{01103} / CyO, Kr-Gal4, UAS-GFP ; ry^{506} / +$

$w^* ; Df(2R)BSC26 / CyO, Kr-Gal4, UAS-GFP$

$y^* w^* ey-Flp, Rh6-mCD8-GFP ; GMR-Gal4 / CyO$

$y^* w^* ; Pin^* / CyO$

$y^* w^* ; omb-Gal4, UAS-GFPnls / FM7c$

Virginator balancer stocks

$y^* w^* / Y, hs-hid ; Pin^* / CyO$

$y^* w^* / Y, hs-hid ; sens^{Ly-1} / TM3, Sb^1$

The following fly stocks were used to obtain these genotypes:

$y^* w^* ; Pin^* / CyO$

$y^* w^* ; sens^{Ly-1} / TM3, Sb^1$

$w^{1118} / Y, hs-hid$

Double balancer stock

$y^* w^* ; wg^{Sp-1} / CyO ; MKRS / TM3, Sb^1 Ser^1, y^+$

The following fly stocks were used to obtain this genotype:

$y^* w^* ; wg^{Sp-1} / CyO ; MKRS / TM2, y^+$

$y^* w^* ; D^* gl^* / TM3, Sb^1 Ser^1, y^+$

2.3 Other fly stocks

All other fly stocks that were used are listed below.

Stocks from the Suzuki lab stock collection

<i>y* w* ey-Flp ; gogo^{D869} FRT80B / TM6B, y⁺</i>	stock Y95
<i>y* w* ey-Flp ; gogo^{D1600} FRT80B / TM6B, y⁺</i>	stock Y99
<i>y* w* ey-Flp ; gogo^{H1675} FRT80B / TM6B, y⁺</i>	stock Y136
<i>P{UAS-gogo}T1 / CyO</i>	stock T152
<i>P{UAS-gogo}T3 / TM6B, y⁺</i>	stock T153
<i>y* w* ey-Flp GMR-lacZ ; wg^{Sp-1} / CyO, y⁺ ; MKRS / TM6B, y⁺</i>	stock M1
<i>y* w* ey-Flp GMR-lacZ ; RpS17^A P{w⁺}70C FRT80B / TM6B, y⁺</i>	stock M35
<i>y* w* ; Pin* / CyO</i>	stock M43
<i>y* w* ; sens^{Ly-1} / TM3, Sb¹</i>	stock M44
<i>w¹¹¹⁸</i>	stock M45
<i>w¹¹¹⁸ / Y, hs-hid</i>	stock M46
<i>GMR-hid, y* w* FRT19A ; ey-Gal4 UAS-Flp</i>	stock M52
<i>y* w* ey-Flp GMR-lacZ ; FRT42D</i>	stock M77
<i>w* ; L² Pin¹ / CyO, Kr-Gal4, UAS-GFP</i>	stock M89
<i>y* w* ; D* gl* / TM3, Sb¹ Ser¹, y⁺</i>	stock M92
<i>y* w* ; wg^{Sp-1} / CyO ; MKRS / TM2, y⁺</i>	stock M151
<i>y* w* , omb-Gal4, UAS-GFPnls / FM7c</i>	stock M344
<i>y* w* ; ey1x-Flp.Exel / CyO ; GMR-mCD8-KO, tubP-Gal80 FRT80B / TM6B, y⁺</i>	stock M412
<i>elav-Gal4, UAS-mCD8-GFP, hs-Flp ; GMR-mCD8-KO, tubP-Gal80 FRT80B / TM6B, y⁺</i>	stock M415
<i>y* w* ; GMR-Gal4, P{UAS-gogo}T1 / CyO</i>	stock M434
<i>w* / + ; mδ-lacZ / CyO, Kr-Gal4, UAS-GFP ; gogo^{D1600} FRT80B / TM6B, y⁺</i>	stock M451
<i>y* w* , Rh6-mCD8-GFP ; gogo^{D869} FRT80B / TM6B, y⁺</i>	stock M481
<i>y* w* ey-Flp, Rh6-mCD8-GFP ; FRT80B / TM3, Sb¹</i>	stock M510
<i>y* w* ey-Flp, Rh6-mCD8-GFP ; gogo^{D869} FRT80B / TM3, Sb¹</i>	stock M513
<i>y* w* ey-Flp, Rh6-mCD8-GFP ; GMR-Gal4 / CyO</i>	stock M527
<i>y* w* ey-Flp, Rh6-mCD8-GFP ; GMR-Gal4, P{UAS-gogo}T1 / CyO</i>	stock M528
<i>y* w* ey-Flp GMR-lacZ ; GMR-Gal4 ; ato-tau-Myc FRT80B / TM6B, y⁺</i>	stock M558

Stocks from the Bloomington *Drosophila* stock center

$v^1 swa^1 / FM3$	FlyBase ID: FBst0003162
$y^1 cv^1 swa^3 v^1 f^1 / FM3$	FlyBase ID: FBst0002174
$cn^1 P\{PZ\}hts^{01103} / CyO ; ry^{506}$	FlyBase ID: FBst0010989
$Df(2R)BSC26 / CyO$	FlyBase ID: FBst0006866

Stocks from other sources

$y^* w^* ey-Flp, Rh6-mCD8-GFP ; FRT42D hts^{null} / CyO, y^+$
 $y^* w^* ey-Flp, Rh6-mCD8-GFP ; FRT42D P\{PZ\}hts^{01103} / CyO, y^+$
 $y^* w^* ey-Flp, Rh6-mCD8-GFP ; FRT42D P\{w^+\}47A I(2)cl-R11^1 / CyO, y^+$
 from Satoko Hakeda-Suzuki, Suzuki Lab.

β -Spec^{G113} FRT19A / FM7a

from Christian Klämbt, Westfälische Wilhelms-Universität, Münster, Germany (stock T0516).

$w^* ; nub^* b^* pr^* hts^{W532X} bw^* / CyO, b^*$
 $w^* ; nub^* b^* pr^* hts^{4G} bw^* / CyO, b^*$

from Lynn Cooley, Yale University, New Haven, Connecticut.

2.4 Fly genotypes

The full genotypes of the flies used in this work are listed below.

Figure 3.1.2

- A: $y^* w^* ey-Flp GMR-lacZ / Y ; RpS17^A P\{w^+\}70C FRT80B / gogo^{D869} FRT80B$
 B: $y^* w^* ey-Flp GMR-lacZ / y^* w^* or Y ; + / P\{GMR-gogo^{4C}-Myc\}2A ; RpS17^A P\{w^+\}70C FRT80B / gogo^{D869} FRT80B$
 C: $y^* w^* ey-Flp GMR-lacZ / y^* w^* or Y ; + / P\{GMR-gogo-Myc\}2A ; RpS17^A P\{w^+\}70C FRT80B / gogo^{D869} FRT80B$
 D: $y^* w^* ey-Flp GMR-lacZ / w^*, P\{GMR-gogo^{4C}-Myc\}XA ; RpS17^A P\{w^+\}70C FRT80B / gogo^{D869} FRT80B$
 E: $y^* w^* ey-Flp GMR-lacZ / w^*, P\{GMR-gogo-Myc\}XA ; RpS17^A P\{w^+\}70C FRT80B / gogo^{D869} FRT80B$
 F: $y^* w^* ey-Flp GMR-lacZ / Y ; RpS17^A P\{w^+\}70C FRT80B / gogo^{D1600} FRT80B$
 G: $y^* w^* ey-Flp GMR-lacZ / y^* w^* or Y ; + / P\{GMR-gogo^{4C}-Myc\}2A ; RpS17^A P\{w^+\}70C FRT80B / gogo^{D1600} FRT80B$
 H: $y^* w^* ey-Flp GMR-lacZ / y^* w^* or Y ; + / P\{GMR-gogo-Myc\}2A ; RpS17^A P\{w^+\}70C FRT80B / gogo^{D1600} FRT80B$
 I: $y^* w^* ey-Flp GMR-lacZ / w^*, P\{GMR-gogo^{4C}-Myc\}XA ; RpS17^A P\{w^+\}70C FRT80B / gogo^{D1600} FRT80B$
 J: $y^* w^* ey-Flp GMR-lacZ / w^*, P\{GMR-gogo-Myc\}XA ; RpS17^A P\{w^+\}70C FRT80B / gogo^{D1600} FRT80B$

The following fly stocks were used to obtain these genotypes:

- $y^* w^* ; P\{GMR-gogo^{4C}-Myc\}2A$
 $y^* w^* ; P\{GMR-gogo-Myc\}2A$
 $w^*, P\{GMR-gogo^{4C}-Myc\}XA$
 $w^*, P\{GMR-gogo-Myc\}XA$

$y^* w^* ey-Flp ; gogo^{D869} FRT80B / TM6B, y^+$
 $y^* w^* ey-Flp ; gogo^{D1600} FRT80B / TM6B, y^+$
 $y^* w^* ey-Flp GMR-lacZ ; RpS17^4 P\{w^*\}70C FRT80B / TM6B, y^+$

Figure 3.1.3

A: w^{1118} / w^{1118} or Y
 B: $y^* w^* / y^* w^*$ or Y ; $P\{GMR-gogo^{1C}-Myc\}2A$
 C: $y^* w^* / y^* w^*$ or Y ; $P\{GMR-gogo-Myc\}2A$

Figure 3.2.1

A: w^{1118} / w^{1118} or Y
 B: $y^* w^* / y^* w^*$ or Y ; $P\{GMR-gogo^{cyto}-Myc\}3B$

Figure 3.2.2

A: w^{1118} / w^{1118} or Y
 $y^* w^* / y^* w^*$ or Y ; $P\{GMR-gogo^{cyto}-Myc\}3B$
 B: w^{1118} / w^{1118} or Y
 $y^* w^* / y^* w^*$ or Y ; $P\{GMR-gogo^{cyto}-Myc\}3B$

Figure 3.3

w^{1118} / w^{1118} or Y

Figure 3.4

A: $y^* w^* ey-Flp, Rh6-mCD8-GFP ; nub^* b^* pr^* hts^{4G} bw^*$
 B: $y^* w^* ey-Flp, Rh6-mCD8-GFP ; nub^* b^* pr^* hts^{W532X} bw^*$
 C: $y^* w^* ey-Flp, Rh6-mCD8-GFP ; Df(2R)BSC26 / cn^1 P\{PZ\}hts^{01103}$
 D: $y^* w^* ey-Flp, Rh6-mCD8-GFP ; FRT42D P\{w^*\}47A I(2)cl-R11^1 / FRT42D P\{PZ\}hts^{01103}$
 E: $y^* w^* ey-Flp, Rh6-mCD8-GFP ; FRT42D hts^{null}$
 F: $y^* w^* ey-Flp, Rh6-mCD8-GFP ; FRT42D P\{w^*\}47A I(2)cl-R11^1 / FRT42D hts^{null}$
 G: $y^* w^* ey-Flp, Rh6-mCD8-GFP ; FRT42D P\{w^*\}47A I(2)cl-R11^1 / FRT42D$

The following fly stocks were used to obtain these genotypes:

$y^* w^* ey-Flp, Rh6-mCD8-GFP ; nub^* b^* pr^* hts^{4G} bw^* / CyO, y^+$
 $y^* w^* ey-Flp, Rh6-mCD8-GFP ; nub^* b^* pr^* hts^{W532X} bw^* / CyO, y^+$
 $y^* w^* ey-Flp, Rh6-mCD8-GFP ; cn^1 P\{PZ\}hts^{01103} / CyO, y^+ ; ry^{506} / +$
 $y^* w^* ey-Flp, Rh6-mCD8-GFP ; Df(2R)BSC26 / CyO, y^+$
 $y^* w^* ey-Flp, Rh6-mCD8-GFP ; FRT42D P\{PZ\}hts^{01103} / CyO, y^+$

$y^* w^* ey-Flp, Rh6-mCD8-GFP ; FRT42D hts^{null} / CyO, y^+$
 $y^* w^* ey-Flp, Rh6-mCD8-GFP ; FRT42D P\{w^+\}47A l(2)cl-R11^1 / CyO, y^+$
 $y^* w^* ey-Flp GMR-lacZ ; FRT42D$

J: w^{1118} / w^{1118} or Y

w^* / w^* or Y ; $nub^* b^* pr^* hts^{\Delta G} bw^*$

w^* / w^* or Y ; $Df(2R)BSC26 / cn^1 P\{PZ\}hts^{01103}$

w^* / w^* or Y ; $nub^* b^* pr^* hts^{W532X} bw^*$

K: w^{1118} / w^{1118} or Y

w^* / w^* or Y ; $nub^* b^* pr^* hts^{\Delta G} bw^*$

w^* / w^* or Y ; $Df(2R)BSC26 / cn^1 P\{PZ\}hts^{01103}$

w^* / w^* or Y ; $nub^* b^* pr^* hts^{W532X} bw^*$

The following fly stocks were used to obtain these genotypes:

w^{1118}

$w^* ; nub^* b^* pr^* hts^{\Delta G} bw^* / CyO, Kr-Gal4, UAS-GFP$

$w^* ; cn^1 P\{PZ\}hts^{01103} / CyO, Kr-Gal4, UAS-GFP ; ry^{506} / +$

$w^* ; Df(2R)BSC26 / CyO, Kr-Gal4, UAS-GFP$

$w^* ; nub^* b^* pr^* hts^{W532X} bw^* / CyO, Kr-Gal4, UAS-GFP$

Figure 3.5

$\beta-Spec^{G113} FRT19A / GMR-hid, y^* w^* FRT19A ; ey-Gal4 UAS-Flp / +$

The following fly stocks were used to obtain this genotype:

$\beta-Spec^{G113} FRT19A / FM7a$

$GMR-hid, y^* w^* FRT19A ; ey-Gal4 UAS-Flp$

Figure 3.6

A: $v^1 swa^1$

B: $y^1 cv^1 swa^3 v^1 f^1$

The following fly stocks were used to obtain these genotypes:

$v^1 swa^1 / FM3$

$y^1 cv^1 swa^3 v^1 f^1 / FM3$

Figure 3.7.1A: $y^* w^*$; $P\{GMR-Add1\}3A$ B: w^* , $P\{GMR-Add1\}XA$ C: $y^* w^*$; $P\{GMR-ShAdd\}3B$ D: w^* , $P\{GMR-ShAdd\}XA$ E: $y^* w^*$; $P\{GMR-htsPD\}3B$ F: w^* , $P\{GMR-htsPD\}XA$ **Figure 3.7.2**A: w^* / Y ; $Df(2R)BSC26 / cn^1 P\{PZ\}hts^{01103}$ B: $w^* / y^* w^* ey-Flp GMR-lacZ$ or $y^* w^*$; $cn^1 P\{PZ\}hts^{01103} / Df(2R)BSC26$; + / $P\{GMR-Add1\}3A$ C: w^* / w^* , $P\{GMR-Add1\}XA$; $Df(2R)BSC26 / cn^1 P\{PZ\}hts^{01103}$ D: $w^* / y^* w^* ey-Flp GMR-lacZ$ or $y^* w^*$; $cn^1 P\{PZ\}hts^{01103} / Df(2R)BSC26$; + / $P\{GMR-ShAdd\}3B$ E: w^* / w^* , $P\{GMR-ShAdd\}XA$; $Df(2R)BSC26 / cn^1 P\{PZ\}hts^{01103}$ F: $w^* / y^* w^* ey-Flp GMR-lacZ$ or $y^* w^*$; $cn^1 P\{PZ\}hts^{01103} / Df(2R)BSC26$; + / $P\{GMR-htsPD\}3B$ G: w^* / w^* , $P\{GMR-htsPD\}XA$; $Df(2R)BSC26 / cn^1 P\{PZ\}hts^{01103}$ H: $y^* w^* / y^* w^*$ or $y^* w^* ey-Flp$ or Y ; $cn^1 P\{PZ\}hts^{01103} / Df(2R)BSC26$; $P\{GMR-htsPD\}3B / P\{GMR-Add1\}3A$ I: $y^* w^* / y^* w^*$ or $y^* w^* ey-Flp$ or Y ; $cn^1 P\{PZ\}hts^{01103} / Df(2R)BSC26$; $P\{GMR-htsPD\}3B$

The following fly stocks were used to obtain these genotypes:

 $y^* w^*$; $P\{GMR-Add1\}3A$ w^* , $P\{GMR-Add1\}XA$ $y^* w^*$; $P\{GMR-ShAdd\}3B$ w^* , $P\{GMR-ShAdd\}XA$ $y^* w^*$; $P\{GMR-htsPD\}3B$ w^* , $P\{GMR-htsPD\}XA$ w^* ; $cn^1 P\{PZ\}hts^{01103} / CyO$, $Kr-Gal4$, $UAS-GFP$; $ry^{506} / +$ w^* ; $Df(2R)BSC26 / CyO$, $Kr-Gal4$, $UAS-GFP$ $y^* w^*$; $cn^1 P\{PZ\}hts^{01103} / CyO$, $Kr-Gal4$, $UAS-GFP$; $P\{GMR-htsPD\}3B$ $y^* w^* / Y$, $hs-hid$; Pin^* / CyO $y^* w^* ey-Flp GMR-lacZ$; wg^{Sp-1} / CyO , y^* ; $MKRS / TM6B$, y^*

Figure 3.9

- A: $y^* w^* ey-Flp, Rh6-mCD8-GFP ; FRT42D P\{w^+\}47A I(2)cl-R11^1 / FRT42D hts^{null} ; + / P\{GMR-Add1\}3A$
 B: $y^* w^* ey-Flp, Rh6-mCD8-GFP ; FRT42D P\{w^+\}47A I(2)cl-R11^1 / FRT42D hts^{null} ; + / P\{GMR-Add1\}3B$
 C: $y^* w^* ey-Flp, Rh6-mCD8-GFP ; FRT42D P\{w^+\}47A I(2)cl-R11^1 / FRT42D hts^{null} ; + / P\{GMR-htsPD\}3A$
 D: $y^* w^* ey-Flp, Rh6-mCD8-GFP ; FRT42D P\{w^+\}47A I(2)cl-R11^1 / FRT42D hts^{null} ; + / P\{GMR-htsPD\}3B$
 E: $y^* w^* ey-Flp, Rh6-mCD8-GFP ; FRT42D P\{w^+\}47A I(2)cl-R11^1 / FRT42D hts^{null}$

The following fly stocks were used to obtain these genotypes:

- $y^* w^* ; P\{GMR-Add1\}3A$
 $y^* w^* ; P\{GMR-Add1\}3B$
 $y^* w^* ; P\{GMR-htsPD\}3A$
 $y^* w^* ; P\{GMR-htsPD\}3B$
 $y^* w^* ey-Flp, Rh6-mCD8-GFP ; FRT42D hts^{null} / CyO, y^+$
 $y^* w^* ey-Flp, Rh6-mCD8-GFP ; FRT42D P\{w^+\}47A I(2)cl-R11^1 / CyO, y^+$

Figure 3.10

- A: w^{118}
 B: $y^* w^* ; P\{GMR-Add1\}3A$
 C: $y^* w^* ; P\{GMR-ShAdd\}3A$
 D: $y^* w^* ; P\{GMR-ShAdd\}3B$

Figure 3.11

- A: $y^* w^*, Rh6-mCD8-GFP / y^* w^* ey-Flp, Rh6-mCD8-GFP ; GMR-Gal4 / + ; + / P\{UAS-hts^{472}-His\}3A$
 B: $y^* w^*, Rh6-mCD8-GFP / y^* w^* ey-Flp, Rh6-mCD8-GFP ; GMR-Gal4 / + ; + / P\{UAS-hts^{472}-His\}3B$
 C: $y^* w^* ey-Flp, Rh6-mCD8-GFP ; GMR-Gal4 / P\{UAS-ShAdd-His\}2A$
 D: $y^* w^* ey-Flp, Rh6-mCD8-GFP ; GMR-Gal4 / P\{UAS-ShAdd-His\}2B$
 E: $y^* w^*, Rh6-mCD8-GFP / y^* w^* ey-Flp, Rh6-mCD8-GFP ; GMR-Gal4 / + ; TM6B, y^+ / +$
 F: $y^* w^* ey-Flp, Rh6-mCD8-GFP ; GMR-Gal4 / P\{UAS-Add1-Myc\}2A$
 G: $y^* w^*, Rh6-mCD8-GFP / y^* w^* ey-Flp, Rh6-mCD8-GFP ; GMR-Gal4 / + ; + / P\{UAS-Add1-Myc\}3A$
 H: $y^* w^*, Rh6-mCD8-GFP / y^* w^* ey-Flp, Rh6-mCD8-GFP ; GMR-Gal4, P\{UAS-gogo\}T1 / + ; TM6B, y^+ / +$
 I: $y^* w^* ey-Flp, Rh6-mCD8-GFP ; GMR-Gal4, P\{UAS-gogo\}T1 / P\{UAS-Add1-Myc\}2A$
 J: $y^* w^*, Rh6-mCD8-GFP / y^* w^* ey-Flp, Rh6-mCD8-GFP ; GMR-Gal4, P\{UAS-gogo\}T1 / + ; + / P\{UAS-Add1-Myc\}3A$
 K: $y^* w^*, Rh6-mCD8-GFP / y^* w^* ey-Flp, Rh6-mCD8-GFP ; GMR-Gal4, P\{UAS-gogo\}T1 / + ; + / P\{UAS-hts^{472}-His\}3A$
 L: $y^* w^*, Rh6-mCD8-GFP / y^* w^* ey-Flp, Rh6-mCD8-GFP ; GMR-Gal4, P\{UAS-gogo\}T1 / + ; + / P\{UAS-hts^{472}-His\}3B$
 M: $y^* w^* ey-Flp, Rh6-mCD8-GFP ; GMR-Gal4, P\{UAS-gogo\}T1 / P\{UAS-ShAdd-His\}2A$
 N: $y^* w^* ey-Flp, Rh6-mCD8-GFP ; GMR-Gal4, P\{UAS-gogo\}T1 / P\{UAS-ShAdd-His\}2B$

The following fly stocks were used to obtain these genotypes:

$y^* w^* ; P\{UAS-hts^{472}-His\}3A$
 $y^* w^* ; P\{UAS-hts^{472}-His\}3B$
 $y^* w^* ; P\{UAS-ShAdd-His\}2A$
 $y^* w^* ; P\{UAS-ShAdd-His\}2B / CyO$
 $y^* w^* ; P\{UAS-Add1-Myc\}2A / CyO$
 $y^* w^* ; P\{UAS-Add1-Myc\}3A$
 $y^* w^* , Rh6-mCD8-GFP ; gogo^{D869} FRT80B / TM6B, y^+$
 $y^* w^* ey-Flp, Rh6-mCD8-GFP ; GMR-Gal4 / CyO$
 $y^* w^* ey-Flp, Rh6-mCD8-GFP ; GMR-Gal4, P\{UAS-gogo\}T1 / CyO$

Figure 3.12.1

A: $y^* w^* ey-Flp, Rh6-mCD8-GFP ; GMR-Gal4 / P\{UAS-gogo\}T1$
 B: $y^* w^* ey-Flp, Rh6-mCD8-GFP ; GMR-Gal4 / + ; + / P\{UAS-gogo\}T3$
 C: $y^* w^* ey-Flp, Rh6-mCD8-GFP ; GMR-Gal4 / P\{UAS-gogo-Myc\}2B$
 D: $y^* w^* ey-Flp, Rh6-mCD8-GFP ; GMR-Gal4 / + ; + / P\{UAS-gogo-Myc\}3B$
 E: $y^* w^* ey-Flp, Rh6-mCD8-GFP ; GMR-Gal4 / + ; + / TM3, Sb^1$

The following fly stocks were used to obtain these genotypes:

$P\{UAS-gogo\}T1 / CyO$
 $P\{UAS-gogo\}T3 / TM6B, y^+$
 $y^* w^* ; P\{UAS-gogo-Myc\}2B / CyO$
 $y^* w^* ; P\{UAS-gogo-Myc\}3B$
 $y^* w^* ey-Flp, Rh6-mCD8-GFP ; FRT80B / TM3, Sb^1$
 $y^* w^* ey-Flp, Rh6-mCD8-GFP ; GMR-Gal4 / CyO$

Figure 3.12.2

A: $y^* w^* ey-Flp, Rh6-mCD8-GFP / y^* w^* ; GMR-Gal4 / P\{UAS-Add1-Myc\}2A$
 B: $y^* w^* ey-Flp, Rh6-mCD8-GFP / y^* w^* ; GMR-Gal4 / + ; + / P\{UAS-Add1-Myc\}3A$

The following fly stocks were used to obtain these genotypes:

$y^* w^* ; P\{UAS-Add1-Myc\}2A / CyO$
 $y^* w^* ; P\{UAS-Add1-Myc\}3A$
 $y^* w^* ey-Flp, Rh6-mCD8-GFP ; GMR-Gal4 / CyO$

Figure 3.13

A: $y^* w^* ey-Flp, Rh6-mCD8-GFP ; GMR-Gal4, P\{UAS-gogo\}T1 / + ; + / TM3, Sb^1$

B: $y^* w^* ey-Flp, Rh6-mCD8-GFP ; GMR-Gal4, P\{UAS-gogo\}T1 / + ; + / P\{GMR-Add1\}3A$

C: $y^* w^* ey-Flp, Rh6-mCD8-GFP ; GMR-Gal4, P\{UAS-gogo\}T1 / + ; + / P\{GMR-Add1\}3B$

D: $y^* w^* ey-Flp, Rh6-mCD8-GFP ; FRT42D hts^{null} / GMR-Gal4, P\{UAS-gogo\}T1$

E: $y^* w^* ey-Flp, Rh6-mCD8-GFP ; FRT42D hts^{null} / CyO, y^+$

The following fly stocks were used to obtain these genotypes:

$y^* w^* ; P\{GMR-Add1\}3A$

$y^* w^* ; P\{GMR-Add1\}3B$

$y^* w^* ey-Flp, Rh6-mCD8-GFP ; FRT42D hts^{null} / CyO, y^+$

$y^* w^* ey-Flp, Rh6-mCD8-GFP ; GMR-Gal4, P\{UAS-gogo\}T1 / CyO$

$y^* w^* ey-Flp, Rh6-mCD8-GFP ; gogo^{D869} FRT80B / TM3, Sb^1$

Figure 3.14.1

A: $y^* w^* ey-Flp, Rh6-mCD8-GFP / y^* w^* ; GMR-Gal4 / + ; + / P\{GMR-Add1\}3A$

B: $y^* w^* ey-Flp, Rh6-mCD8-GFP / y^* w^* ; GMR-Gal4, P\{UAS-gogo\}T1 / + ; + / P\{GMR-Add1\}3A$

D: $y^* w^* ey-Flp, Rh6-mCD8-GFP / y^* w^* ; GMR-Gal4 / + ; + / P\{GMR-Add1\}3B$

E: $y^* w^* ey-Flp, Rh6-mCD8-GFP / y^* w^* ; GMR-Gal4, P\{UAS-gogo\}T1 / + ; + / P\{GMR-Add1\}3B$

The following fly stocks were used to obtain these genotypes:

$y^* w^* ; P\{GMR-Add1\}3A$

$y^* w^* ; P\{GMR-Add1\}3B$

$y^* w^* ey-Flp, Rh6-mCD8-GFP ; GMR-Gal4 / CyO$

$y^* w^* ey-Flp, Rh6-mCD8-GFP ; GMR-Gal4, P\{UAS-gogo\}T1 / CyO$

Figure 3.14.2

A: $y^* w^* ; + / GMR-Gal4, P\{UAS-gogo\}T1 ; P\{GMR-Add1\}3B / +$

& $y^* w^* ; P\{UAS-gogo\}T1 / GMR-Gal4 ; + / P\{GMR-Add1\}3B$

B: $y^* w^* ; + / GMR-Gal4 ; P\{UAS-gogo\}T3 / P\{GMR-Add1\}3B$

C: $y^* w^* ; P\{UAS-gogo-Myc\}2B / GMR-Gal4 ; + / P\{GMR-Add1\}3B$

D: $y^* w^* ; + / GMR-Gal4 ; P\{UAS-gogo-Myc\}3B / P\{GMR-Add1\}3B$

E: $y^* w^* ; CyO / GMR-Gal4 ; + / P\{GMR-Add1\}3B$

The following fly stocks were used to obtain these genotypes:

$y^* w^* ; P\{GMR-Add1\}3B$

$y^* w^* ; GMR-Gal4, P\{UAS-gogo\}T1 / CyO$

$P\{UAS-gogo\}T1 / CyO$

$P\{UAS-gogo\}T3 / TM6B, y^+$

y w* ; P{UAS-gogo-Myc}2B / CyO*

y w* ; P{UAS-gogo-Myc}3B*

y w* ey-Flp GMR-lacZ ; GMR-Gal4 ; ato-tau-Myc FRT80B / TM6B, y**

Figure 3.14.3

A: *y* w* ey-Flp / Y ; gogo^{H1675} FRT80B / GMR-mCD8-KO, tubP-Gal80 FRT80B*

B: *y* w* ey-Flp / y* w* ; + / P{GMR-Add1}2A ; gogo^{H1675} FRT80B / GMR-mCD8-KO, tubP-Gal80 FRT80B*

The following fly stocks were used to obtain these genotypes:

y w* ey-Flp ; gogo^{H1675} FRT80B / TM6B, y**

y w* ; P{GMR-Add1}2A*

*elav-Gal4, UAS-mCD8-GFP, hs-Flp ; GMR-mCD8-KO, tubP-Gal80 FRT80B / TM6B, y**

y w* ; ey1x-Flp.Exel / CyO ; GMR-mCD8-KO, tubP-Gal80 FRT80B / TM6B, y**

2.5 Genetic tools

This section briefly explains the most important genetic tools and lists the genetic elements that were used in this work.

Balancer chromosomes

Keeping a recessive lethal or recessive sterile mutation in a genetically stable stock requires the suppression of recombination. This is achieved by the use of balancer chromosomes. A balancer chromosome is the product of multiple chromosomal inversions and translocations, which prevent recombination with a homologue chromosome whose structure has not been changed.

Usually, a balancer chromosome carries an easily visible marker mutation to facilitate the distinction of progeny that inherited the balancer chromosome from progeny that inherited the homologue chromosome carrying the mutation of interest.

Moreover, balancer chromosomes themselves are recessive lethal or strongly reducing reproductive fitness to prevent the stock from losing the chromosome with the mutation of interest and becoming homozygous for the balancer chromosome.

GFP balancer chromosomes additionally cause a broad expression of GFP during embryonic and larval stages. This allows for the easy distinction of embryos and larvae that have inherited the GFP balancer chromosome from their siblings that have not.

The virginator

For genetic experiments, it is essential that crosses are performed with virgin females that have not been fertilized yet. Usually, virgin females are obtained by manually collecting freshly hatched

females of the desired genotype. However, if many virgins of a particular genotype are needed, the virginator is the method of choice.

The virginator is a Y chromosome that carries a lethal gene under the control of a heat inducible promoter. To obtain virgin flies, the developing flies are heat-shocked by exposing them to 37 °C for 2 h during their larval stages. This kills all male larvae and only females will survive and hatch. The resulting population will consist entirely of female flies, which will not be fertilized and stay virgins due to the lack of males.

The Gal4/UAS system

The Gal4/UAS system was developed in 1993 by Andrea Brand and Norbert Perrimon (Brand and Perrimon 1993). It allows the ectopic expression of any transgene in a wide variety of cell type and tissue specific patterns.

The expression pattern of the transgene is determined by the Gal4 driver used. Gal4 drivers can be generated by inserting the gene encoding the yeast transcription factor Gal4 into the fly genome. Depending on the site of insertion, the expression of Gal4 may then be driven by a particular genomic enhancer, which defines the Gal4 expression pattern. Alternatively, a construct consisting of any fly promoter and the Gal4 encoding gene can be generated in vitro and inserted into the fly genome to drive Gal4 expression from that particular promoter.

The UAS promoter is then, in turn, activated by the transcription factor Gal4. Therefore, any coding sequence that is put under control of the UAS promoter in vitro and inserted into the fly genome will be expressed in those cells that express the Gal4 transcription factor.

The Gal4/UAS system also works in cultured fly cells. When expressing proteins in cell culture, it is often desired to obtain high expression levels in all cells, which is accomplished by the use of a Gal4 driver that is based on a strong promoter with a broad expression pattern, such as an Actin promoter. Conveniently, when the Gal4/UAS system is applied in cell culture, neither the Gal4 driver nor the UAS target(s) have to be inserted into the genome. Instead, both can be supplied from plasmids with which the cells are transfected.

The Flp/FRT system

The Flp/FRT system is also derived from yeast and allows for the generation of mosaic animals that are overall heterozygous but contain tissue homozygous mutant for a lethal mutation. It is based on the protein Flpase that induces recombination between *FRT* sites (Golic and Lindquist 1989). For the generation of mosaic animals, an *FRT* site has been introduced close to the centromere on each chromosome arm (Xu and Rubin 1993). If both homologue chromosome arms, the one that carries the mutation of interest and the one that carries the wild type allele, contain an *FRT* site (Figure 2.5A), a cell contains four *FRT* sites after DNA replication, one on each

chromatid (Figure 2.5B). If Flipase is expressed in this cell, it may mediate the recombination between the *FRT* sites on non-sister chromatids, which leads to an exchange of the chromosome arms (Figure 2.5C) and to two daughter cells of different genotypes. One is homozygous mutant and one is homozygous for the wild type allele (Figure 2.5D). As continued expression of Flipase in the daughter cells can, of course, not restore the heterozygous state, each daughter cell is the founder of a homozygous clone that arises from further cell divisions.

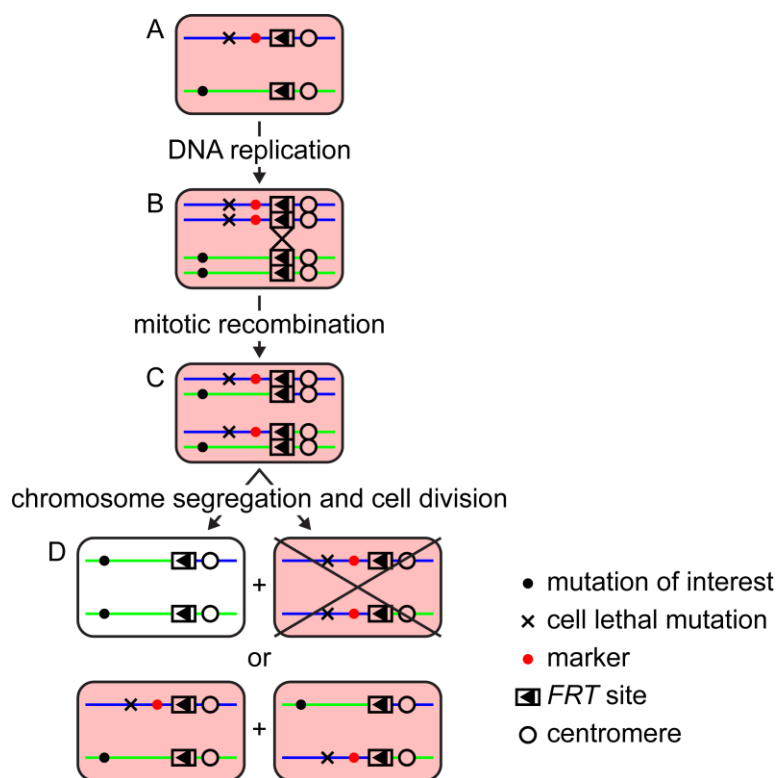


Figure 2.5: The Flp/FRT system

(A) This heterozygous cell contains the mutation of interest on a chromosome arm that features an *FRT* site near the centromere. The homologous chromosome arm possesses an *FRT* site, a marker, and a cell lethal mutation. (B) After DNA replication, the cell contains four *FRT* sites. (C) Expression of Flipase may cause the recombination between two *FRT* sites on non-sister chromatids, which causes the exchange of these two chromatids. (D) After cell division, two daughter cells with different genotypes can occur. One is homozygous for the mutation of interest and lost the marker. It will found an unmarked homozygous mutant clone. Its sister cell is homozygous wild type with regard to the mutation of interest. As it is also homozygous for the cell lethal mutation, it will perish. Alternatively, two marked heterozygous cells can be generated, which can be subject to Flipase mediated mitotic recombination during the next round of cell division.

The spatial and temporal occurrence of mosaic tissue is determined by the activity of the Flipase and thereby by the promoter that controls the expression of Flipase. For the generation of mosaic eyes including the photoreceptors, eye-specific enhancer fragments from the promoter of the gene

ey, the *Drosophila* homologue of *Pax6*, are well suited and were used in this work (Hazelett et al. 1998; Hauck et al. 1999; Newsome et al. 2000a)

To extinguish the clones homozygous for the wild type allele and to enlarge the clones that are homozygous for the mutation of interest, a recessive cell lethal mutation or a lethal transgene can be introduced on the chromosome arm with the wild type allele. Additionally, marking the “wild type” chromosome arm with a w^+ transgene allows for the easy tracing of recombination efficiency in a w background (Figure 2.5D). Usually, more than 90 % of the eye is homozygous for the mutation of interest when a cell lethal mutation is used on the chromosome arm with the wild type allele (Newsome et al. 2000a).

If the wild type chromosome arm carries a gene encoding a fluorescent protein, the homozygous mutant clone can also be identified by the absence of fluorescence. Likewise, a fluorescence marker on the mutant chromosome arm allows for the identification of homozygous wild type clones by the absence of fluorescence.

List of genetic elements that were used

Genetic elements that were used in this work are listed in the following table.

genetic element	FlyBase designation	Flybase ID	use
<i>FM3</i>	<i>FM3</i>	FBba0000002	X chromosome balancer marked by B^l
<i>FM7a</i>	<i>FM7a</i>	FBba0000007	X chromosome balancer marked by B^l
<i>FM7c</i>	<i>FM7c</i>	FBba0000009	X chromosome balancer marked by B^l
<i>CyO</i>	<i>CyO</i>	FBba0000025	2 nd chromosome balancer marked by Cy^l
<i>CyO, y^+</i>	<i>CyO-y^+</i>	FBba0000035	2 nd chromosome balancer marked by Cy^l and y^+
<i>CyO, Kr-Gal4, UAS-GFP</i>	<i>CyO-19</i>	FBba0000315	2 nd chromosome GFP balancer marked by Cy^l
<i>MKRS</i>	<i>MKRS</i>	FBba0000066	3 rd chromosome balancer marked by Sb^l
<i>TM3, Sb^l</i>	<i>TM3-Sb</i>	FBba0000187	3 rd chromosome balancer marked by Sb^l
<i>TM3, Sb^l Ser^l, y^+</i>	<i>TM3-vSc</i>	FBba0000149	3 rd chromosome balancer marked by Sb^l , Ser^l , and y^+

genetic element	FlyBase designation	Flybase ID	use
<i>TM6B, y⁺</i>	<i>TM6B-y⁺</i>	FBba0000339	3 rd chromosome balancer marked by <i>Antp^{Hu}</i> and <i>y⁺</i>
<i>B¹</i>	<i>B¹</i>	FBal0000817	dominant X chromosome marker mutation affects eye shape
<i>Pin*</i>	<i>Pin*</i>	FBgn0003088	dominant 2 nd chromosome marker mutation affects shape of thoracic bristles
<i>wg^{Sp-1}</i>	<i>wg^{Sp-1}</i>	FBal0015984	dominant 2 nd chromosome marker mutation affects number of sternopleural bristles
<i>Cy¹</i>	<i>Cy¹</i>	FBal0002196	dominant 2 nd chromosome marker mutation affects wing shape
<i>sens^{Ly-1}</i>	<i>sens^{Ly-1}</i>	FBal0011759	dominant 3 rd chromosome marker mutation affects wing shape
<i>Sb¹</i>	<i>Sb¹</i>	FBal0015145	dominant 3 rd chromosome marker mutation affects shape of thoracic bristles
<i>Ser¹</i>	<i>Ser¹</i>	FBal0015427	dominant 3 rd chromosome marker mutation affects wing shape
<i>Antp^{Hu}</i>	<i>Antp^{Hu}</i>	FBal0000583	dominant 3 rd chromosome marker mutation affects number of humeral bristles
<i>w*</i>	<i>w*</i>	FBgn0003996	recessive X chromosome marker mutation
<i>w¹¹¹⁸</i>	<i>w¹¹¹⁸</i>	FBal0018186	affects eye color, complemented by <i>w⁺</i>
<i>y*</i>	<i>y*</i>	FBgn0004034	recessive X chromosome marker mutation affects body color, complemented by <i>y⁺</i>
<i>Y, hs-hid</i>	<i>P{hs-hid}Y</i>	FBti0017539	virginator
<i>ey-Gal4</i>	<i>P{GAL4-ey.H}SS5</i>	FBti0012711	<i>ey</i> Gal 4 driver
<i>GMR-Gal4</i>	<i>P{GAL4-ninaE.GMR}12</i>	FBti0002994	<i>GMR</i> Gal4 driver
<i>P{UAS-gogo}T1</i>	<i>gogo^{Scer^{UAS.T1}}</i>	FBal0248994	full-length Gogo from <i>UAS</i> promoter inserted on 2 nd chromosome
<i>P{UAS-gogo}T3</i>	-	-	full-length Gogo from <i>UAS</i> promoter inserted on 3 rd chromosome
<i>UAS-Flp</i>	<i>P{UAS-FLP1.D}JD2</i>	FBti0012285	Flipase from <i>UAS</i> promoter

genetic element	FlyBase designation	Flybase ID	use
<i>ey-Flp</i>	<i>P{ey-FLP.N}2</i>	FBti0015982	Flipase from <i>ey</i> promoter
<i>FRT19A</i>	<i>P{neoFRT}19A</i>	FBti0000870	<i>FRT</i> site for mitotic recombination X chromosome
<i>FRT42D</i>	<i>P{neoFRT}42D</i>	FBti0002072	<i>FRT</i> site for mitotic recombination right arm of 2 nd chromosome
<i>FRT80B</i>	<i>P{neoFRT}80B</i>	FBti0002073	<i>FRT</i> site for mitotic recombination left arm of 3 rd chromosome
<i>GMR-hid</i>	<i>P{GMR-hid}SS1</i>	FBti0012707	kills photoreceptor cells inserted on X chromosome
<i>l(2)cl-R11¹</i>	<i>l(2)cl-R11¹</i>	FBal0104506	recessive lethal mutation on right arm of 2 nd chromosome
<i>RpS17⁴</i>	<i>RpS17⁴</i>	FBal0011935	recessive lethal mutation on left arm of 3 rd chromosome
<i>P{w⁺}47A</i>	<i>P{white-un1}47A</i>	FBti0001286	<i>w⁺</i> marker on right arm of 2 nd chromosome
<i>P{w⁺}70C</i>	<i>P{white-un1}70C</i>	FBti0001287	<i>w⁺</i> marker on left arm of 3 rd chromosome
<i>GMR-lacZ</i>	<i>P{GMR-lacZ.C(38.1)}TPN1</i>	FBti0015985	β -galactosidase marker marks all photoreceptor axons
<i>GMR-mCD8-KO</i>	<i>P{GMR-mCD8mKOrange}</i>	FBtp0052779	KO marker marks all photoreceptor axons
<i>Rh6-mCD8-GFP</i>	<i>P{Rh6-mCD8-GFP}</i>	FBtp0052780	GFP marker marks R8 axons
<i>swa¹</i>	<i>swa¹</i>	FBal0016664	<i>swallow</i> mutation
<i>swa³</i>	<i>swa³</i>	FBal0016666	<i>swallow</i> mutation
<i>β-Spec^{G113}</i>	<i>β-Spec^{G113}</i>	FBal0213000	<i>β-Spectrin</i> mutation
<i>gogo^{D869}</i>	<i>gogo^{D869}</i>	FBal0242619	<i>gogo</i> mutation
<i>gogo^{D1600}</i>	<i>gogo^{D1600}</i>	FBal0242620	<i>gogo</i> mutation

genetic element	FlyBase designation	Flybase ID	use
<i>gogo</i> ^{H1675}	<i>gogo</i> ^{H1675}	FBal0242620	<i>gogo</i> mutation
<i>hts</i> ^{null}	<i>hts</i> ^{null}	FBal0248988	<i>hts</i> mutation
<i>hts</i> ^{ΔG}	<i>hts</i> ^{ΔG}	FBal0212993	<i>hts</i> mutation
<i>hts</i> ^{W532X}	<i>hts</i> ^{W532X}	FBal0212992	<i>hts</i> mutation
<i>P{PZ}hts</i> ⁰¹¹⁰³	<i>P{PZ}hts</i> ⁰¹¹⁰³	FBti0005179	<i>hts</i> mutation caused by P- element insertion
<i>Df(2R)BSC26</i>	<i>Df(2R)BSC26</i>	FBab0029945	deficiency covering <i>hts</i> locus

Table 2.5: List of genetic elements that were used

The genetic elements used in this work are listed in the first column. The second column gives the corresponding FlyBase designations and the third column the corresponding FlyBase IDs. The fourth column gives a short description of the purpose of each genetic element.

2.6 Molecular biology

This section describes all the plasmids that have been used in this work and their construction. Most of the plasmids were generated using the Gateway cloning system from Invitrogen (Carlsbad, California).

The Gateway cloning system

The Gateway cloning system is based on the site-specific recombination system of the *E. coli* bacteriophage λ (reviewed by Landy 1989). The circular λ phage contains a DNA sequence called *attP* that recombines with the *attB* site in the bacterial chromosome to mediate the integration of the λ phage into the host chromosome. The DNA sequences that are formed by the recombination of *attP* and *attB* are called *attL* and *attR*, which, in turn, are able to recombine with each other to mediate the excision of bacteriophage λ from the host chromosome. Integration and excision are driven by two different yet overlapping sets of proteins. The *attB* site has been modified to generate the distinct recombination sites *attB1* and *attB2*. Likewise, *attP1* and *attP2* are modified *attP* sites (Hartley et al. 2000). *attB1* specifically recombines with *attP1* and *attB2* specifically with *attP2*. To subclone a piece of DNA by the Gateway cloning system, it can be amplified by PCR using a 5' primer that adds the 25 bp *attB1* site and a 3' primer that adds the 25 bp *attB2* site. The

PCR product is then mixed with a so-called donor vector and the commercially available BP clonase, an enzyme mix that mediates the recombination between *attB* and *attP* (Figure 2.6). Instead of an MCS, the donor vector contains the Gateway cassette, which consists of an *attP1* and an *attP2* site flanking the *ccdB* gene. *ccdB* inhibits the growth of most bacterial strains (Bernard and Couturier 1992). Therefore, after transformation, only bacteria that contain the recombinant plasmid with the DNA of interest flanked by *attL1* and *attL2*, referred to as entry clone, will form colonies, but not those that contain the original donor vector with the *ccdB* gene.

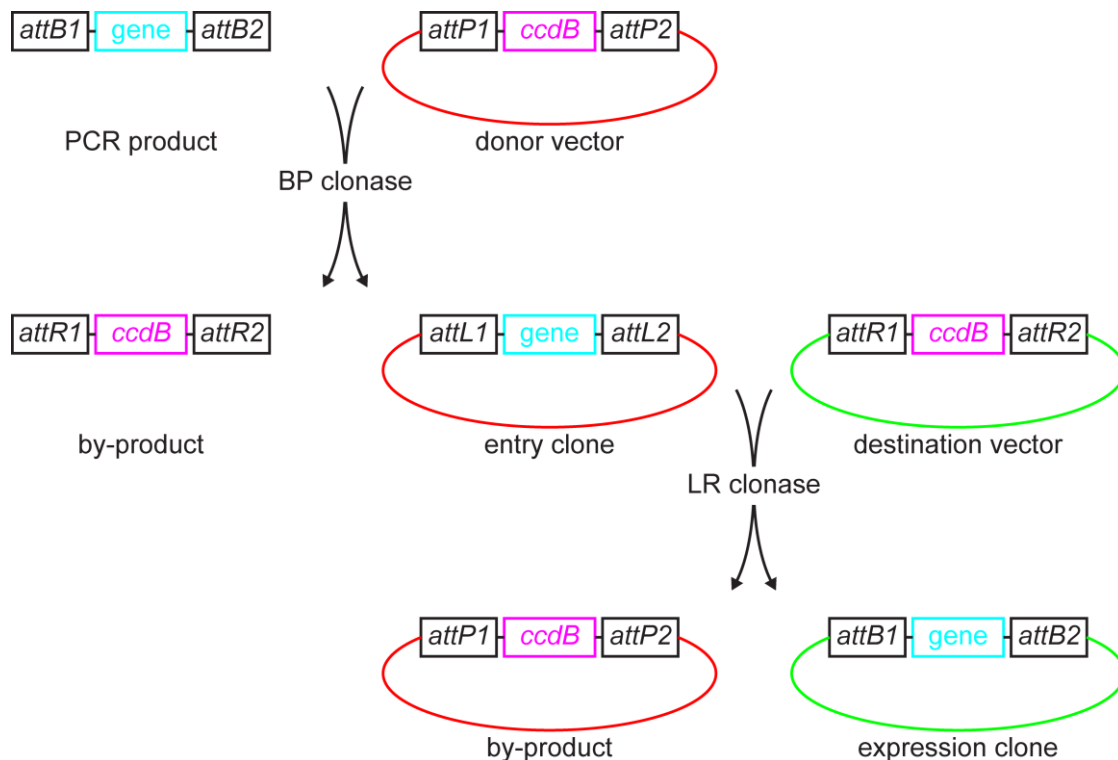


Figure 2.6: The Gateway system

The *attB* sites can be added to the gene of interest (cyan) by PCR. BP recombination between the PCR product and a donor vector containing *attP* sites that flank the *ccdB* gene (magenta) is mediated by BP clonase. It generates an entry clone containing the gene of interest flanked by *attL* sites and, as a by-product, the *ccdB* gene flanked by *attR* sites. LR recombination between the entry clone and a destination vector with the *ccdB* gene flanked by *attR* sites is mediated by LR clonase and generates the expression clone, which contains the gene of interest flanked by *attB* sites. As a by-product, a plasmid consisting of the donor vector's / entry clone's backbone, *attP* sites and the *ccdB* gene is generated.

From the entry clone, the DNA of interest can be shuttled into any destination vector by simply mixing entry clone, destination vector and LR clonase enzyme mix, yielding the so-called expression clone (Figure 2.6). A destination vector can be obtained from a conventional plasmid vector by inserting a Gateway cassette consisting of the *ccdB* gene flanked by *attR* sites into its MCS. The destination vector / expression clone should confer a different antibiotic resistance than

the donor vector / entry clone to allow for the specific selection of bacteria with the expression clone but not those with the entry clone after LR recombination. The Gateway cassette to generate a destination vector is available in different reading frames. This allows adjusting the reading frame of the subcloned DNA to the reading frame of the vector when fusion proteins should be produced.

Expression clones

All expression clones that were used in this work are listed below.

expression clone	destination vector	entry clone
<i>pGMR-gogo-Myc</i>	<i>pGMR-W-Myc</i>	<i>pDONR221-gogo+</i>
<i>pGMR-gogo^{ΔC}-Myc</i>	<i>pGMR-W-Myc</i>	<i>pDONR221-gogo^{ΔC}+</i>
<i>pGMR-gogo^{cyto}-Myc</i>	<i>pGMR-myr-W-Myc</i>	<i>pDONR221-gogo^{cyto}+</i>
<i>pGMR-Add1</i>	<i>pGMR-W-His</i>	<i>pDONR221-Add1.stop</i>
<i>pGMR-ShAdd</i>	<i>pGMR-W-His</i>	<i>pDONR221-ShAdd.stop</i>
<i>pGMR-htsPD</i>	<i>pGMR-W-His</i>	<i>pDONR221-htsPD.stop</i>
<i>pUAST-gogo-Myc</i>	<i>pUAST-W-Myc</i>	<i>pDONR221-gogo+</i>
<i>pUAST-gogo^{FFD}-Myc</i>	<i>pUAST-W-Myc</i>	<i>pDONR221-gogo^{FFD}+</i>
<i>pUAST-gogo^{DDD}-Myc</i>	<i>pUAST-W-Myc</i>	<i>pDONR221-gogo^{DDD}+</i>
<i>pUAST-Add1-Myc</i>	<i>pUAST-W-Myc</i>	<i>pDONR221-Add1+</i>
<i>pUAST-htsPD-Myc</i>	<i>pUAST-W-Myc</i>	<i>pDONR221-htsPD+</i>
<i>pUAST-Add1-His</i>	<i>pUAST-W-His</i>	<i>pDONR221-Add1+</i>
<i>pUAST-ShAdd-His</i>	<i>pUAST-W-His</i>	<i>pDONR221-ShAdd+</i>
<i>pUAST-htsPD-His</i>	<i>pUAST-W-His</i>	<i>pDONR221-htsPD+</i>
<i>pUAST-hts⁴⁷²-His</i>	<i>pUAST-W-His</i>	<i>pDONR221-hts⁴⁷²+</i>
<i>pUAST-hts⁶⁵⁸-His</i>	<i>pUAST-W-His</i>	<i>pDONR221-hts⁶⁵⁸+</i>
<i>pUAST-hts^{AAA}-His</i>	<i>pUAST-W-His</i>	<i>pDONR221-hts^{AAA}+</i>
<i>pUAST-hts^{DEDE}-His</i>	<i>pUAST-W-His</i>	<i>pDONR221-hts^{DEDE}+</i>
<i>pUAST-GFP-His</i>	<i>pUAST-W-His</i>	<i>pDONR221-GFP+</i>
<i>pUAST-Wnk-Myc</i>	Klaudiusz Mann, Suzuki Lab	

Table 2.6.1: List of expression clones

The expression clones are listed in the first column. They were obtained from LR recombinations between the destination vectors quoted in the second and the entry clones in the third column or from the quoted source.

Destination vectors

All destination vectors that were used in this work are listed below.

destination vector	vector backbone	insert
<i>pGMR-W-Myc</i>	<i>pCaSpeR-GMR-gogo</i> (KpnI + XbaI)	<i>pBSIIKS(+)-W-Myc</i> (KpnI + XbaI)
<i>pGMR-myr-W-Myc</i>	<i>pCaSpeR-GMR-gogo</i> (KpnI + XbaI)	<i>pBSIIKS(+)-myr-W-Myc</i> (KpnI + XbaI)
<i>pGMR-W-His</i>	<i>pCaSpeR-GMR-gogo</i> (KpnI + XbaI)	<i>pBSIIKS(+)-W-His</i> (KpnI + XbaI)
<i>pUAST-W-Myc</i>	<i>pCaSpeR-UAS-gogo</i> (KpnI + XbaI)	<i>pBSIIKS(+)-W-Myc</i> (KpnI + XbaI)
<i>pUAST-W-His</i>	<i>pCaSpeR-UAS-gogo</i> (KpnI + XbaI)	<i>pBSIIKS(+)-W-His</i> (KpnI + XbaI)

Table 2.6.2: List of destination vectors

The destination vectors are listed in the first column. Their vector backbones were obtained from digesting the plasmids listed in the second column with the restriction enzymes indicated. They were ligated to the inserts derived from restriction digests of the plasmids listed in the third column with the indicated restriction enzymes.

Entry clones

All entry clones that were used in this work are listed below.

entry clone	template	primers
<i>pDONR221-gogo+</i>	<i>pCaSpeR-UAS-gogo</i>	SO001 + SO016
<i>pDONR221-gogo^{ΔC}+</i>	<i>pCaSpeR-UAS-gogo</i>	SO001 + SO015a
<i>pDONR221-gogo^{cyto}+</i>	<i>pCaSpeR-UAS-gogo</i>	SO008 + SO016
<i>pDONR221-Add1.stop</i>	<i>pDONR221-Add1+</i>	SO151 + SO202
<i>pDONR221-ShAdd.stop</i>	<i>pDONR221-ShAdd+</i>	SO151 + SO203
<i>pDONR221-htsPD.stop</i>	<i>pDONR221-htsPD+</i>	SO151 + SO204
<i>pDONR221-Add1+</i>	<i>Add1</i> cDNA	SO 151 + SO153
<i>pDONR221-ShAdd+</i>	<i>ShAdd</i> cDNA	SO 151 + SO154
<i>pDONR221-htsPD+</i>	<i>htsPD</i> cDNA	SO 151 + SO155
<i>pDONR221-hts⁴⁷²+</i>	<i>pDONR221-ShAdd+</i>	SO151 + SO205
<i>pDONR221-hts⁶⁵⁸+</i>	<i>pDONR221-htsPD+</i>	SO151 + SO207
<i>pDONR221-hts^{AAAA}+</i>	<i>pDONR221-hts⁶⁵⁸+</i>	SO151 + AAAA megaprimer
<i>pDONR221-hts^{DEDE}+</i>	<i>pDONR221-hts⁶⁵⁸+</i>	SO151 + DEDE megaprimer
<i>pDONR221-GFP+</i>	<i>pUAST-DEST12</i>	SO252 + SO253
<i>pDONR221-gogo^{FFD}+</i>	Si-Hong Luu, Suzuki Lab (pSL6)	
<i>pDONR221-gogo^{DDD}+</i>	Si-Hong Luu, Suzuki Lab (pSL7)	

Table 2.6.3: List of entry clones

The entry clones listed in the first column were obtained from BP recombinations between the *pDONR221* vector and the products of PCRs using the templates in the second and the primers in the third column or from the quoted source.

Add1 cDNA, *ShAdd* cDNA and *htsPD* cDNA were amplified by PCR from the embryonic GH cDNA library, a gift from Gaja Tavosanis (Max-Planck Institute of Neurobiology), using the primers SO173 and SO175, SO176 or SO177. The AAAA megaprimer was generated by a PCR using *pDONR221-hts⁶⁵⁸* + as template and the primers SO217a and SO207. The DEDE megaprimer was generated by a PCR using *pDONR221-hts⁶⁵⁸* + as template and the primers SO218b and SO207.

Other plasmids

All other plasmids that were used in this work are listed below.

plasmid	vector backbone	insert
<i>pBSIIKS(+)-W-Myc</i>	<i>pBSIIKS(+)-Myc</i> (EcoRV)	<i>pBSIIKS(+)-rfA</i> (EcoRV)
<i>pBSIIKS(+)-myr-W-Myc</i>	<i>pBSIIKS(+)-myr-Myc</i> (EcoRV)	<i>pBSIIKS(+)-rfA</i> (EcoRV)
<i>pBSIIKS(+)-W-His</i>	<i>pBSIIKS(+)-W-Myc</i> (BglII/XbaI)	<i>6xHis</i> (BglII + XbaI)
<i>pBSIIKS(+)-Myc</i>	<i>pBSIIKS(+)-[KSEBX]</i> (BglII/XbaII)	<i>pBS-AGAP(N-C)-Myc</i> (BglII + XbaI)
<i>pBSIIKS(+)-myr-Myc</i>	<i>pBSIIKS(+)-Myc</i> (KpnI/SphI)	<i>myr</i> (KpnI + SphI)
<i>pBSIIKS(+)-rfA</i>	<i>pBSIIKS(+)</i> (EcoRV)	<i>rfA</i>
<i>pBSIIKS(+)-[KSEBX]</i>	<i>pBSIIKS(+)</i> (KpnI/XbaI)	<i>[KSEBX]</i>
<i>pCaSpeR-GMR-gogo</i>	Takashi Suzuki (pTS65)	
<i>pCaSpeR-UAS-gogo</i>	Takashi Suzuki (pTS67)	
<i>pBS-AGAP(N-C)-Myc</i>	Takashi Suzuki (pTS15)	
<i>pBSIIKS(+)</i>	Stratagene (La Jolla, California)	
<i>pDONR221</i>	Invitrogen (Carlsbad, California)	
<i>pUAST-DEST12</i>	Frederik Wirtz-Peitz, Perrimon Lab, Harvard Medical School, Boston, Massachusetts	
<i>actin-Gal4</i>	Takashi Suzuki	
transposase helper plasmid	Takashi Suzuki	

Table 2.6.4: List of other plasmids

All other plasmids that have been used in this work are listed in the first column. For newly generated plasmids, the second column states the source of the vector backbones, which were obtained from digesting the listed plasmids with the indicated restriction enzymes. They were ligated to the inserts listed in the third column, which were obtained from digesting the listed plasmids with the stated restriction enzymes when indicated. For all other plasmids, the source has been quoted.

6xHis was generated by simply mixing oligonucleotides SO063 and SO064. The myristoylation signal *myr* was the product of a PCR using SO045 and SO046a as primers and genomic DNA from a *w¹¹¹⁸* fly as template. The Gateway cassette *rfA* is commercially available from Invitrogen (Carlsbad, California). The multiple cloning site *[KSEBX]* was obtained by mixing oligonucleotides SO055 and SO056.

Oligonucleotides

All oligonucleotides mentioned in this work were synthesized by Metabion (Martinsried, Germany).

name	sequence
SO001	GGGGACAAGTTTGTACAAAAAAGCAGGCTCAAA ATG CGG AAA AAC TCA AAG GAA
SO008	G GGG ACA AGT TTG TAC AAA AAA GCA GGC TGG GCC CAA TAT GTG GTG CGA TAT
SO015a	GGG GAC CAC TTT GTA CAA GAA AGC TGG GTG TTC GTC CTG TCG CCG AGC CAC
SO016	GGG GAC CAC TTT GTA CAA GAA AGC TGG GTG CAC GGC CAC TTC CTT TGA CTT
SO045	GGGGTACC CAAA ATG GGC AAC AAA TGC TGC AGC
SO046a	GG GCA TGC ACC GGT TGG TGT GGT GCG TGG
SO055	CGCATGCGATATCCAGATCTT
SO056	CTAGAAGATCTGGATATCGCATGCGGTAC
SO063	GG AGA TCT CAT CAC CAT CAC CAT CAC GTC TA GAC C
SO064	GGT CTA GAC GTG ATG GTG ATG GTG ATG AGA TCT CC
SO151	GGGGACAAGTTTGTACAAAAAAGCAGGCTTCAAA ATG ACT GAA GTT GAG CAA CCG
SO153	GGG GAC CAC TTT GTA CAA GAA AGC TGG GTG GGC CTC GGC CTT CTT CTT CTC
SO154	GGG GAC CAC TTT GTA CAA GAA AGC TGG GTG TTT TCC CTC AAT CTC CTT AAG
SO155	GGG GAC CAC TTT GTA CAA GAA AGC TGG GTG TTT TAT GAA CGC CGT ACA ACA
SO173	AAAGTATTATAACCACGCAACAAATTC
SO175	AAGATTGCTACTCCTACGGATCAC
SO176	TAAAGAGTTGAAGGATTCGGTGTC
SO177	GGATTGATGTGCTGTCGTATTG
SO202	GGGGACCACTTTGTACAAGAAAGCTGGGT CTA GGC CTC GGC CTT CTT CTT CTC
SO203	GGGGACCACTTTGTACAAGAAAGCTGGGT CTA TTT TCC CTC AAT CTC CTT AAG
SO204	GGGGACCACTTTGTACAAGAAAGCTGGGT CTA TTT TAT GAA CGC CGT ACA ACA
SO205	GGG GAC CAC TTT GTA CAA GAA AGC TGG GTG CTT TGT AAT CTT CTT GGG ATC
SO207	GGG GAC CAC TTT GTA CAA GAA AGC TGG GTG ATC GCT CAG CAC GAC TTC CGC
SO217a	ACA AAG TGG GTG GCT GAG GGT GCC CCC GCC CAC GCA GCG CCA GTG AGG ATA GAA GAT C
SO218b	ACA AAG TGG GTG GCT GAG GGT GAC CCC GAA CAC GAC GAG CCA GTG AGG ATA GAA GAT CC
SO252	GGGGACAAGTTTGTACAAAAAAGCAGGCTTCAAA ATG GTG AGC AAG GGC GAG GAG
SO253	GGG GAC CAC TTT GTA CAA GAA AGC TGG GTG CTT GTA CAG CTC GTC CAT GCC G

Table 2.6.5: List of oligonucleotides

The sequences of the oligonucleotides listed in the left column are specified in the right column from 5' (left) to 3' (right). Green indicates nucleotides complementary to the PCR template. Blue indicates *attB* recombination sites. Kozak sequences and stop codons are in magenta, recognition sequences for restriction enzymes in cyan. Red indicates nucleotides that are not complementary to the PCR template in order to introduce mutations into the PCR product.

2.7 Identification of Hts as a Gogo binding protein

To identify proteins that physically interact with the cytoplasmic part of Gogo, a large amount of eye imaginal discs from late 3rd instar larvae expressing Gogo^{cyto}-Myc (Figure 3.1.1) was mechanically isolated as described previously (1979 Eugene). Gogo^{cyto}-Myc was immunoprecipitated from the lysate of these discs, and co-precipitated proteins were separated by PAGE, detected by Coomassie staining and identified by mass spectrometry.

Solutions

Organ Medium:

25 mM	glycerol phosphate disodium salt
10 mM	KH ₂ PO ₄
30 mM	KCl
10 mM	MgCl ₂
3 mM	CaCl ₂
162 mM	sucrose
10 U/ml	Penicillin
10 µg/ml	Streptomycin

Ringer's solution:

130 mM	NaCl
5 mM	KCl
1.5 mM	CaCl ₂

TENT buffer (pH 7.5):

25 mM	TrisCl
5 mM	EDTA
250 mM	NaCl
0.5 %	Triton X-100
1 mM	PMSF
2 mM	DTT
10 µM	pepstatin
1x	Roche complete protease inhibitor

HNGT buffer (pH 7.4):

20 mM	HEPES
150mM	NaCl
10 %	glycerol
0.1 %	Triton X-100

Disc isolation

Imaginal discs were isolated from each approximately 250 ml of 3rd instar transgenic larvae expressing Gogo^{cyto}-Myc and of control *w¹¹¹⁸* larvae. To obtain the larvae, eggs were collected on apple juice agar plates for a period of 8 h and allowed to develop to the 3rd instar larval stage directly on the collection plates while being fed with yeast paste. The larvae were washed with tap water to get rid of yeast and pupae, which, in contrast to larvae, float on top.

The larvae were suspended in 500 ml Organ Medium and grinded by means of a Model 4-E grinding mill (QCG Systems, Phoenixville, Pennsylvania). The ground material was passed through two screens with 2 mm and 0.8 mm openings, respectively (Retsch, Haan, Germany) and through a polyamide sieve mesh with 150 µm openings (Fisher Scientific, Schwerte, Germany). To maximize the yield, any material left on the grinding plates and the sieves was flushed with additional Organ Medium.

The material was allowed to settle for 30', and the supernatant was reduced to a total volume of 1.4 l by aspiration from the surface. 2.5 l of fresh Organ Medium were added, the material was allowed to settle for 10', and the total volume was reduced to 200 ml. As additional washing steps, the total volume was brought to 500 ml with fresh Organ Medium, the material was allowed to settle for 10', and the supernatant was aspirated to a total volume of 100 to 200 ml for three times. Then, the supernatant was reduced to a minimum and the remainder was centrifuged for 1' at 800 g and 4 °C. The supernatant was discarded. The pellet was resuspended in 40 ml 14 % Ficoll. Each 10 ml were layered onto a discontinuous density gradient in a 50 ml Falcon tube consisting of a bottom layer containing 15 ml 50 % sucrose, an intermediate layer of 10 ml 21 % Ficoll in Organ Medium, and a top layer containing 12.5 ml 14 % Ficoll in Organ Medium. The gradients were spun for 8' at 800 g and 4 °C. Air bubbles and other undesired material at the top were aspirated and discarded. Imaginal discs were enriched near the top of the 14 % Ficoll layer and at the interface between the 14 % and the 21 % Ficoll layer. They were collected, put into 150 ml Ringer's solution, and allowed to settle for 20'. The volume was reduced to 50 ml and 150 ml of additional Ringer's solution were added. The discs were allowed to settle for 10'. The volume again was reduced to 50 ml. After centrifuging for 1' at 800 g and 4 °C, the supernatant was aspirated, and approximately 1 ml of isolated imaginal discs was obtained.

Immunoprecipitation

To the 1 ml of imaginal discs in Ringer's solution, 2 ml of TENT buffer were added. The discs were transferred to a 3 ml tissue grinder potter (Fisher Scientific, Schwerte, Germany) and homogenized by 20 strokes with the pestle. After 30' on ice, the lysate was cleared by a 15' centrifugation at 10 000 g and 4 °C, followed by a 15' centrifugation at 16 000 g and 4 °C. 40 µl of a slurry of anti c-Myc antibody conjugated to agarose beads (Sigma-Aldrich, St. Louis, Missouri) were added to

2 ml of cleared lysate. After 2 h at 4 °C with agitation, the beads were washed five times for each 15' with 1 ml of HNGT buffer at 4 °C. 40 µl Laemmli buffer were added to the beads. After cooking 10' at 94 °C and centrifuging 1' at 16 000 g, 30 µl of the cleared Laemmli buffer were subjected to SDS-PAGE.

Detection and identification of co-immunoprecipitated proteins

After SDS-PAGE, the gels were stained with EZBlue gel staining reagent (Sigma-Aldrich, St. Louis, Missouri). Protein bands that occurred only in the lane with the proteins from Gogo^{cyto}-Myc expressing larvae but not in the control lane were cut out. The proteins were identified by mass spectrometry (Toplab, Martinsried, Germany).

2.8 Cell culture binding assay

The *Drosophila* Schneider cell line was derived from a primary culture of late stage, 20 to 24 h old *D. melanogaster* embryos (Schneider 1972). Some of its properties suggest that it descends from a macrophage-like lineage. Schneider cells, like flies, grow at temperatures from 18 to 28 °C. They form semi-adherent monolayers in tissue culture flasks. They grow in ambient air and do not require supplemental CO₂.

Transfection

Schneider cells were cultivated at 25 to 28 °C in Schneider's *Drosophila* medium (PromoCell, Heidelberg, Germany) supplemented with 10 % FCS. Shortly before forming a confluent layer, the cells of a 75 cm² cell culture flask were resuspended and divided to the wells of a 6-well multiwell plate for transfection. They were allowed to settle over night. One well was used per transfection.

For a single transfection, each 1.5 to 2 µg of the *actin-Gal4* plasmid and the expression plasmid(s) encoding the desired protein(s) under control of the *UAS* promoter were diluted in 100 µl serum-free medium. 10 µl Cellfectin (Invitrogen, Carlsbad, California) were diluted in another 100 µl of serum-free medium. The diluted cellfectin and the diluted DNA were mixed and left for 30', during which the cells were washed with 1 ml of serum-free medium. Then, the medium was removed from the cells and replaced by the DNA-Cellfectin mix to which 800 µl of additional serum-free medium were added. Transfection was allowed to proceed for at least 6 h up to 1 d.

Then, the transfection mix was removed from the cells and replaced by 2 ml of fresh medium supplemented with FCS. The cells were incubated for 3 d to allow for the expression of the desired proteins.

Immunoprecipitation

The cells were resuspended and harvested by centrifugation at 1 000 *g* for 5' at room temperature. The supernatant was discarded, and the cells were resuspended in 500 μ l lysis buffer. Lysis took place on ice for 30'. The lysate was cleared by a 15' centrifugation at 16 000 *g* and 4 °C. 10 μ l of the cleared lysate were kept back as input control, 400 μ l were used for the immunoprecipitation. To the latter, 20 μ l of a slurry of anti c-Myc antibody conjugated to agarose beads (Sigma-Aldrich, St. Louis, Missouri) were added. After 2 to 4 h at 4 °C with agitation, the beads were collected by centrifugation at 800 *g* for 5' at 4 °C. The beads were washed three times for each 10' to 20' with 300 to 500 μ l lysis buffer at 4 °C. Then, 20 μ l Laemmli buffer were added to the beads and 10 μ l Laemmli buffer were added to the input control. After cooking 10' at 94 °C and centrifuging 1' at 16 000 *g*, 20 μ l of the cleared Laemmli buffer were subjected to SDS-PAGE.

Solutions

Lysis buffer (pH 8.0) (Figures 3.2.3A-C, 3.8, 3.15):

25 mM	TrisCl
27.5 mM	NaCl
20 mM	KCl
25 mM	sucrose
10 mM	EDTA
10 mM	EGTA
0.75 %	Nonidet P-40
10 %	glycerol
20 mM	NaF
2 mM	sodium pyrophosphate
1 mM	PMSF
1 mM	DTT
1x	Roche complete protease inhibitor

Lysis buffer (pH 7.5) (Figures 3.2.3D-E):

50 mM	TrisCl
150 mM	NaCl
1 %	Nonidet P-40
1x	Roche complete protease inhibitor

2.9 Preparation of lysates from larval brains

Per lane, 15 hand-dissected larval brains were directly put into 15 μ l Laemmli loading buffer, cooked for 10' at 94 °C, crushed with a plastic pestle and cooked for another 10'. The proteins in the lysate were separated by PAGE and Hts was detected by western blot.

2.10 Western blot

After PAGE, proteins were transferred onto Amersham Hybond ECL membrane (GE Healthcare, Waukesha, Wisconsin). The transfer was controlled by staining the membrane with Ponceau S afterwards. Then, the membrane was blocked with 5 % milk powder in PBS for 1 h at room temperature. The blocked membrane was incubated with the primary antibody in 5 % milk powder in PBS over night at 4 °C. The membrane was washed three times with PBS for 10' each and then incubated with the secondary antibody in PBS for 4 h at room temperature. The membrane was washed thrice with PBS for 10' each, once with PBS containing 0.1 % Tween 20 for 10', and once shortly with PBS. The membrane was submerged in Amersham ECL detection reagent (GE Healthcare, Waukesha, Wisconsin). Exposure times of the films ranged from 5'' to several h.

Membrane stripping

If a second protein was to be detected on the same membrane, the antibodies were stripped off the membrane by submerging it for 1 h in strip solution at 65 °C. Starting with the blocking step, the detection procedure was then repeated as described above.

Strip solution (pH 7.5)

100 mM	TrisCl
0.2 %	SDS
100 mM	2-mercaptoethanol

2.11 Immunostaining of adult brain cryosections

Adult flies were anesthetized with carbonic acid gas. Body and proboscis were removed from the head. For fixation, the heads were put into PBS containing 2 % formaldehyde and 0.05 % Triton X-100 for 60' to 90' at 4 °C. After washing the heads with PBS, they were transferred into a 12 % sucrose solution. The sucrose solution was allowed to infiltrate the tissue for 16 h at 4 °C. Then, the heads were submerged in a drop of Tissue Tek O.C.T. Compound (Sakura Finetek Europe, Zoeterwoude, The Netherlands). The heads were allowed to be permeated for 10' to 30' at room temperature, embedded and aligned in Peel-A-Way embedding molds (Polysciences, Warrington, Pennsylvania) and frozen on an ethanol bath with dry ice. The embedded heads were cut in 10 to 14 μ m thick horizontal slices with a cryostat microtome.

The slices were deposited on SuperFrost Plus microscope slides (Gerhard Menzel Glasbearbeitungswerk, Braunschweig, Germany), dried for 5' at room temperature, subjected to fixation in PBS containing 0.5 % formaldehyde for 20' to 60' at room temperature, washed with PBS three times for 3' each, blocked in PBS containing 0.3 % Triton X-100 and 1 % BSA for 30' and washed three times for 10' each with PBS containing 0.3 % Triton X-100. The primary antibody was applied over night at 4 °C in PBS containing 0.3 % Triton X-100 and 5 % NGS. After several washings with PBS containing 0.3 % Triton X-100, the HRP conjugated secondary antibody was applied in PBS containing 0.3 % Triton X-100 and 5 % NGS for 4 h at room temperature, followed by another round of washings with PBS containing 0.3 % Triton X-100. Then, the staining reaction was started by applying 0.05 % diaminobenzidine in 0.003 % hydrogen peroxide, monitored, and, when proceeded to the desired stage, stopped by washing with PBS. The samples were embeded in PBS containing 70 % glycerol and covered with cover slips.

2.12 Whole mount immunostaining of larval and adult brains

To obtain larval brains, late 3rd instar larvae that were crawling on the wall of the culture vial were collected and dissected in PBS containing up to 0.1 % Triton X-100.

Adult flies were anesthetized with carbonic acid gas, immersed in ethanol for 30'' to remove hydrophobic compounds from their cuticle, and dissected in PBS containing up to 0.1 % Triton X-100. The tracheae covering the brain were removed.

Directly after dissection, the brains were transferred into PBS containing up to 0.1 % Triton X-100 and stored on ice. Fixation was performed by adding formaldehyde to a final concentration of approximately 3.5 % and agitating for 20' to 35' at room temperature. The brains were washed three times for at least 10' each with PBS containing 0.1 to 0.5 % Triton X-100 and blocked for 30' with 5 % NGS in PBS containing 0.1 to 0.5 % Triton X-100 at room temperature. Then, the primary antibodies were added and left on at least over night at 4 °C with agitation.

After washing the brains again three times for at least 10' each with PBS containing 0.1 to 0.5 % Triton X-100, the fluorescently labeled secondary antibodies were applied in PBS containing 5 % NGS and 0.1 to 0.5 % Triton X-100 and left on at least over night at 4 °C with agitation.

Finally, the brains were washed again three times for at least 10' each with PBS containing 0.1 to 0.5 % Triton X-100, transferred into Vectashield Mounting Medium (Vector Laboratories, Burlingame, California) and mounted on microscope slides.

2.13 Estimation of Add1 levels in R axons in the medulla

The ratio of the mean fluorescence intensity of the axons to the mean fluorescence intensity of the background was determined for htsF and 24B10 immunostainings by means of Adobe Photoshop CS3. In the channel displaying the 24B10 immunostaining, the average intensity value of the

medulla was determined. All pixels with a higher intensity value, considered to represent the axons, were selected and their average intensity value was divided by the average intensity value of the remaining pixels, considered as background, to get the relative fluorescence intensity of the 24B10 staining. Then, the average intensity values of the selected area and the remaining pixels were determined in the channel displaying the htsF immunostaining, and the ratio of both values was calculated to obtain the relative fluorescence intensity of the htsF immunostaining.

2.14 Antibodies

The following antibodies were used in this work.

Antibody used for immunoprecipitations

For immunoprecipitations, anti c-Myc antibody raised in rabbit and conjugated to agarose beads (Sigma-Aldrich, St. Louis, Missouri) was used.

Antibodies used for western blots

The antibodies used for western blots are listed below.

antibody	host species	dilution	source
htsF (anti Hts)	rat	1:5000	Lynn Cooley, Yale University, New Haven, Connecticut
1B1 (anti Hts)	mouse monoclonal	1:10	Developmental Studies Hybridoma Bank, Iowa City, Iowa
HIS.H8 (anti 6xHis)	mouse monoclonal	1:1000	Abcam, Cambridge, United Kingdom
9E10 (anti c-Myc)	mouse monoclonal	1:100	Santa Cruz Biotechnology, Santa Cruz, California
anti mouse IgG HRP conjugated	sheep	1:4000 to 1:5000	GE Healthcare, Waukesha, Wisconsin
anti rat IgG HRP conjugated	goat	1:3000	GE Healthcare, Waukesha, Wisconsin

Table 2.14.1: List of antibodies used for western blots

The antibodies are listed in the first column. The second column quotes the host species it was raised in, the third the dilution it was used at, and the fourth the source from which it was obtained.

Antibodies used for immunostainings

The antibodies used in immunostainings are listed below. Alexa Fluor 488 conjugated anti GFP antibody was included in both the primary and the secondary staining step.

antibody	host species	dilution	source
anti β -galactosidase	mouse (monoclonal)	1:300	Promega, Madison, Wisconsin
anti Gogo	rabbit	1:1000	Takashi Suzuki
htsF (anti Hts)	rat	1:400 to 1:500	Lynn Cooley, Yale University, New Haven, Connecticut
1B1 (anti Hts)	mouse (monoclonal)	1:5 to 1:10	Developmental Studies Hybridoma Bank, Iowa City, Iowa
anti c-Myc	rabbit	1:300	Gramsch Laboratories, Schwabhausen, Germany
24B10 (anti Chaoptin)	mouse (monoclonal)	1:5 to 1:50	Developmental Studies Hybridoma Bank, Iowa City, Iowa
anti GFP Alexa Fluor 488 conjugated	rabbit	1:100 to 1:500	Invitrogen, Carlsbad, California
anti mouse IgG HRP conjugated	goat	1:600	Jackson ImmunoResearch Laboratories, West Grove, Pennsylvania
anti mouse IgG Alexa Fluor 488 conjugated	goat	1:200 to 1:250	Invitrogen, Carlsbad, California
anti rabbit IgG Alexa Fluor 488 conjugated	goat	1:200 to 1:300	Invitrogen, Carlsbad, California
anti rat IgG Alexa Fluor 488 conjugated	goat	1:200	Invitrogen, Carlsbad, California
anti mouse IgG Alexa Fluor 568 conjugated	goat	1:200 to 1:500	Invitrogen, Carlsbad, California
anti rat IgG Alexa Fluor 568 conjugated	goat	1:200	Invitrogen, Carlsbad, California
anti mouse IgG Alexa Fluor 633 conjugated	goat	1:200	Invitrogen, Carlsbad, California
anti rat IgG Alexa Fluor 633 conjugated	goat	1:200 to 1:500	Invitrogen, Carlsbad, California

Table 2.14.2: List of antibodies used for immunostainings

The antibodies are listed in the first column. The second column quotes the host species it was raised in, the third the dilution it was used at, and the fourth the source from which it was obtained.

3. RESULTS

3.1 Gogo requires its cytoplasmic part to function in photoreceptor axon guidance

Gogo was proposed to function as an axon guidance receptor in R8 (Tomasi et al. 2008), and the aim of this thesis was to elucidate the molecular mechanisms that underlie its function during axon guidance by identifying proteins that physically interact with Gogo. Unlike its N-terminal extracellular part that contains well-defined protein domains and presumably senses the growth cone's environment by binding to as yet unidentified ligands, the cytoplasmic C-terminus of Gogo lacks any such domain (Figure 1.5 and Tomasi et al. 2008). It appeared especially exciting to clarify how this uncharacterized region would transmit the information required for proper axon guidance into the growing axon. To ensure that the cytoplasmic part of Gogo is indeed essential for proper photoreceptor axon guidance, a C-terminally 4xMyc-tagged fragment of Gogo lacking almost all the cytoplasmic part (Gogo^{ΔC}-Myc, Figure 3.1.1) was tested for its ability to rescue *gogo* mutants.

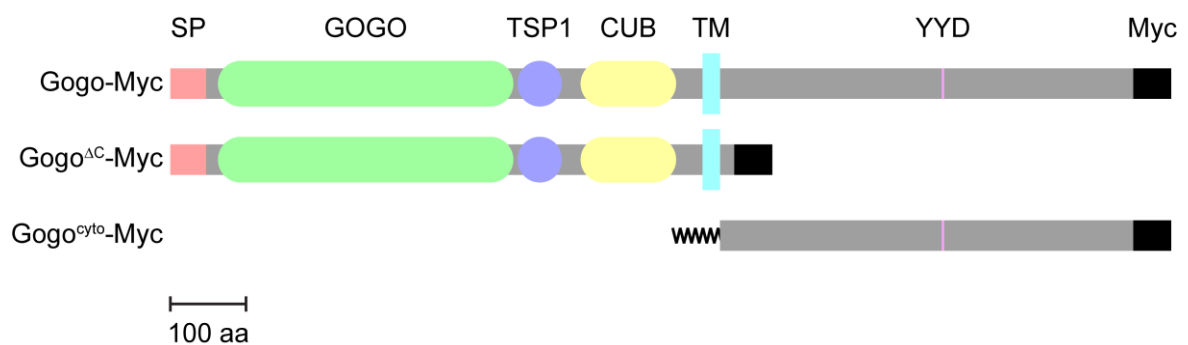


Figure 3.1.1: Schematic of the different artificial Gogo constructs used

Gogo-Myc comprises the complete full-length Gogo protein, whereas Gogo^{ΔC}-Myc lacks almost all the cytoplasmic part. In Gogocyto-Myc, the extracellular part and the transmembrane domain were replaced by a myristoylation signal. All constructs feature a C-terminal 4xMyc-tag (Myc). SP: signal peptide. TM: transmembrane domain. Same color indicates same sequence. Scale bar: 100 aa.

In mosaic flies that are overall heterozygous but have eyes homozygous mutant for the *gogo* null allele *gogo*^{D869}, the medullae are severely disrupted, and the regular array of R7 and R8 axons is lost (Figure 3.1.2A). This defect can be restored by expressing C-terminally 4xMyc-tagged full-length Gogo (Gogo-Myc, Figure 3.1.1) under direct control of the *GMR* promoter (Figure 3.1.2C). The *GMR* promoter drives expression in all differentiating cells of the developing eye, including all photoreceptors (Ellis et al. 1993). Expressing Gogo^{ΔC}-Myc does not restore the defects caused by *gogo*^{D869} (Figure 3.1.2B), indicating that Gogo requires its cytoplasmic region for its function in photoreceptor axon guidance. This result was confirmed with each a second transgenic insertion of

GMR-gogo^{ΔC}-Myc (Figure 3.1.2D) and *GMR-gogo-Myc* (Figure 3.1.2E) as well as with another *gogo* null allele, *gogo^{D1600}* (Figures 3.1.2F-J).

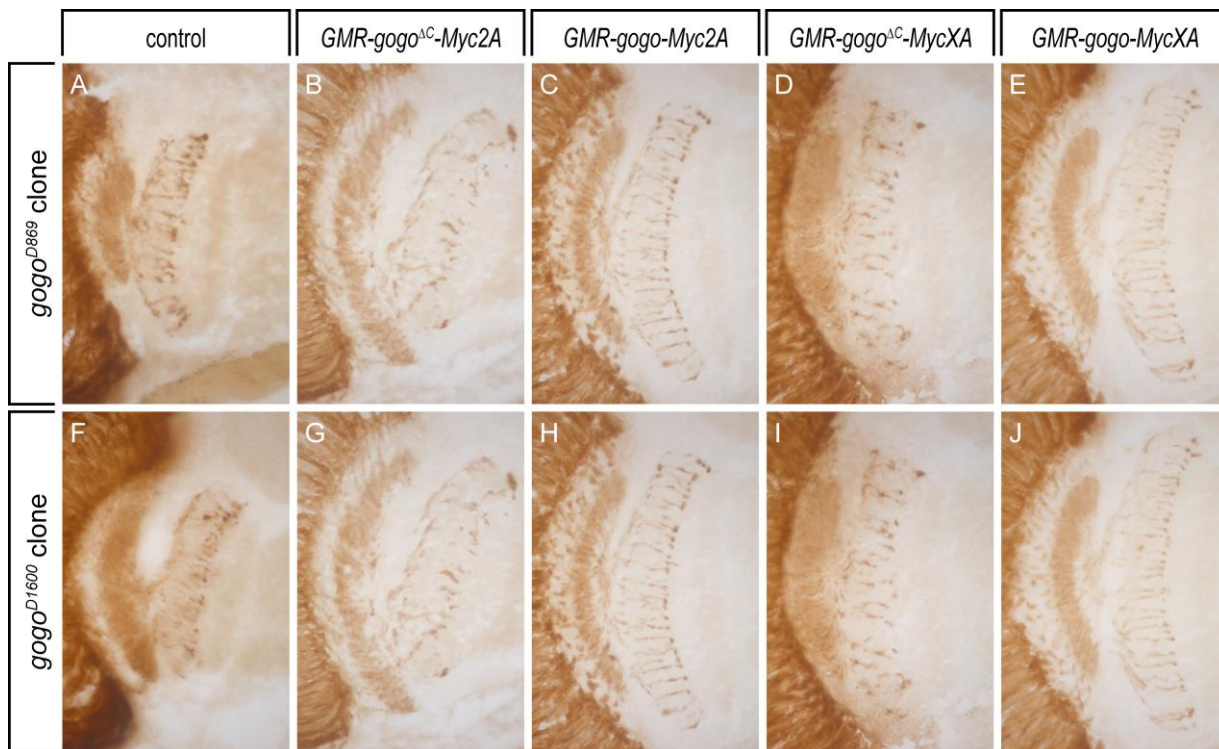


Figure 3.1.2: Gogo requires its cytoplasmic part to function in photoreceptor axon guidance

Horizontal head sections of (A-E) *gogo^{D869}* or (F-J) *gogo^{D1600}* *ey-Flp* mosaic flies carrying the *gl-lacZ* reporter and the indicated transgene stained for β -galactosidase. The defects caused by (A,F) *gogo* null mutations are restored by (C,E,H,J) *GMR-gogo-Myc* but not by (B,D,G,I) *GMR-gogo^{ΔC}-Myc*.

To exclude that the inability of *GMR-gogo^{ΔC}-Myc* to rescue *gogo* mutants was merely an unspecific secondary effect of reduced expression, protein instability or mislocalization, optic lobes of transgenic *GMR-gogo^{ΔC}-Myc* or *GMR-gogo-Myc* late 3rd instar larvae were stained with anti-Myc antibody. Both Gogo^{ΔC}-Myc (Figure 3.1.3B) and Gogo-Myc (Figure 3.1.3C) are detected along photoreceptor axons, in the lamina plexus, and at the tips of R7 / R8 axons in the developing medulla. The staining intensity of Gogo^{ΔC}-Myc appears to be somewhat lower compared to Gogo-Myc, but apart from that, there is no obvious overall difference between the appearance of Gogo^{ΔC}-Myc and Gogo-Myc. The staining is specific as it is absent from the negative control (Figure 3.1.3A).

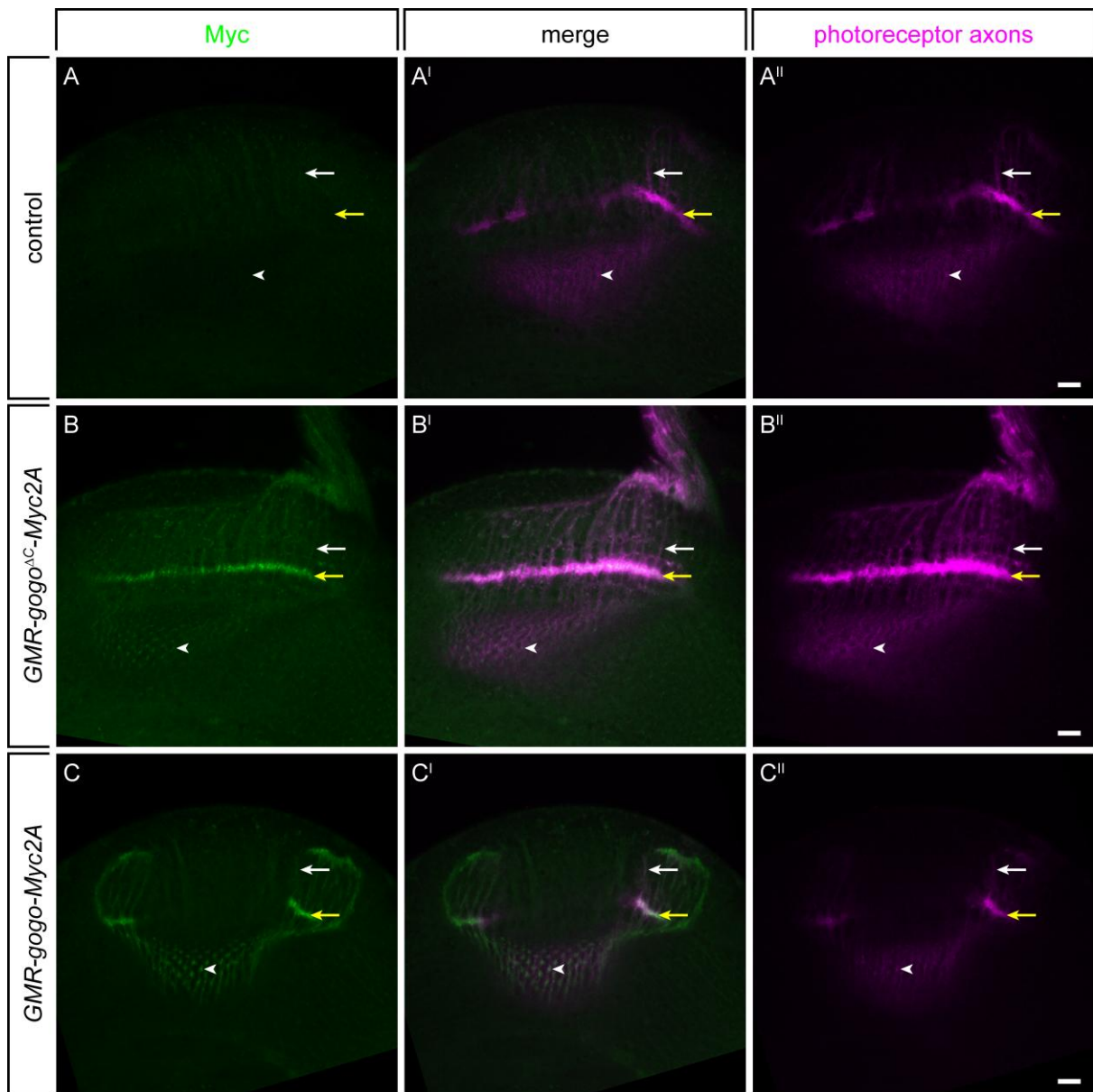


Figure 3.1.3: Gogo^{ΔC}-Myc and Gogo-Myc are present in larval photoreceptor axons

Whole mount immunostainings of optic lobes from (A) *w¹¹¹⁸*, (B) transgenic *GMR-gogo^{ΔC}-Myc*, and (C) transgenic *GMR-gogo-Myc* late 3rd instar larvae. Both (B) Gogo^{ΔC}-Myc and (C) Gogo-Myc are detected along photoreceptor axons (white arrows), in the lamina plexus (yellow arrows), and at the tips of R7 / R8 axons (arrowheads). The staining is specific as it is absent from the (A) negative control. All genotypes were imaged at the same settings. Scale bars: 10 μm.

3.2 Gogo physically interacts with Hts

To identify proteins that physically interact with Gogo, transgenic flies that express a myristoylated, C-terminally 4xMyc-tagged version of the cytoplasmic part of Gogo (Gogo^{cyto}-Myc, Figure 3.1.1) under direct control of the *GMR* promoter were generated.

Gogo^{cyto}-Myc is present in photoreceptor axons of late 3rd instar larvae, as shown by immunostaining with anti-Myc antibody (Figure 3.2.1).

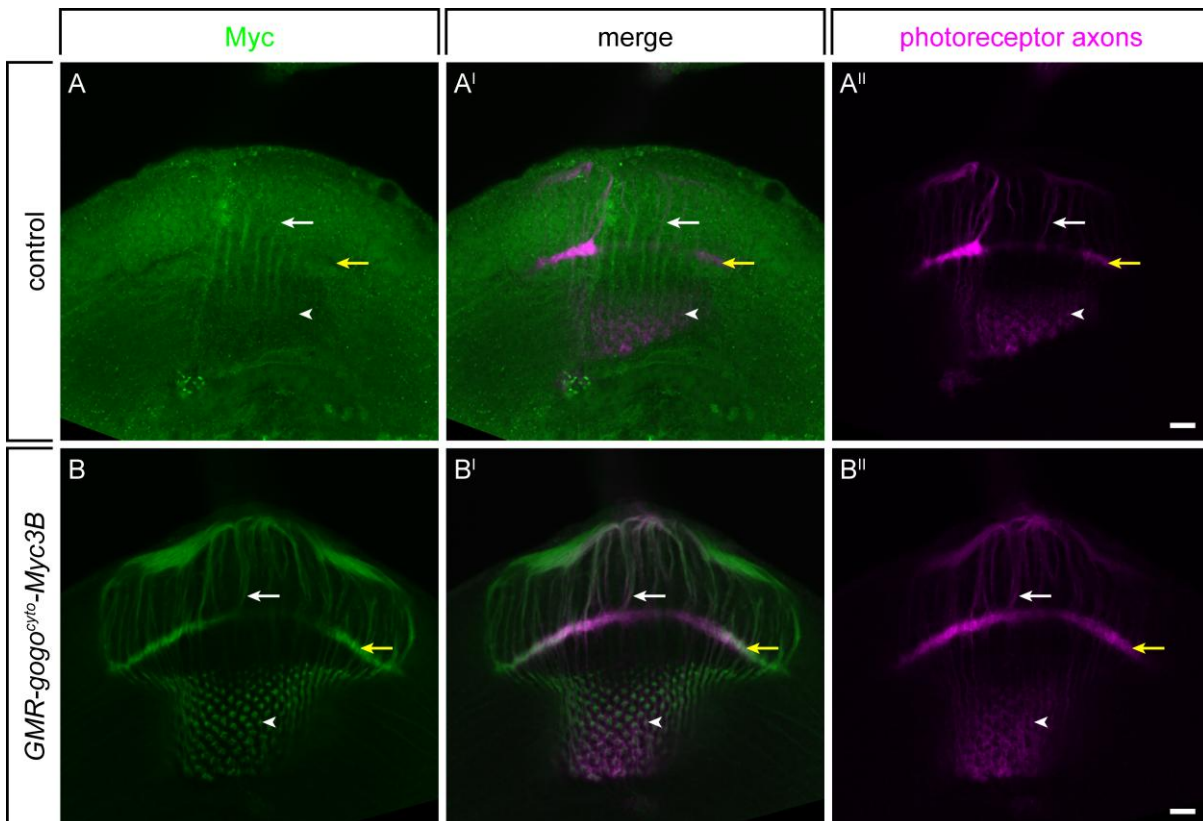


Figure 3.2.1: Gogo^{cyto}-Myc is present in larval photoreceptors

Whole mount immunostainings of optic lobes from (A) *w¹¹¹⁸* and (B) *GMR-gogo^{cyto}-Myc3B* 3rd instar larvae. Gogo^{cyto}-Myc is detected along photoreceptor axons (white arrows), in the lamina plexus (yellow arrows), and at the tips of R7 / R8 axons (arrowheads). The staining is specific as it is absent from the (A) negative control. Scale bars: 10 μ m.

Using an antibody directed against the Myc-epitope, Gogo^{cyto}-Myc was immunoprecipitated from a large amount of mechanically isolated 3rd instar larval imaginal discs. Coimmunoprecipitated proteins were separated by PAGE and detected by Coomassie staining (Figure 3.2.2A). A protein with an apparent molecular weight of approximately 93 kDa appeared specifically together with Gogo^{cyto}-Myc but not in the control performed with *w¹¹¹⁸* discs. It was identified as Hts by mass spectrometry, but the obtained set of peptide masses did not allow for the unambiguous identification of the specific isoform observed. However, the apparent molecular weight of 93 kDa points to Add1 or Add2 that have been described to appear as a doublet at around 90 kDa on western blots (Petrella et al. 2007).

The identity of Gogo^{cyto}-Myc was proven by western blot (Figure 3.2.2B).

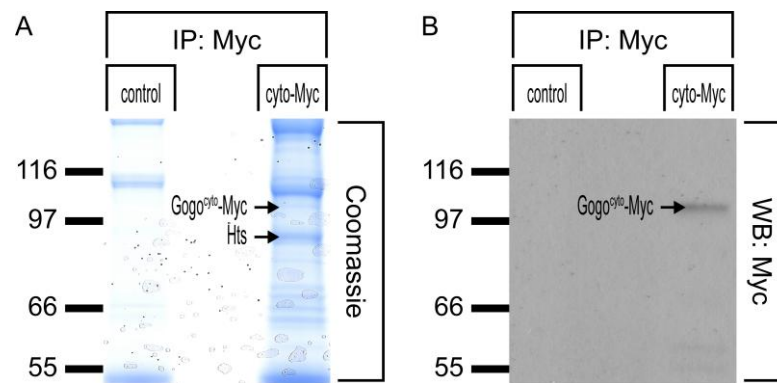


Figure 3.2.2: Hts physically interacts with Gogo^{cyto}-Myc

Gogo^{cyto}-Myc was immunoprecipitated from lysates of imaginal discs from late 3rd instar larvae. Proteins were separated by PAGE and detected by (A) Coomassie. A band that appeared together with Gogo^{cyto}-Myc but not in the control was identified as Hts by mass spectrometry. The identity of Gogo^{cyto}-Myc was proven by (B) western blot.

The physical interaction was verified by coimmunoprecipitation from lysates of Schneider cells that coexpressed a C-terminally 6xHis-tagged version of Add1 (Add1-His) and Gogo-Myc. As the YYD motif is the only outstanding structure in the cytoplasmic part of Gogo and functionally important (Luu 2008), two mutant versions of Gogo-Myc have also been tested for their ability to bind to Add1-His. In one of these mutants, the Tyrosine residues of the YYD motif have been replaced by Phenylalanine residues (Gogo^{FFD}-Myc), which does not affect the function of Gogo, and in the other one by Aspartic acid residues (Gogo^{DDD}-Myc), which compromises Gogo's function (Luu 2008). Add1-His appears on the western blot together with immunoprecipitated Gogo-Myc, Gogo^{FFD}-Myc and Gogo^{DDD}-Myc, but not in the control lacking any Gogo constructs (Figure 3.2.3A). No difference was observed in Add1-His binding to Gogo-Myc, Gogo^{FFD}-Myc or Gogo^{DDD}-Myc. Analogous experiments showed that also the Hts isoforms ShAdd (Figure 3.2.3B) and HtsPD (Figure 3.2.3C) are able to bind to Gogo, suggesting that binding to Gogo is mediated by the region of Hts that is common to all isoforms (Figure 1.6). This was directly shown by coexpressing Gogo-Myc and a 6xHis-tagged version of this common region (Hts⁴⁷²-His), followed by immunoprecipitation and western blot (Figure 3.2.3D). To prove that the physical interaction is indeed specific for Hts and Gogo, two unrelated proteins, Wnk and GFP, were supplied with a 4xMyc and a 6xHis tag in an identical way as Gogo-Myc and Hts⁴⁷²-His, respectively. Hts⁴⁷²-His did not coimmunoprecipitate with Wnk-Myc, and GFP-His not with Gogo-Myc, demonstrating that the binding between Hts⁴⁷²-His and Gogo-Myc is specific for Hts and Gogo. As the expression level of Gogo-Myc and GFP-His was very low when both were coexpressed, this control was repeated using double the amount of cells coexpressing Gogo-Myc and GFP-His as cells coexpressing Gogo-Myc and Hts⁴⁷²-His (Figure 3.2.3E). Again, the interaction between Hts⁴⁷²-His and Gogo-Myc could be shown to be specific for Hts.

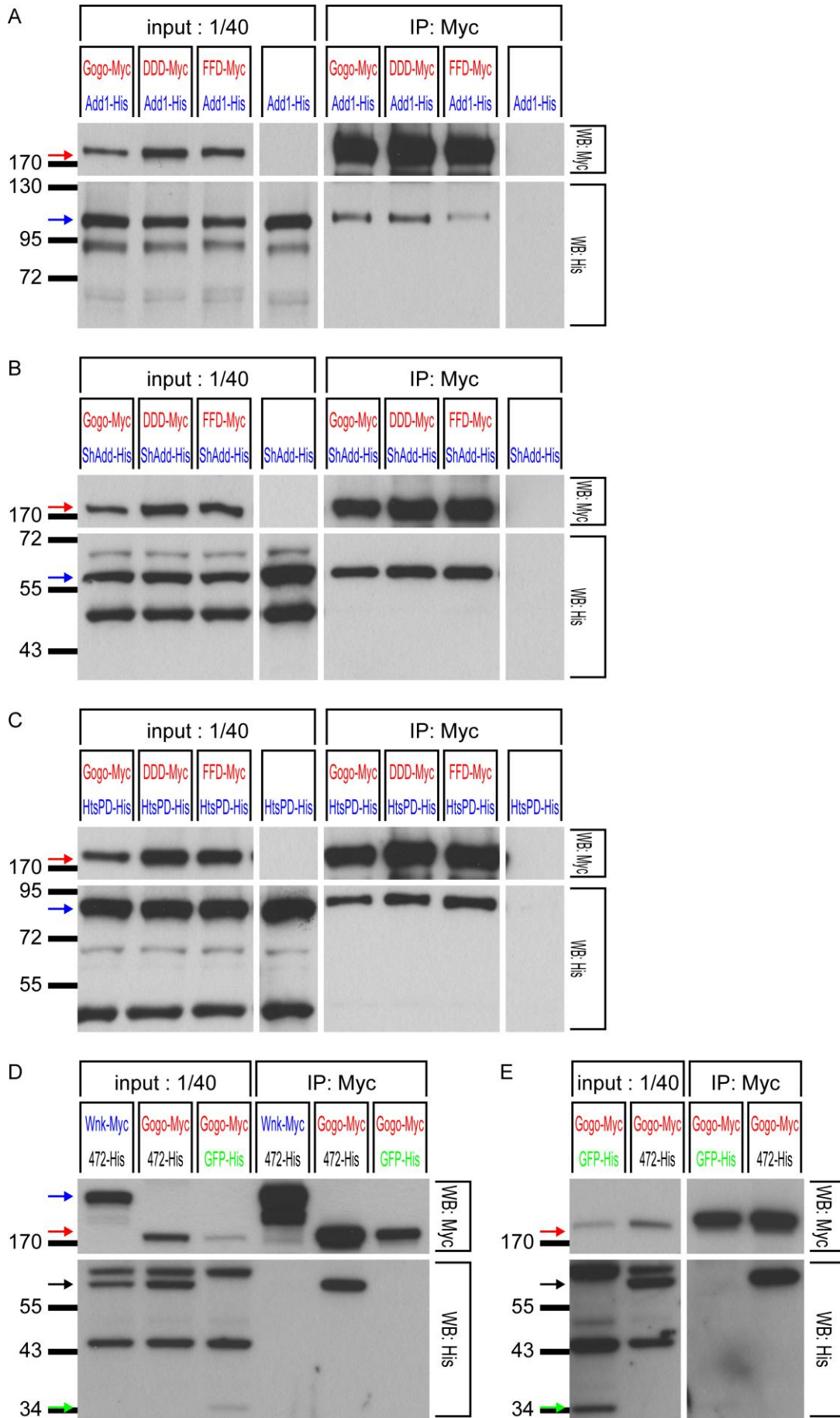


Figure 3.2.3: Gogo binds to all Hts isoforms independently of its YYD motif

(A) Schneider cells expressed Add1-His alone (lane 4) or together with the indicated Gogo construct (lanes 1 to 3). Add1-His coimmunoprecipitated with Gogo-Myc (lane 5), Gogo^{DDD}-Myc (lane 6) and Gogo Gogo^{FFD}-Myc (lane 7) but was absent from the control (lane 8). Analogous results were obtained for (B) ShAdd-His and (C) HtsPD-His. (D) The N-terminal 472 aa of Hts are sufficient for the interaction with Gogo. The cells coexpressed Gogo-Myc and Hts⁴⁷²-His (lane 2), Wnk-Myc and Hts⁴⁷²-His (lane 1) or Gogo-Myc and GFP-His (lane 3). Hts⁴⁷²-His coimmunoprecipitated with Gogo-Myc (lane 5). Hts⁴⁷²-His did not coimmunoprecipitate with Wnk-Myc (lane 4) and GFP-His not with Gogo-Myc (lane 6), demonstrating that the physical interaction is specific for Gogo and Hts. (E) To compensate for the low expression level of Gogo-Myc and GFP-His when they are coexpressed, lysate from twice the amount of cells coexpressing Gogo-Myc and GFP-His (lane 1) than from those coexpressing Gogo-Myc and Hts⁴⁷²-His (lane 2) was used. Hts⁴⁷²-His coimmunoprecipitated with Gogo-Myc (lane 4), but GFP-His did not (lane 3).

3.3 Hts can be detected in larval photoreceptor axons

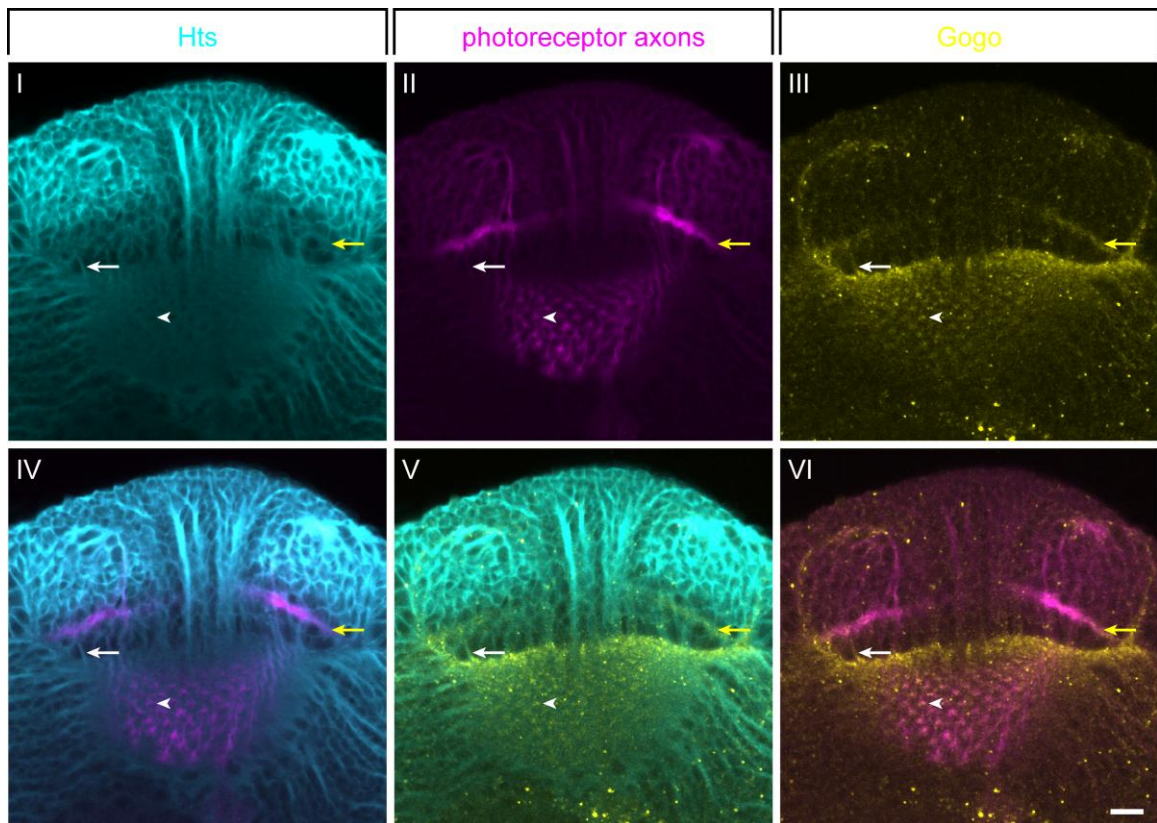


Figure 3.3: Hts in optic lobes of wild type larvae

Wild type 3rd instar larval optic lobes were immunostained with (I) anti-Hts antibody htsF, (II) antibody 24B10 to visualize photoreceptor axons, and (III) anti-Gogo antibody. Hts is ubiquitously expressed. It is detected along photoreceptor axons (white arrows) and in the lamina plexus (yellow arrows) where R1 to R6 terminate. R7 / R8 termini (arrowheads) stain strongly positive for Gogo but show a reduction of the otherwise uniform Hts staining of the medulla. (IV) Merge of I and II. (V) Merge of I and III. (VI) Merge of II and III. Scale bar: 10 μ m.

As revealed by immunostaining with the anti-Hts antibody htsF, Hts is ubiquitously expressed in the optic lobes of late 3rd instar wild type larvae (Figure 3.3). htsF labels photoreceptor axons and the termini of R1 to R6 in the lamina plexus. The medulla exhibits an overall uniform and diffuse staining, but interestingly, the signal is reduced at the termini of R7 / R8 axons that stain strongly positive for Gogo (Figure 3.3 and Tomasi et al. 2008).

3.4 Loss of Hts severely affects axon guidance in the visual system

As Adducin was not known to be involved in axon guidance yet and research on Hts in *Drosophila* so far focused on its role during oogenesis, it was interesting to see if *hts* mutant flies would show defects in photoreceptor axon guidance.

The mutant analysis started with the two point mutations *hts*^{4G} (Koundakjian et al. 2004) and *hts*^{W532X} (Petrella et al. 2007) that both cause premature stop codons (Petrella et al. 2007). The latter has been suggested to be a null mutant based on the lack of detectable amounts of Hts protein on western blots from mutant ovaries, whereas a truncated form of Hts protein is expressed in *hts*^{4G} mutants (Petrella et al. 2007). Both mutants are homozygous viable, and adult homozygous mutant flies expressing GFP as a marker in R8 were tested for axon guidance defects in the medulla. *hts*^{4G} did not cause any observable defects (n=5, Figure 3.4A, Table 3.4), but the majority of *hts*^{W532X} mutant medullae (3 of n=5, Table 3.4) showed sporadic irregularities. Approximately 3 % (21 of 616) of the columns in the medulla contained aberrant axons (Figure 3.4B).

Another *hts* mutant, namely *hts*⁰¹¹⁰³ (Spradling et al. 1999), is caused by a P-element insertion into an intron of the 5' UTR (Figure 3.4H) that strongly reduces Hts protein amount and function (Wilson 2005). *hts*⁰¹¹⁰³ hemizygous flies are viable and show a severe disruption of the medulla in adult flies (29 of n=30, Figure 3.4C, Table 3.4). When compared to the wild type (Figure 3.4G), the regular array of R7 and R8 axons is lost and instead, axons clump together, forming irregularly spaced thick bundles and gaps in between. Instead of going straight from M1 to M3 and M6, respectively, R8 and R7 axons follow disordered paths from M1 to their respective target layer and R8 often overshoots its correct target layer M3.

As *hts*^{W532X} was supposed to be a null mutant, it was surprising to see this much stronger phenotype in *hts*⁰¹¹⁰³ hemizygous flies. To clarify this inconsistency, the expression of Hts proteins in the three mutants was analyzed using the antibody htsF that recognizes all Hts isoforms (Petrella et al. 2007). On western blots from lysates of late 3rd instar larval brains, htsF detected full-length Add1/2 and ShAdd from wild type larvae and a truncated protein plus ShAdd from *hts*^{4G} mutant larvae (Figure 3.4J), as expected. htsF did not detect any clear band from *hts*⁰¹¹⁰³ hemizygous larvae, but surprisingly, it detected not only ShAdd but two additional weak but definite bands from *hts*^{W532X} mutant brains.

genotype	no defects (e.g. Fig. 3.4A)	rare defects (e.g. Fig. 3.4B)	intermediate defects (e.g. Fig. 3.4F)	strong defects (e.g. Fig. 3.4C)
<i>hts</i> ^{AG} homozygous (n=5)	5 / 100 %	0	0	0
<i>hts</i> ^{W532X} homozygous (n=5)	1 / 20 %	3 / 60 %	1 / 20 %	0
<i>hts</i> ⁰¹¹⁰³ hemizygous (n=31)	0	1 / 3 %	5 / 16 %	25 / 81 %
<i>hts</i> ^{null} homozygous (n=4)	0	0	0	4 / 100 %
<i>hts</i> ⁰¹¹⁰³ mosaic (n=3)	3 / 100 %	0	0	0
<i>hts</i> ^{null} mosaic (n=31)	0	2 / 6 %	12 / 39 %	17 / 55 %
<i>hts</i> ^{wt} mosaic (n=5)	5 / 100 %	0	0	0

Table 3.4: Severity of the defects observed in different *hts* mutants

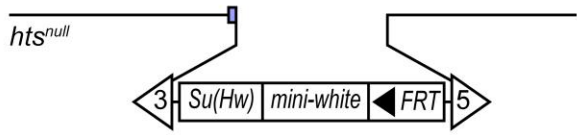
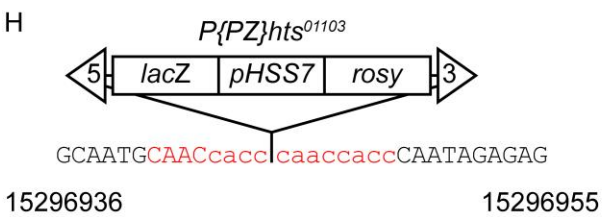
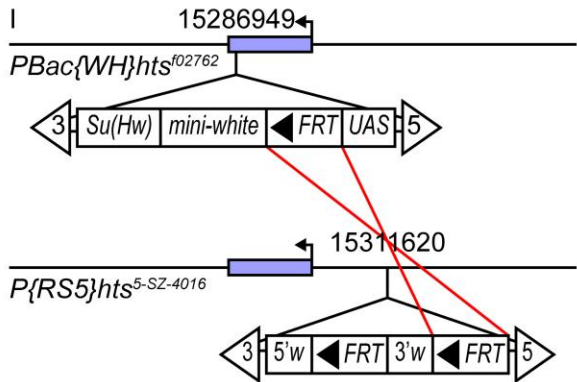
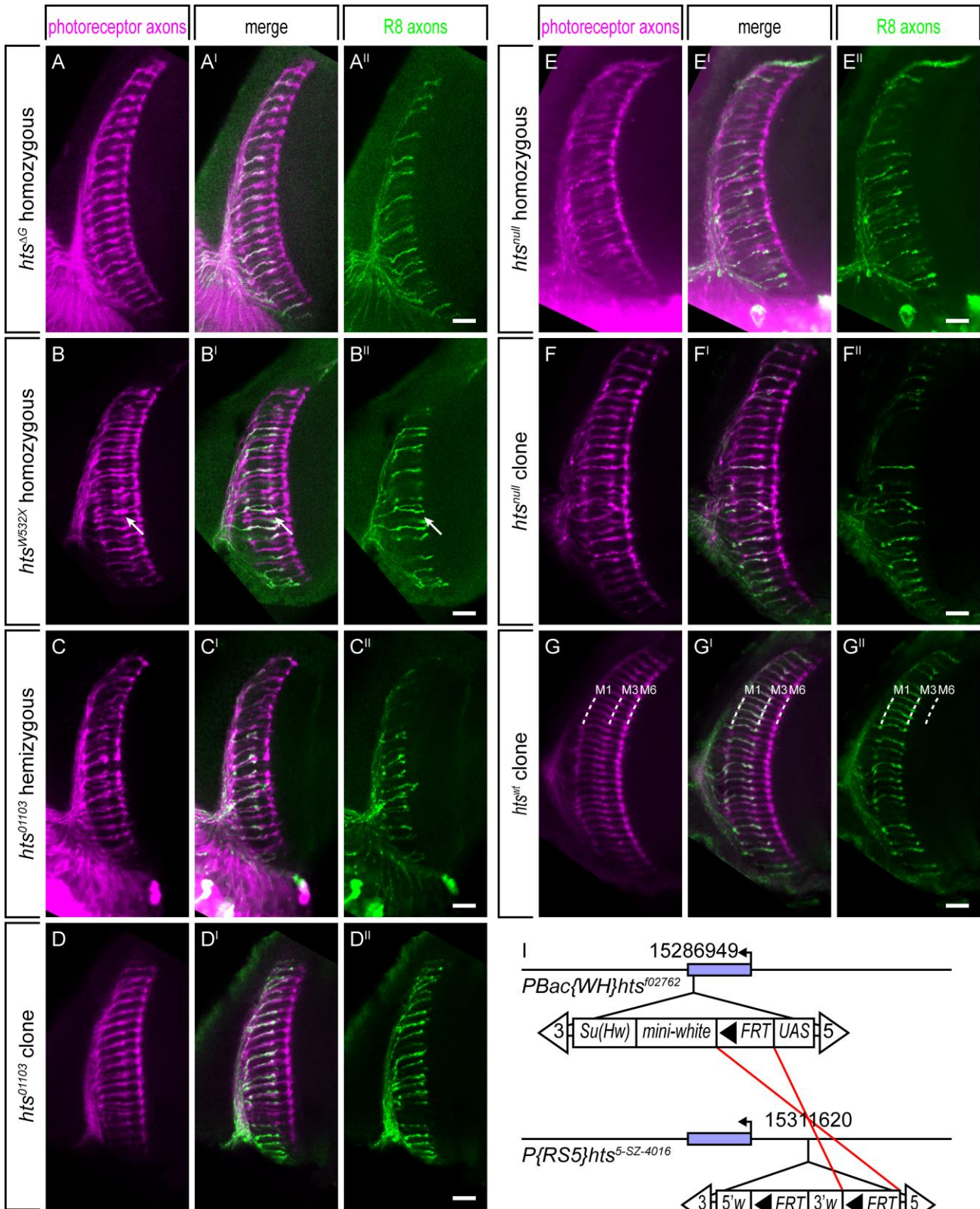
For each genotype listed in the left column, the number / percentage of medullae that had no defective phenotype, showed only sporadic irregularities, had an intermediate or a strongly defective phenotype is denoted.

Based on their apparent molecular weights, they can be considered as the truncated protein caused by the premature stop codon and full-length Add1/2, respectively. Since a comparable band corresponding to full-length Add1/2 is absent from both *hts*^{AG} and *hts*⁰¹¹⁰³, it seems unlikely that the detected full-length protein is maternally contributed. Rather, it could be attributed to stop codon readthrough as it was reported for other nonsense mutations in *Drosophila* (Washburn and O'Tousa 1992; Samson et al. 1995).

The result found using *hts*F was confirmed with another antibody against Hts. 1B1 (Zaccai and Lipshitz 1996a) recognizes all Hts isoforms but ShAdd (Whittaker et al. 1999; Petrella et al. 2007) and detected exactly the same pattern of protein bands except for the lack of bands corresponding to ShAdd (Figure 3.4K).

Although Hts could not be detected unambiguously in *hts*⁰¹¹⁰³ hemizygous brains, there is no obvious defect in the medullae of mosaic animals that are overall heterozygous but have homozygous *hts*⁰¹¹⁰³ mutant eyes including the photoreceptors (n=3, Figure 3.4D, Table 3.4), suggesting that *hts*⁰¹¹⁰³ is not a null mutant either.

To abolish any doubt about the nature of the mutation, a definite *hts* null mutation (*hts*^{null}) was generated by removing almost the complete *hts* coding sequence (Figure 3.4I). *hts*^{null} is recessive lethal at 25 °C, but a few escapers survive when the flies are raised at 18 °C. The medullae of both homozygous *hts*^{null} (n=4, Figure 3.4E, Table 3.4) and *hts*^{null} mosaic (29 of n=31, Figure 3.4F, Table 3.4) animals show severe defects that resemble the *hts*⁰¹¹⁰³ hemizygous phenotype. The overall structure of the medulla is disrupted. Axons lose their regular array and clump together. Some R8 axons overshoot M3, and abnormally thick swellings at the axon termini and at the M1 layer can be observed.



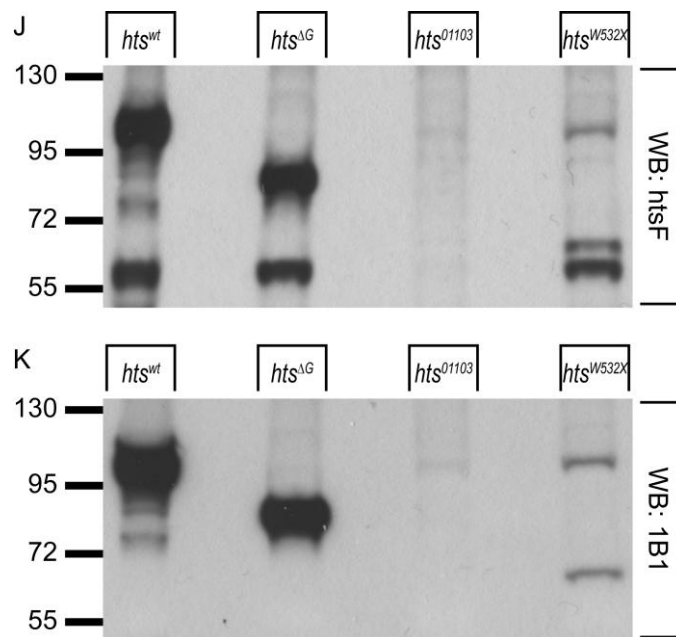


Figure 3.4: Loss of Hts severely affects axon guidance in the visual system

(A-G) Photoreceptor axons in the medulla of flies with the indicated genotype and GFP as a marker in R8 axons. (A) Homozygous *hts*^{ΔG} mutants do not exhibit defects. (B) In homozygous *hts*^{W532X} mutants, single axons occasionally enter the wrong column and inappropriately fasciculate with neighboring axons (arrow). (C) In *hts*⁰¹¹⁰³ hemizygous flies, the medulla looks overall disorganized and the regular array of photoreceptor axons is lost. (D) Mosaic flies with eye-specific clones homozygous for *hts*⁰¹¹⁰³ do not exhibit defects in the medulla. (E) Homozygous *hts*^{null} mutants show strong defects similar to *hts*⁰¹¹⁰³ hemizygous flies. (F) Compared to *hts*⁰¹¹⁰³ hemizygous flies, mosaic flies with eye-specific clones homozygous for *hts*^{null} more often show only an intermediately defective phenotype as shown here with large areas of the medulla unaffected. However, the majority exhibits equally strong defects. (G) Wild type control. Layers M1, M3, and M6 are denoted by dashed lines. Anterior up, lateral left. Scale bars: 10 μm. (H) Genomic site of the *P{PZ}hts*⁰¹¹⁰³ insertion. Genomic sequence in capital letters, 8 bp direct repeat flanking *P{PZ}* in red. (I) Generation of the *hts*^{null} mutation. Almost the complete region of the *hts* locus containing exons (blue box) was removed by Flp mediated recombination of *FRT* sites in the P-elements *PBac{WH}hts*⁰²⁷⁶² and *P{RS5}hts*^{5-SZ-4016}. (J-K) Immunoblots of lysates from eye-brain complexes of control (lane 1), homozygous *hts*^{ΔG} (lane 2), hemizygous *hts*⁰¹¹⁰³ (lane 3) and homozygous *hts*^{W532X} (lane 4) 3rd instar larvae probed with Hts antibody (J) htsF or (K) 1B1.

The majority of medullae from both *hts*^{null} mosaic and *hts*⁰¹¹⁰³ hemizygous flies have strong defects (Table 3.4), but compared to the latter ones, medullae from *hts*^{null} mosaic flies more often exhibit still severe yet somewhat milder defects (Figure 3.4F). This finding may be explained by the different genetic backgrounds, but it may also be attributed to the use of the Flp/FRT system. In the mosaic flies, the majority of the cells of the eye are homozygous for *hts*^{null}, but a small fraction stays heterozygous as the rest of the body does. Moreover, some wild type Hts protein from their heterozygous progenitors may persist in these homozygous mutant cells. Both could contribute to the attenuation of the defects observed in *hts*^{null} mosaic flies compared to the *hts*⁰¹¹⁰³ hemizygous

flies. Assuming that a low amount of Hts protein that is below the detection limit of western blots is expressed from the *hts*⁰¹¹⁰³ allele, the use of the Flp/FRT system in addition to the doubled gene dosage in homozygous *hts*⁰¹¹⁰³ compared to hemizygous cells may also explain the absence of defects in *hts*⁰¹¹⁰³ mosaic flies.

3.5 β -Spectrin mutants show defects in photoreceptor axon guidance

The close functional conjunction of human Adducin and Spectrin and the kindred localization of Hts and Spectrin to fusomes, spectrosomes and the submembranous regions of follicle cells (Lin et al. 1994; de Cuevas et al. 1996) suggested that Hts may cooperate with Spectrin also in flies. Indeed, mosaic flies with homozygous β -*Spec*^{G113} (Hulsmeier et al. 2007) mutant eyes show defects in the medulla qualitatively similar to, but even more severe than those caused by the loss of *hts*. All of the medullae examined (n=6) appeared overall disorganized (Figure 3.5). Axons took aberrant pathways within the medulla and formed inappropriate bundles, destroying the regular array of axons.

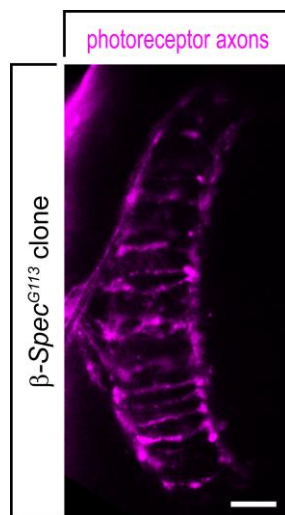


Figure 3.5: β -Spectrin mutants show defects in photoreceptor axon guidance

Medullae of flies with eye clones homozygous for the β -Spectrin mutation β -*Spec*^{G113} exhibit defects qualitatively similar but more severe compared to the defects caused by the loss of *hts*. Anterior up, lateral left. Scale bar: 10 μ m.

The resemblance between the defects caused by β -Spectrin and *hts* mutations affirms the assumption that Hts may collaborate with Spectrin to execute its function in photoreceptor axon guidance.

3.6 *swallow* mutants do not show defects in photoreceptor axon guidance

mRNA trafficking and local protein synthesis in the axon, especially of cytoskeletal and cytoskeleton associated proteins, are essential for proper axon pathfinding (reviewed by Yoon et al. 2009)). For example, the steering of *X. laevis* retinal growth cones towards Netrin-1 requires the local synthesis of β -Actin in the axon (Campbell and Holt 2001; Leung et al. 2006), whereas their collapse mediated by the repellent Slit-2 requires local translation of cofilin (Piper et al. 2006).

In the *Drosophila* oocyte and early embryo, the targeting of specific mRNAs to distinct subcellular compartments is required to establish the anterior-posterior and the dorsal-ventral axes (reviewed by Bashirullah et al. 1998)). One of these localized mRNAs is encoded by *hts*, and its correct localization in the oocyte and the embryo is dependent on maternal *swallow* (Yue and Spradling 1992; Ding et al. 1993; Whittaker et al. 1999). Although only the localization of the *hts* transcript encoding Ovhts has been shown to be affected by *swallow* mutations, it was tempting to test if *swallow* mutants would show defects in photoreceptor axon pathfinding. Two *swallow* alleles that both were shown to affect *hts* mRNA localization in the Oocyte (Ding et al. 1993; Whittaker et al. 1999; Pokrywka et al. 2004), *swa*¹ and *swa*³, were tested for defects in the adult medulla. However, neither homozygous *swa*¹ (n=3, Figure 3.6A) nor homozygous *swa*³ (n=3, Figure 3.6B) mutants showed any observable defect in the medulla.

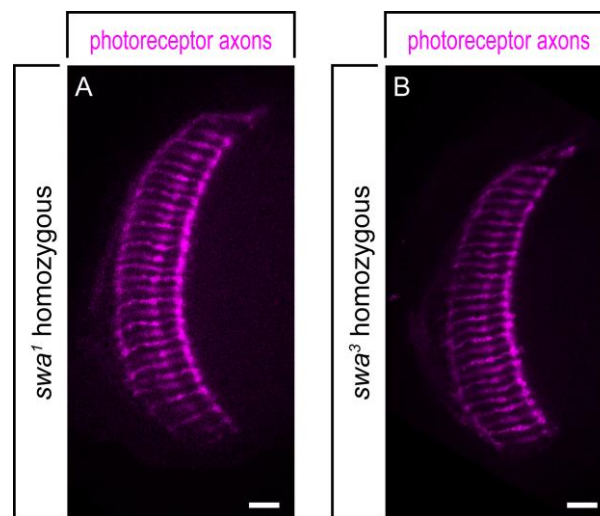


Figure 3.6: *swallow* mutants do not show defects in photoreceptor axon guidance

Neither (A) homozygous *swa*¹ nor (B) homozygous *swa*³ mutants show observable defects due to impaired photoreceptor axon guidance in the adult medulla. Anterior up, lateral left. Scale bars: 10 μ m.

3.7 Add1 and HtsPD rescue *hts*⁰¹¹⁰³ hemizygous flies but ShAdd does not

To test which of the Hts protein isoforms function in photoreceptor axon guidance in vivo, transgenic flies were generated that hold constructs encoding the different Hts isoforms under

direct control of the *GMR* promoter. Two independent transgenic insertions of each construct were tested for their ability to rescue *hts*⁰¹¹⁰³ hemizygous flies. To exclude that their presence causes severe defects in the medulla on its own, flies holding the constructs in a wild type background were examined. In none of them any obvious defect in the medulla was observed (Figure 3.7.1, n=4 each).

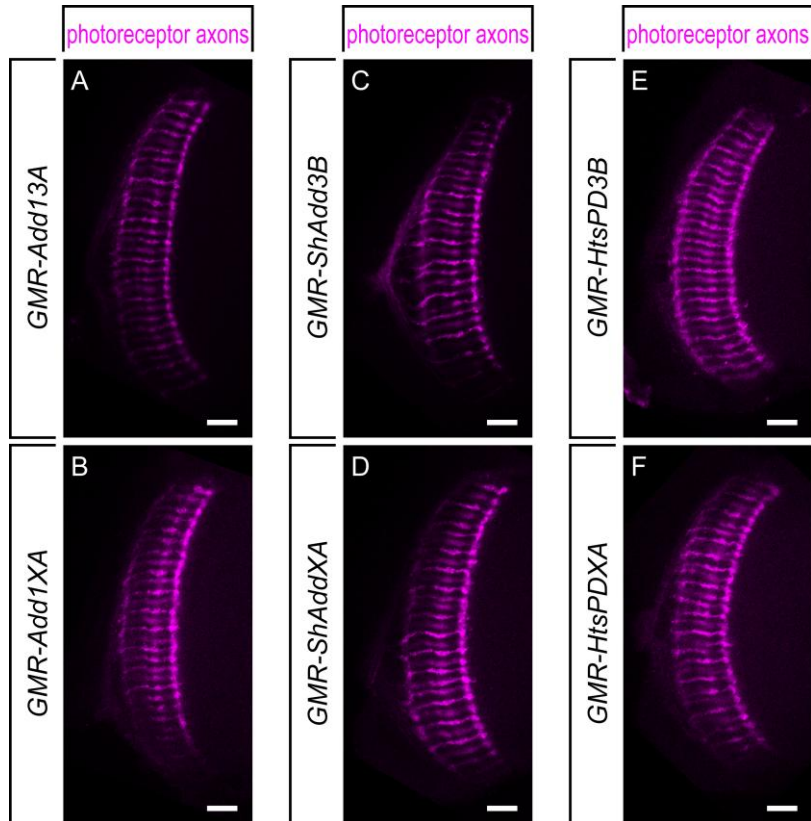


Figure 3.7.1: The *hts* rescue constructs do not cause defects in the medulla on their own

None of each two independent insertions of the *hts* rescue constructs encoding (A-B) Add1, (C-D) ShAdd or (E-F) HtsPD causes detectable defects in the adult medulla. Anterior up, lateral left. Scale bars: 10 μ m.

To test their ability to rescue *hts*⁰¹¹⁰³ hemizygous flies, the extent of defects in the medulla of flies holding the different rescue constructs in the mutant background was estimated blindly. Whereas almost always more than 50 % of the medulla was defective when no rescue construct (8 of n=9, Figure 3.7.2A, Table 3.7) or *GMR-ShAdd* (13 of n=14, Figure 3.7.2D and 8 of n=10, Figure 3.7.2E, Table 3.7) was present, both *GMR-Add1* and *GMR-HtsPD* eliminated the defects to a large extent. At least approximately half of the medullae from flies holding *GMR-Add1* (8 of n=17, Figure 3.7.2B and 8 of n=10, Figure 3.7.2C, Table 3.7) or *GMR-HtsPD* (16 of n=16, Figure 3.7.2F and 5 of n=10, Figure 3.7.2G, Table 3.7) were defective only up to 50 %.

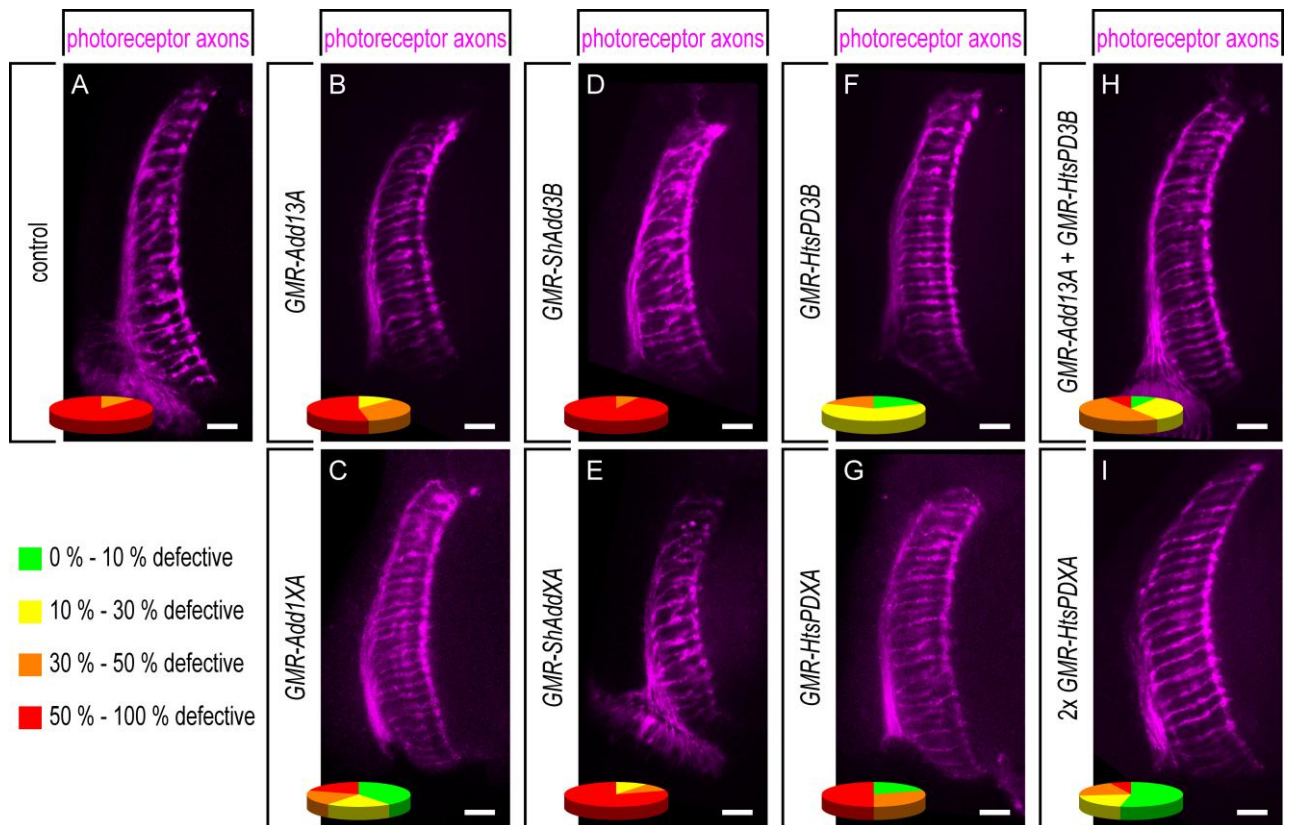


Figure 3.7.2: Ability of different rescue constructs to rescue *hts*⁰¹¹⁰³ hemizygous flies

The indicated rescue constructs were tested for their ability to compensate for the (A) defects in the medulla of *hts*⁰¹¹⁰³ hemizygous flies. Pie charts show the fraction of examined medullae that are defective to 0 % - 10 % (green), 10 % - 30 % (yellow), 30 % - 50 % (orange) and 50 % - 100 % (red), respectively (see also Table 3.7). (B-C) Two independent insertions of *GMR-Add1* rescued the mutants at least partially. (D-E) None of the two insertions of *GMR-ShAdd* that were tested clearly reduced the defects in the medulla. (F-G) At least half of the medullae of *hts*⁰¹¹⁰³ hemizygous flies expressing HtsPD in their photoreceptors are defective only up to 50 %. (H) *GMR-Add1* and *GMR-HtsPD* together do not reduce the defects better than (I) two copies of *GMR-HtsPD* do. Anterior up, lateral left. Scale bars: 10 μ m.

Since none of the rescue constructs eliminated the defects completely, it seemed possible that both Hts protein isoforms Add1 and HtsPD instead of either one may be required for proper axon guidance. This was tested by coexpressing both Add1 and HtsPD in *hts*⁰¹¹⁰³ hemizygous photoreceptors. To exclude that a better rescue potentially observed in the flies expressing both protein isoforms could be ascribed rather to a higher amount of Hts protein in general than to the presence of the two different isoforms, flies holding two copies of *GMR-HtsPD* were used as control. However, the extent of defects in the medulla of flies with the combination of *GMR-Add1* and *GMR-HtsPD* was not less than in flies holding two copies of *GMR-HtsPD* (Figures 3.7.2H-I, Table 3.7).

rescue construct	0 % - 10 % defective	10 % - 30 % defective	30 % - 50 % defective	50 % - 100 % defective
none (n=9)	0	0	1 / 11 %	8 / 89 %
<i>GMR-Add13A</i> (n=17)	0	2 / 12 %	6 / 35 %	9 / 53 %
<i>GMR-Add1XA</i> (n=10)	4 / 40 %	2 / 20 %	2 / 20 %	2 / 20 %
<i>GMR-ShAdd3B</i> (n=14)	0	0	1 / 7 %	13 / 93 %
<i>GMR-ShAddXA</i> (n=10)	0	1 / 10 %	1 / 10 %	8 / 80 %
<i>GMR-HtsPD3B</i> (n=16)	3 / 19 %	10 / 63 %	3 / 19 %	0
<i>GMR-HtsPDXA</i> (n=10)	2 / 20 %	0	3 / 30 %	5 / 50 %
<i>GMR-Add13A</i> <i>GMR-HtsPD3B</i> (n=12)	1 / 8 %	4 / 33 %	6 / 50 %	1 / 8 %
<i>GMR-HtsPD3B</i> <i>GMR-HtsPD3B</i> (n=15)	8 / 53 %	3 / 20 %	3 / 20 %	1 / 7 %

Table 3.7: Ability of different rescue constructs to rescue *hts*⁰¹¹⁰³ hemizygous flies

Flies that were hemizygous for *hts*⁰¹¹⁰³ and held the rescue constructs listed in the left column were assayed blindly for defects in the medulla. Each two independent transgenic insertions were used. Also flies that held both *GMR-Add1* and *GMR-HtsPD* were examined as were flies with two copies of *GMR-HtsPD*. For each genotype, the numbers / percentages of medullae that were defective up to 10 %, to 10 % - 30 %, to 30 % - 50 % or to more than 50 % are quoted.

3.8 Mutating putative phosphorylation sites in Hts does not affect its interaction with Gogo

Adducin is functionally regulated by Calmodulin binding to its MARCKS-related domain and by phosphorylation (Ling et al. 1986; Gardner and Bennett 1987; Matsuoka et al. 1996; Matsuoka et al. 1998). α -Adducin is phosphorylated by PKA, PKC, and Rho-kinase at Serine or Threonine residues at positions 408, 436, 445, 480, and 481, which lie within or a little downstream of the neck domain, and at two Serine residues in the MARCKS related domain (Matsuoka et al. 1996; Fukata et al. 1999).

The physical interaction between Gogo and Hts suggests that they may form a functional complex that guides photoreceptor axons. The function of this complex could be controlled by regulating the binding of Hts and Gogo, potentially via phosphorylation of Hts. Candidate phosphorylation sites that may regulate the binding of Hts to Gogo to form a functional complex should be common among Add1 and HtsPD, because both protein isoforms are able to function in photoreceptor axon guidance. Contrarily, they should not be included in ShAdd, as it does not function in photoreceptor axon guidance. The only phosphorylation sites of α -Adducin that lie within a region that fulfills these criteria are the Threonine residue at position 480 and the Serine residue at position 481. In

its homologous region, Hts possesses a Serine residue at position 478, a Threonine residue at position 480, a Serine residue at position 482, and a Threonine residue at position 483.

To test the relevance of these amino acid residues for the interaction between Hts and Gogo, three artificial constructs were generated that comprise the amino acid residues 1 to 658 of Hts that constitute the part of Hts that is common to Add1 and HtsPD (Figure 1.6). In one construct (Hts^{AAAA}-His), the above mentioned amino acid residues were changed to Alanine residues, preventing phosphorylation. In the second one (Hts^{DEDE}-His), they were changed to Aspartic acid and Glutamic acid residues, respectively, which can partially mimic phosphorylated Serine or Threonine residues (Thomas et al. 1998). No changes to the wild type sequence were made in the third one (Hts⁶⁵⁸-His). All three Hts fragments feature a C-terminal 6xHis-tag.

As revealed by coimmunoprecipitation with Gogo-Myc from the lysates of *Drosophila* Schneider cells that coexpressed Hts⁶⁵⁸-His, Hts^{AAAA}-His or Hts^{DEDE}-His, all three Hts fragments bind equally well to Gogo (Figure 3.8). The putative phosphorylation sites in Hts are not required for the binding to Gogo.

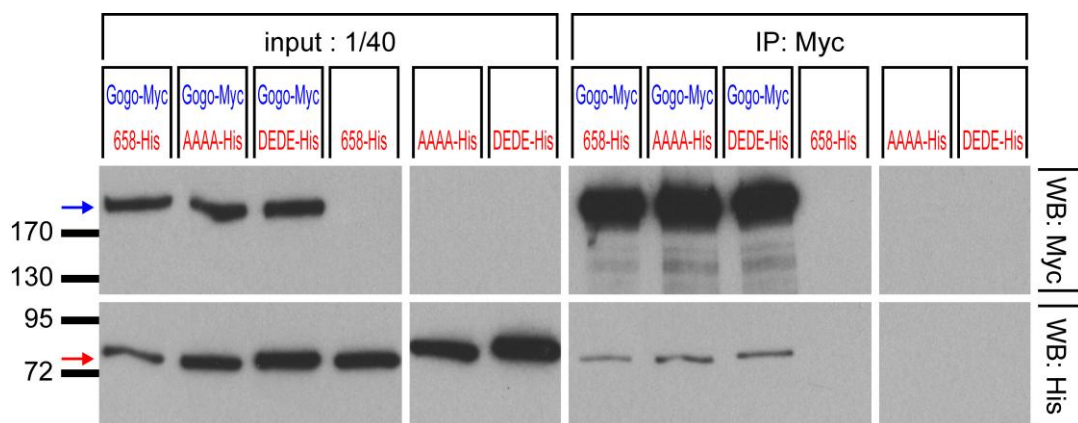


Figure 3.8: Mutating putative phosphorylation sites in Hts does not affect Gogo binding

Drosophila Schneider cells expressed the indicated Hts construct alone as control (lanes 4 to 6) or together with Gogo-Myc (lanes 1 to 3). Hts⁶⁵⁸-His, Hts^{AAAA}-His, and Hts^{DEDE}-His all coimmunoprecipitated with Gogo-Myc (lanes 7 to 9) but were absent from the control (lanes 10 to 12).

3.9 Add1 and HtsPD rescue *hts*^{null} mosaic flies

The different rescue constructs were also tested for their ability to rescue *hts*^{null} mosaic flies that expressed GFP as a marker to label R8 axons. Here, flies that had inherited the rescue construct could not be distinguished by eye from their siblings that had not. Instead, htsF antibody staining was used to identify flies that possessed the rescue construct. Again, two independent insertions of each construct were used.

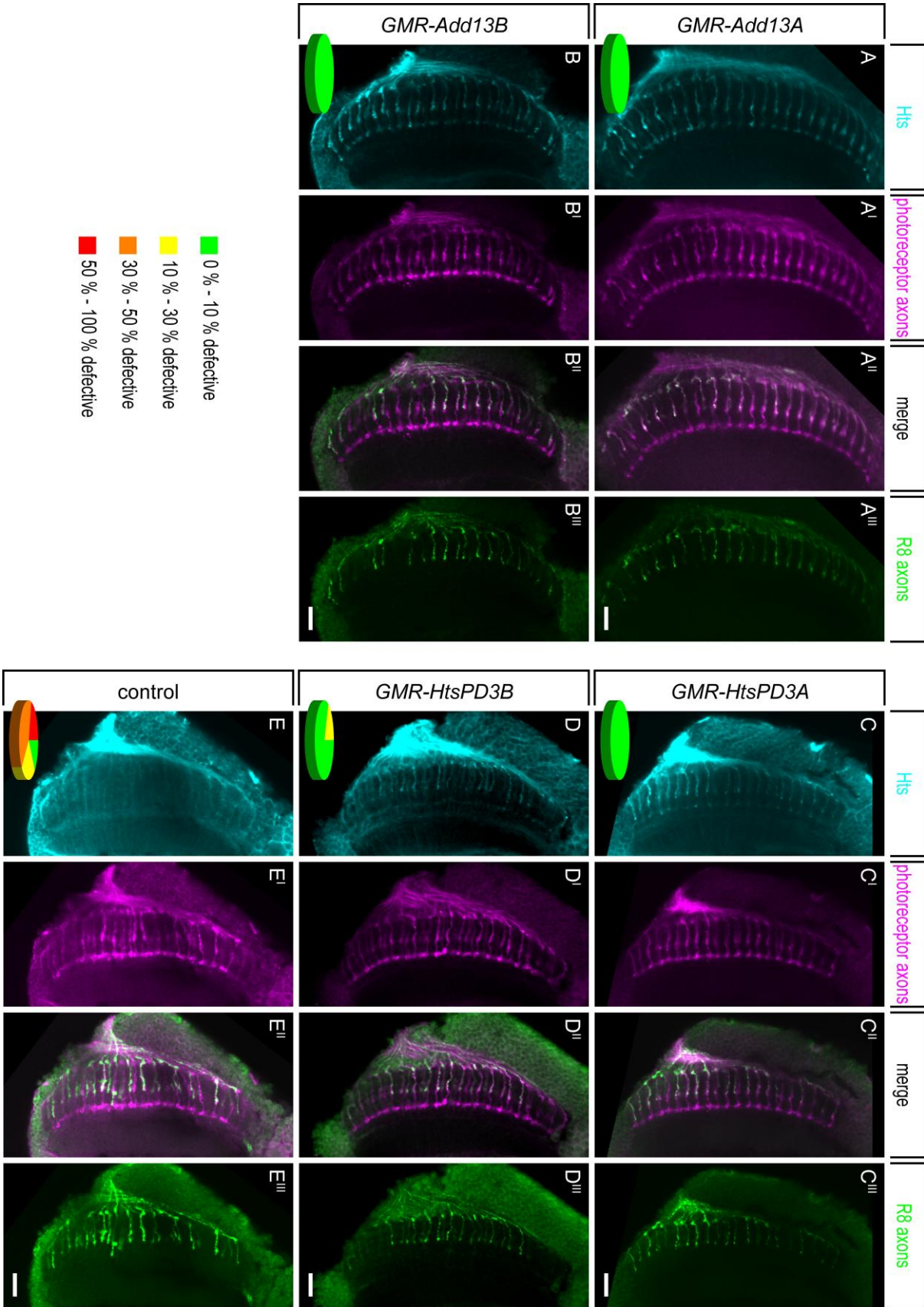


Figure 3.9: Add1 and HtsPD rescue *hts^{null}* mosaic flies

Mosaic flies that were overall heterozygous but had eyes consisting almost completely of cells homozygous for *hts^{null}* expressed the indicated Hts isoform under direct control of the *GMR* promoter. Each two independent insertions of the rescue constructs were used. Both (A-B) Add1 and (C-D) HtsPD almost completely suppressed the defects seen in the medulla of (E) control flies that did not exhibit detectable Hts protein in the photoreceptors in the medulla. Pie charts show the fraction of examined medullae that are defective to 0 % - 10 % (green), 10 % - 30 % (yellow), 30 % - 50 % (orange) and 50 % - 100 % (red), respectively (see also Table 3.9). Anterior up, lateral left. Scale bars: 10 μ m.

As expected, Add1 could be detected in some (6 of n=14, Figure 3.9A and 12 of n=21, Figure 3.9B, respectively) medullae of flies tested for *GMR-Add13A* or *GMR-Add13B*, but not in their siblings. Similarly, some (8 of n=17, Figure 3.9C and 11 of n=14, Figure 3.9D, respectively) medullae were positive for HtsPD and the remaining ones were not when tested for *GMR-HtsPD3A* or *GMR-HtsPD3B*. However, ShAdd was never detected in the medulla when flies were tested for either *GMR-ShAdd3A* (n=13) or *GMR-ShAdd3B* (n=14).

Both Add1 and HtsPD were able to rescue the defects caused by *hts^{null}* in the medulla. When the extent of defects in the medulla was estimated blindly, all medullae with photoreceptor axons positive for either Add1 (n=6, Figure 3.9A and n=8, Figure 3.9B) or HtsPD (n=8, Figure 3.9C and n=11, Figure 3.9D) were rated to be defective up to 30 % at the most (Table 3.9). Contrariwise, the majority (18 of n=29) of medullae with photoreceptor axons negative for Hts were rated to be defective to at least 30 % (Figure 3.9E, Table 3.9).

rescue construct	0 % - 10 % defective	10 % - 30 % defective	30 % - 50 % defective	50 % - 100 % defective
none (n=29)	4 / 14 %	7 / 24 %	12 / 41 %	6 / 21 %
<i>GMR-Add13A</i> (n=6)	6 / 100 %	0	0	0
<i>GMR-Add13B</i> (n=12)	12 / 100 %	0	0	0
<i>GMR-HtsPD3A</i> (n=8)	8 / 100 %	0	0	0
<i>GMR-HtsPD3B</i> (n=11)	9 / 82 %	2 / 18 %	0	0

Table 3.9: Ability of different rescue constructs to rescue *hts^{null}* mosaic flies.

Heterozygous flies with eyes comprising large clones of *hts^{null}* homozygous cells that held the rescue constructs listed in the left column were assayed blindly for defects in the medulla. Each two independent transgenic insertions were used. For each genotype, the numbers / percentages of medullae that were defective up to 10 %, to 10 % - 30 %, to 30 % - 50 % or to more than 50 % are quoted.

Interestingly, the isoform-specific rescue experiment shows that the C-terminal MARCKS-related domain included in Add1 but not HtsPD is not required to rescue the defects in the medulla caused by *hts*. This is consistent with the lack of defects in homozygous *hts^{4G}* mutant flies (Figure 3.4A, Table 3.4), which have only truncated Hts protein lacking the MARCKS-related domain. Both were

surprising, since the MARCKS-related domain of Adducin has been shown to be required for all of its known activities in vitro (Li et al. 1998; Matsuoka et al. 2000).

3.10 ShAdd does not localize to photoreceptor axons

ShAdd was never detected in photoreceptor axons in the medulla when looking for flies that had inherited the *GMR-ShAdd* rescue construct, suggesting that ShAdd may not be able to localize to photoreceptor axons. To test this, transgenic flies that held the *GMR-ShAdd* rescue construct in an otherwise wild type background were probed with htsF antibody. Indeed, htsF did not label the photoreceptor axons in the medulla of any of the two transgenic lines tested (Figures 3.10C-D) or in wild type flies without a transgenic construct (Figure 3.10A) but did clearly label them in control flies that expressed Add1 (Figure 3.10B).

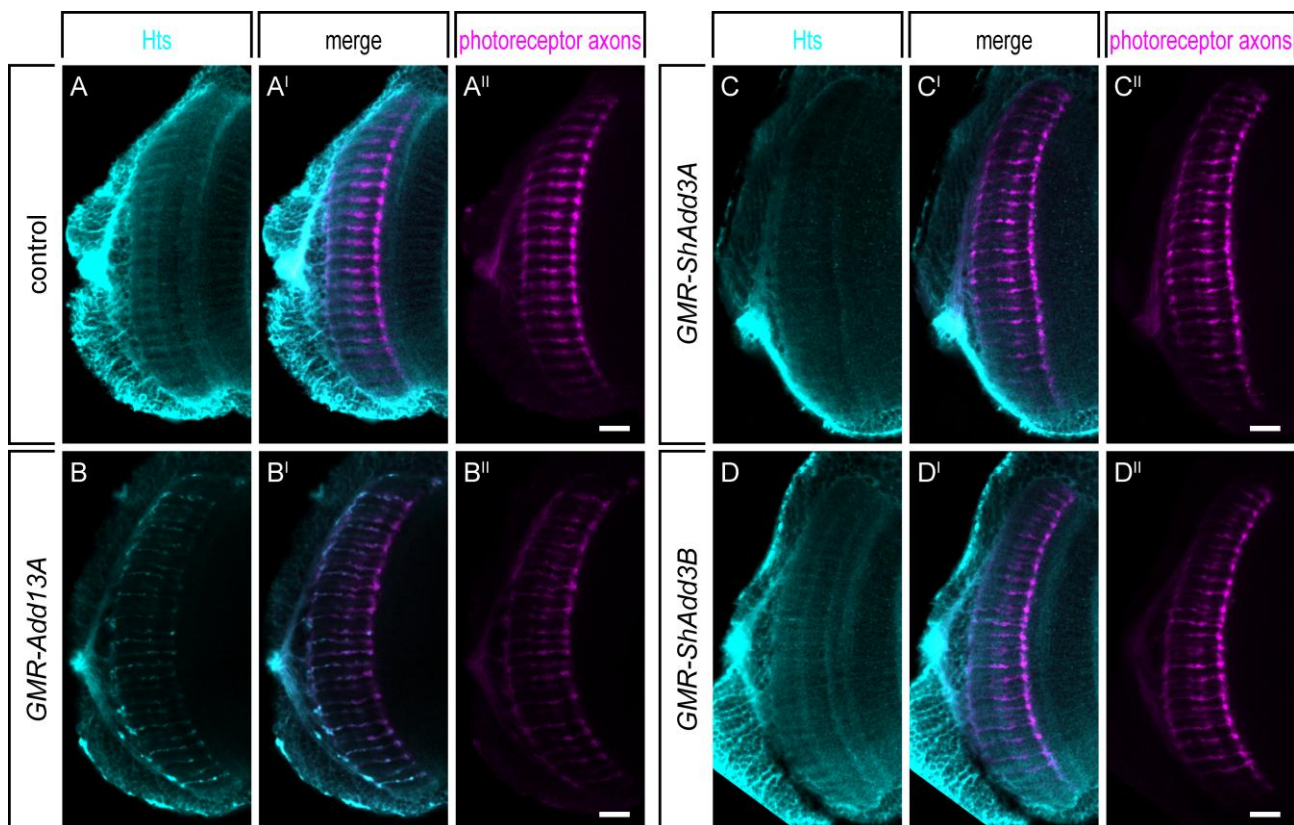


Figure 3.10: ShAdd does not localize to photoreceptor axons

(A) The antibody htsF does not label photoreceptor axons in the medulla of wild type flies (n=5). (B) Add1 is clearly detected in photoreceptor axons of *GMR-Add13A* transgenic flies that served as a positive control (n=9). In contrast, the photoreceptor axons are not labeled in the medullae of (C) *GMR-ShAdd3A* (n=6) or (D) *GMR-ShAdd3B* (n=5) transgenic flies. Anterior up, lateral left. Scale bars: 10 μ m.

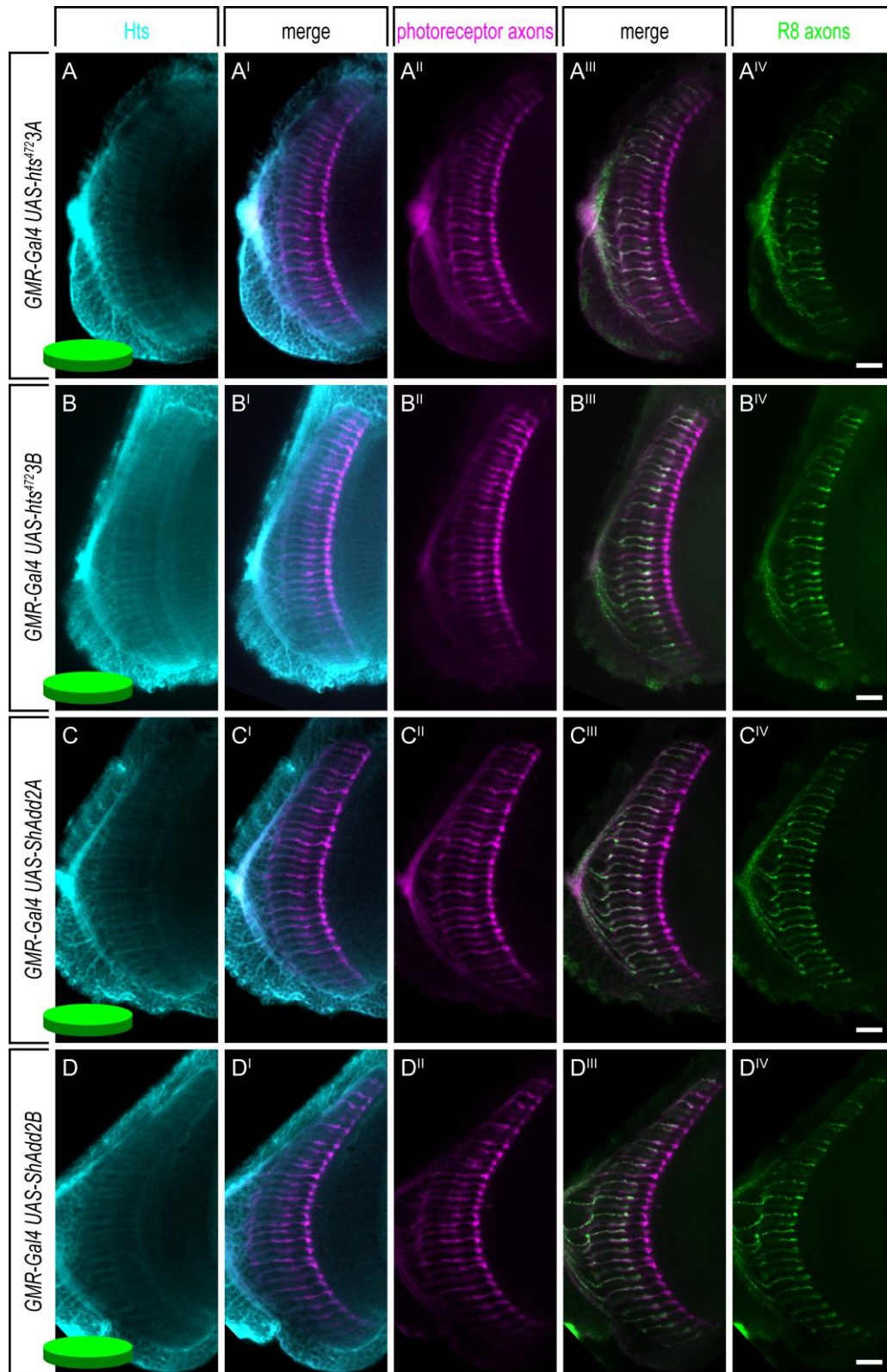
The same result was obtained when ShAdd and Add1, respectively, were encoded by *UAS* constructs. The examined flies possessed the *GMR-Gal4* driver and a construct encoding ShAdd or Add1 under control of the *UAS* promoter. Again, each two independent insertions were used. *htsF* clearly labels the photoreceptor axons in the medulla of flies expressing Add1 (n=10, Figure 3.11F and 8 of n=13, Figure 3.11G), but does not label them in flies with a *UAS* construct encoding ShAdd (n=5, Figure 3.11C and n=3, Figure 3.11D) or in flies with only the Gal4 driver but without a *UAS* target (n=6, Figure 3.11E). This indicates that at least some part of the tail domain of Hts that is covered by Add1 and HtsPD but not ShAdd is required for the presence of Hts in photoreceptor axons or, alternatively, that the unique 23 amino acids at the C-terminus of ShAdd are responsible for its absence from the axons.

It was not ascertained if this absence of ShAdd was due to reduced translation, degradation, impaired transport to or efficient removal from the axon. Either way, the absence of ShAdd protein from photoreceptor axons can account for the failure of *GMR-ShAdd* to rescue the defects caused by *hts*.

3.11 The tail domain of Hts is required for its localization to the axon

To test whether the absence of ShAdd from R7 / R8 axons was due to the lack of the tail domain or to the presence of its unique 23 amino acids, Hts⁴⁷², the part of Hts which is common to all Hts protein isoforms, was tested for its localization to photoreceptor axons in the medulla.

The examined flies possessed the *GMR-Gal4* driver and a construct encoding Hts⁴⁷² under control of the *UAS* promoter. As usual, two independent insertions were examined. In none of them did *htsF* detect Hts⁴⁷² in the photoreceptor axons in the medulla (n=4, Figure 3.11A and n= 4, Figure 3.11B), revealing that the tail domain of Hts is indeed required for the presence of Hts in R7 / R8 axons.



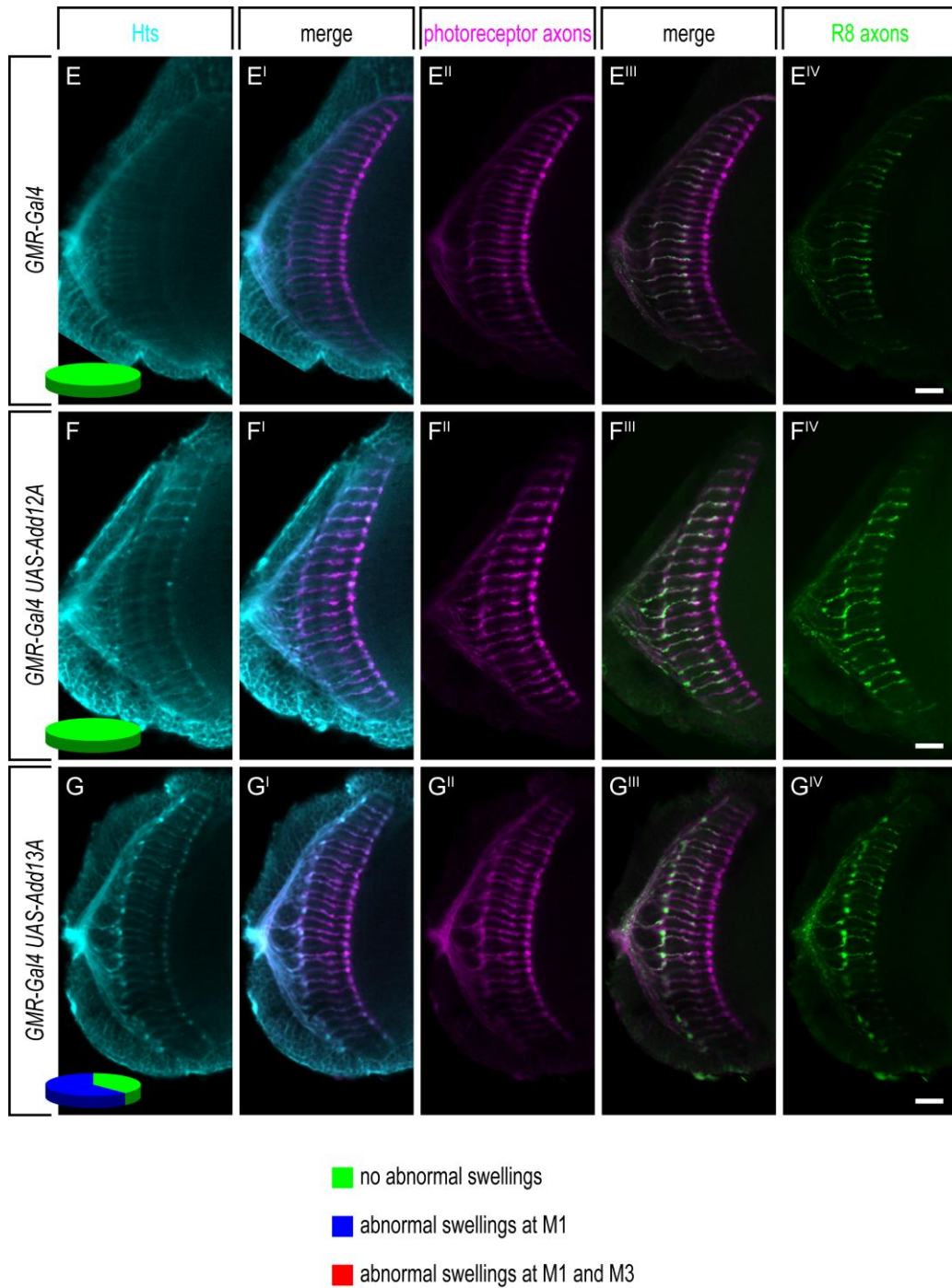
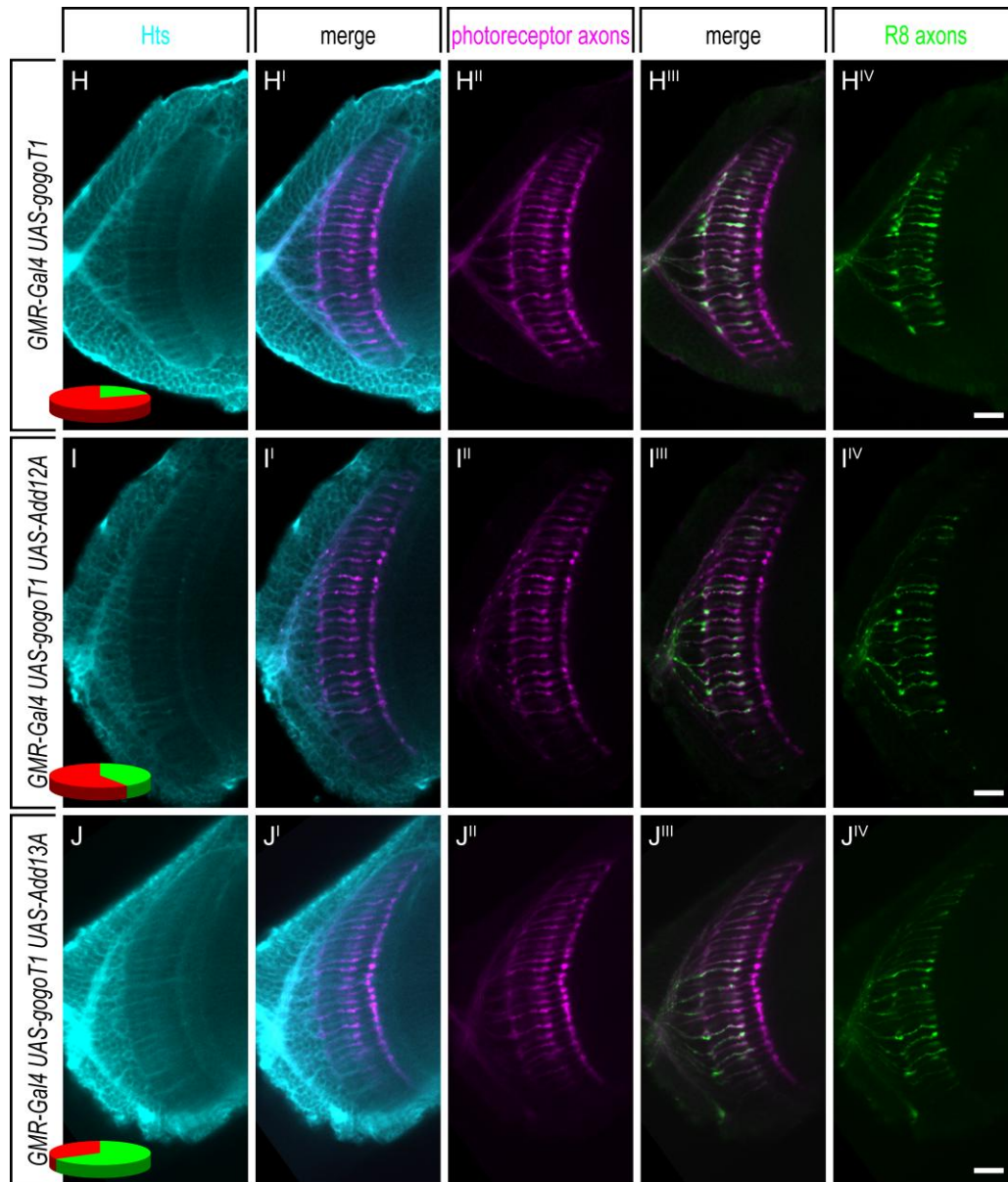
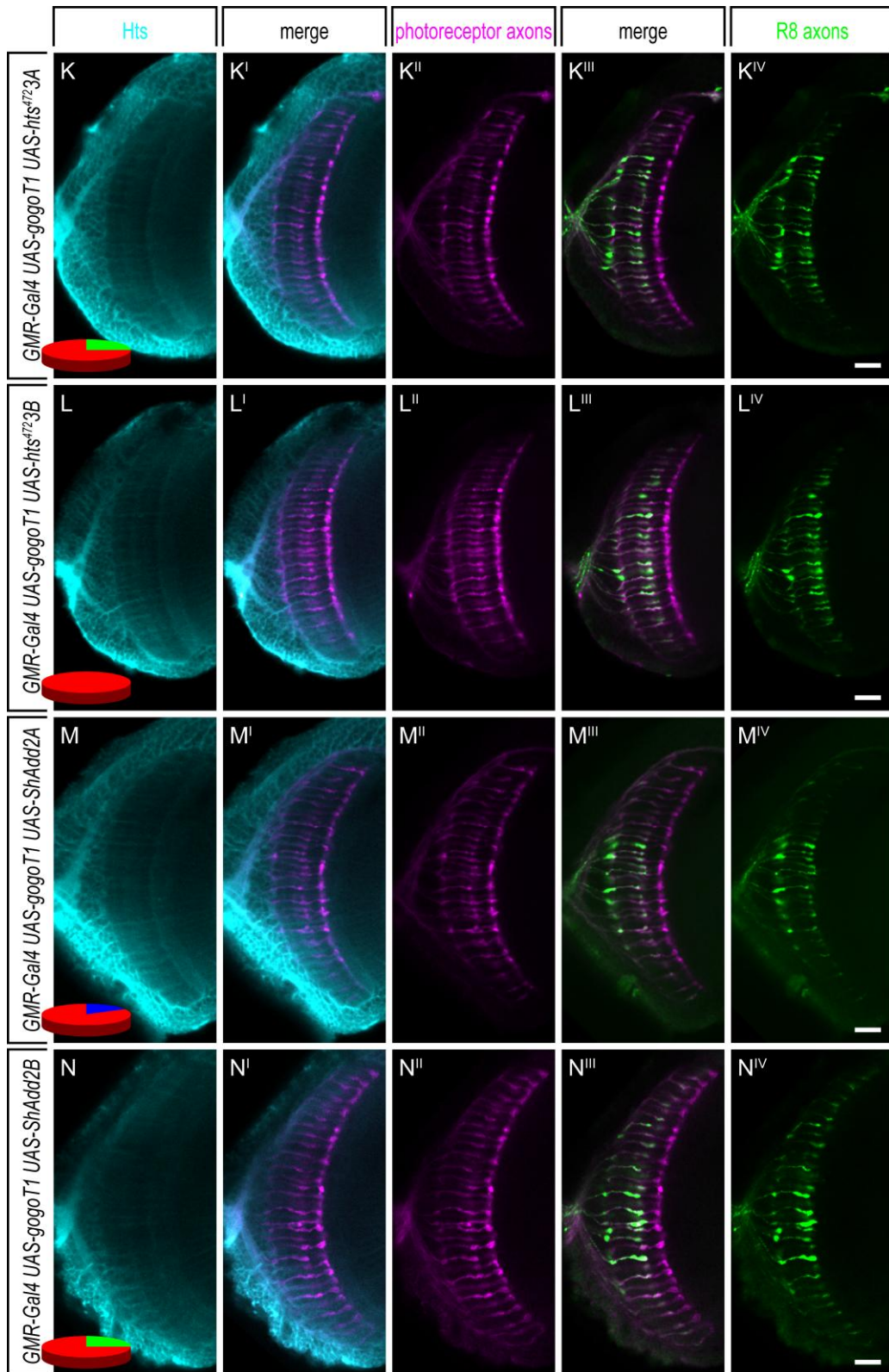


Figure 3.11: Overexpression of different Hts constructs

(A-B) Hts can not be detected by immunostaining in photoreceptor axons of flies that have the *GMR-Gal4* driver and either of two independent insertions of a construct encoding Hts⁴⁷² under control of the *UAS* promoter. Neither of the two insertions causes any abnormality in the medulla. (C-D) The same holds true for a construct encoding ShAdd under control of the *UAS* promoter. Hts can not be detected in photoreceptor axons and neither of two independent insertions causes abnormalities in the medulla. Unlike in the (E) control, Add1 can be detected when expressed from either of the two transgenic insertions (F) *UAS-Add12A* or (G) *UAS-Add13A*. Expression of Add1 from *UAS-Add13A* causes R8



axons to form abnormally thick swellings at the M1 layer of the medulla. (H) Excessive Gogo causes R8 axons to form abnormally thick swellings at both the M1 and the M3 layer. (I-J) These abnormal swellings are suppressed when Add1 is co-overexpressed from either of the two insertions *UAS-Add12A* or *UAS-Add13A*. Moreover, the amount of Add1 protein seems to be dramatically decreased when compared to flies with an endogenous Gogo level. Neither of each two independent insertions encoding (K-L) *Hts*⁴⁷² or (M-N) ShAdd under control of the *UAS* promoter has a marked effect on the defects caused by excessive Gogo. Anterior up, lateral left. Scale bars: 10 μ m.



genotype	no abnormal swellings	swellings at M1	swellings at M1 and M3
<i>GMR-Gal4</i> (n=6)	6 / 100 %	0	0
<i>GMR-Gal4 UAS-hts⁴⁷²3A</i> (n=4)	4 / 100 %	0	0
<i>GMR-Gal4 UAS-hts⁴⁷²3B</i> (n=4)	4 / 100 %	0	0
<i>GMR-Gal4 UAS-Add12A</i> (n=10)	10 / 100 %	0	0
<i>GMR-Gal4 UAS-Add13A</i> (n=13)	5 / 38 %	8 / 62 %	0
<i>GMR-Gal4 UAS-ShAdd2A</i> (n=5)	5 / 100 %	0	0
<i>GMR-Gal4 UAS-ShAdd2B</i> (n=3)	3 / 100 %	0	0
<i>GMR-Gal4 UAS-gogoT1</i> (n=5)	1 / 20 %	0	4 / 80 %
<i>GMR-Gal4 UAS-gogoT1</i> <i>UAS-hts⁴⁷²3A</i> (n=4)	1 / 25 %	0	3 / 75 %
<i>GMR-Gal4 UAS-gogoT1</i> <i>UAS-hts⁴⁷²3B</i> (n=4)	0	0	4 / 100 %
<i>GMR-Gal4 UAS-gogoT1</i> <i>UAS-Add12A</i> (n=17)	7 / 41 %	0	10 / 59 %
<i>GMR-Gal4 UAS-gogoT1</i> <i>UAS-Add13A</i> (n=9)	6 / 67 %	0	3 / 33 %
<i>GMR-Gal4 UAS-gogoT1</i> <i>UAS-ShAdd2A</i> (n=6)	0	1 / 17 %	5 / 83 %
<i>GMR-Gal4 UAS-gogoT1</i> <i>UAS-ShAdd2B</i> (n=4)	1 / 25 %	0	3 / 75 %

Table 3.11: Effects of different transgenic *hts* constructs

Flies with the *GMR-Gal4* driver and the transgenic insertions listed in the left column were assayed blindly for abnormal swellings of R8 axons. For each genotype, the numbers / percentages of medullae assessed to have no remarkable swellings, abnormal swellings at the M1 or at the M1 and the M3 layer are quoted.

3.12 Overexpression of Add1 and Gogo cause similar but different defects in the medulla

In flies that expressed GFP as a marker in R8 axons and that possessed the *GMR-Gal4* driver, the presence of the *UAS-Add13A* insertion caused R8 axons to form abnormally thick swellings at the M1 layer (8 of n=13, Figure 3.11G, Table 3.11). Interestingly, a similar gain-of-function phenotype was reported for Gogo. When it is expressed from the transgenic insertion *UAS-gogoT1*, R8 axons exhibit abnormal swellings at the M1 and the M3 layer (4 of n=5, Figure 3.11H, Table 3.11 and Tomasi et al. 2008). The same defects were also observed when *gogo* was expressed from other transgenic insertions. *UAS-gogoT3* is another insertion of the same construct as in *UAS-gogoT1*,

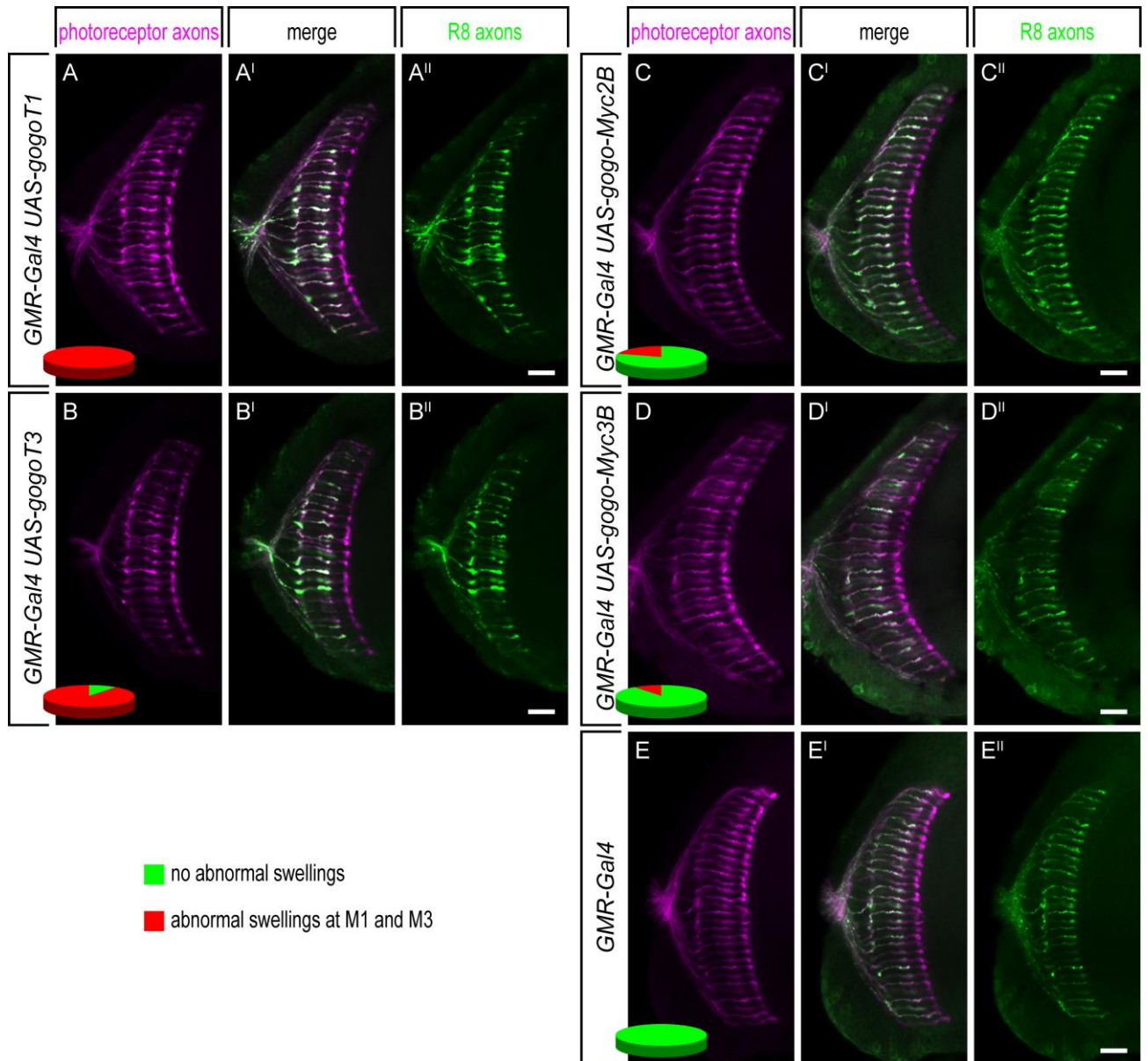


Figure 3.12.1: Defects of photoreceptor axons in the medulla caused by excessive Gogo

Medullae of flies with the indicated genotype were assayed blindly for abnormal swellings of R8 axons at M1 and M3. Almost all medullae from flies overexpressing Gogo from the (A) *UAS-gogoT1* or the (B) *UAS-gogoT3* insertion were assessed to have abnormal swellings at M1 and M3. When Gogo was expressed from either the (C) *UAS-gogo-Myc2B* or the (D) *UAS-gogo-Myc3B* insertion, only a small fraction of the medullae examined were assessed to show these abnormal swellings. (E) Medullae from control flies with the *GMR-Gal4* driver but no *UAS* target always look normal, demonstrating that the defects are indeed due to the excessive Gogo protein. See also Table 3.12. Anterior up, lateral left. Scale bars: 10 μ m.

which encodes untagged full-length Gogo. *UAS-gogo-Myc2B* and *UAS-gogo-Myc3B* are two independent insertions of a construct that encodes C-terminally 4xMyc-tagged full-length Gogo.

Abnormal swellings at M1 and M3 were observed at least in a small fraction of medullae from flies that had either one of these transgenic *gogo* insertions and the *GMR-Gal4* driver, but never in the control flies that had the *GMR-Gal4* driver without a *UAS* target (Figure 3.12.1, Table 3.12). Therefore, *hts* and *gogo* cause not only similar loss-of-function, but also similar gain-of-function phenotypes, indicating again that they act together in a common pathway to guide photoreceptor axons.

genotype	no abnormal swellings	swellings at M1	swellings at M1 and M3
<i>GMR-Gal4 UAS-gogoT1</i> (n=10)	0	0	10 / 100 %
<i>GMR-Gal4 UAS-gogoT3</i> (n=10)	1 / 10 %	0	9 / 90 %
<i>GMR-Gal4 UAS-gogo.Myc2B</i> (n=10)	8 / 80 %	0	2 / 20 %
<i>GMR-Gal4 UAS-gogo-Myc3B</i> (n=10)	9 / 90 %	0	1 / 10 %
<i>GMR-Gal4</i> (n=18)	18 / 100 %	0	0

Table 3.12: Penetrance of several insertions of constructs encoding Gogo

Flies with the *GMR-Gal4* driver and the transgenic insertions listed in the left column were assayed blindly for abnormal swellings of R8 axons. For each genotype, the numbers / percentages of medullae assessed to have no remarkable swellings, abnormal swellings at the M1 or at the M1 and the M3 layer are quoted.

However, a second transgenic insertion of the *UAS-Add1* construct, *UAS-Add12A*, did not cause any noticeable abnormalities (n=10, Figure 3.11F, Table 3.11). This is probably due to the lower expression level of *Add1* from this transgenic insertion, as judged from the intensity of *Hts* immunostainings (Figure 3.12.2).

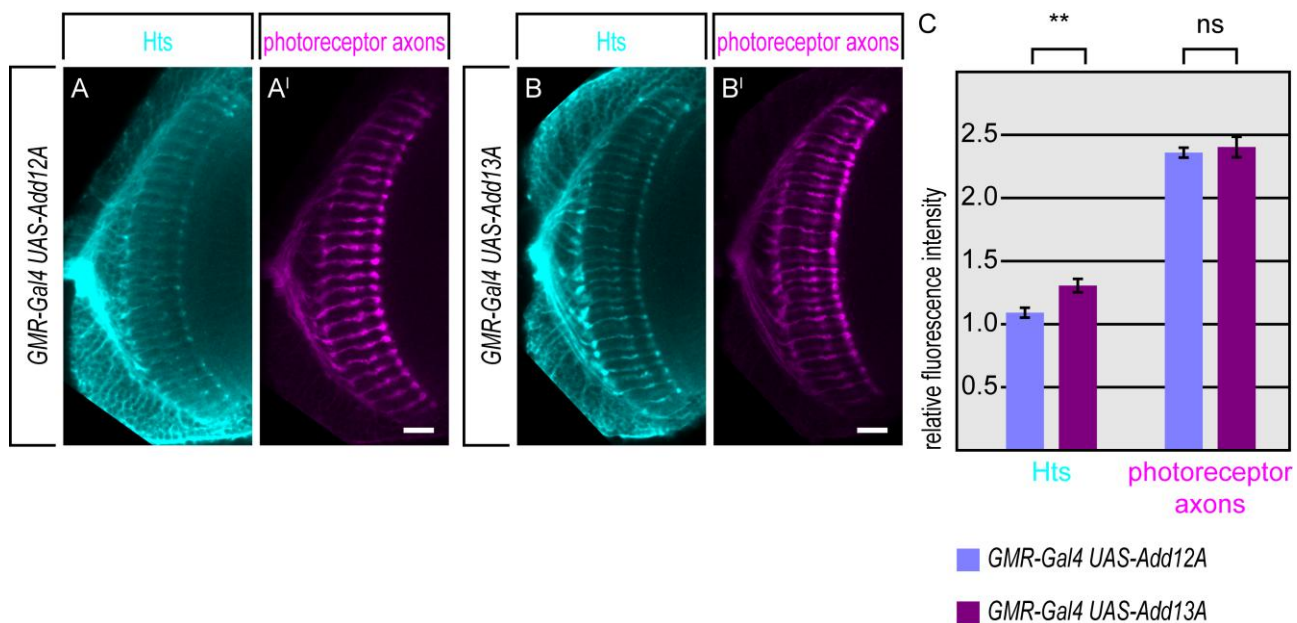


Figure 3.12.2: *UAS-Add13A* produces more axonal Hts protein than *UAS-Add12A*

Medullae of flies expressing Add1 from the two transgenic insertions (A) *UAS-Add12A* (n=10) and (B) *UAS-Add13A* (n=9) were immunostained with htsF antibody. (C) As judged from the fluorescence intensities of the immunostainings, the photoreceptor axons in the medulla contain more Hts protein when they express it from the *UAS-Add13A* than from the *UAS-Add12A* insertion. ns: not significant. **: P<0.01, Mann Whitney test. Error bars represent the SEM. All samples were imaged at the same settings. Anterior up, lateral left. Scale bars: 10 μ m.

None of the insertions of the *UAS-hts*⁴⁷² (n=4, Figure 3.11A and n=4, Figure 3.11B) or the *UAS-ShAdd* (n=10, Figure 3.11C and n=13, Figure 3.11D) construct tested caused any abnormalities when compared to the control (n=6, Figure 3.11E, Table 3.11).

3.13 *hts* antagonizes *gogo* overexpression

The physical interaction between Hts and Gogo, the similar defects caused by the loss of either *hts* or *gogo*, and the similarity of the defects caused by an excess of either Gogo or Hts suggested a collaborative function of Hts and Gogo in photoreceptor axon guidance. However, the co-overexpression of both *gogo* and *hts* in photoreceptor axons using the Gal4/UAS system gave an unexpected result. In many cases, the abnormal swellings caused by excessive Gogo (Figure 3.11H) were dramatically reduced both at the M1 and the M3 layer, and the R8 axons appeared almost like wild type R8 axons when Add1 was co-overexpressed (Figures 3.11I-J, Table 3.11). In contrast, no reduction of the defects caused by excessive Gogo could be attributed to the constructs *UAS-hts*⁴⁷² (Figures 3.11K-L) and *UAS-ShAdd* (Figures 3.11M-N, Table 3.11).

As both Add1 and Gogo were expressed by means of the Gal4/UAS system, the same amount of Gal4 transcription factor but double the dose of *UAS* promoters was present in cells that possessed both a *UAS-Add1* and a *UAS-gogo* construct compared to cells that had only one type of *UAS* target. This could potentially result in lower protein levels of each Add1 and Gogo when both are co-expressed, which then could explain the mutual suppression of their overexpression phenotypes. To confirm that the mutual suppression of their overexpression phenotypes is not an unspecific implication of the change in the Gal4 / *UAS* ratio resulting in lower protein levels, the finding was reproduced with flies that expressed only Gogo by means of the Gal4/UAS system but Add1 under direct control of the *GMR* promoter. Again, the abnormal swellings caused by an excess of Gogo (Figure 3.13A) were strongly reduced when Add1 was co-expressed (Figures 3.13B-C, Table 3.13).

Conversely, the effect of *gogo* overexpression was enhanced by removing one copy of *hts*. Both number and size of swellings were increased in *gogo* overexpressing, *hts*^{null} heterozygous flies, especially at the M1 layer (Figures 3.13D,F), although heterozygosity for *hts*^{null} did not cause any obvious abnormalities of R8 axons in the medulla on its own (Figure 3.13E, Table 3.13).

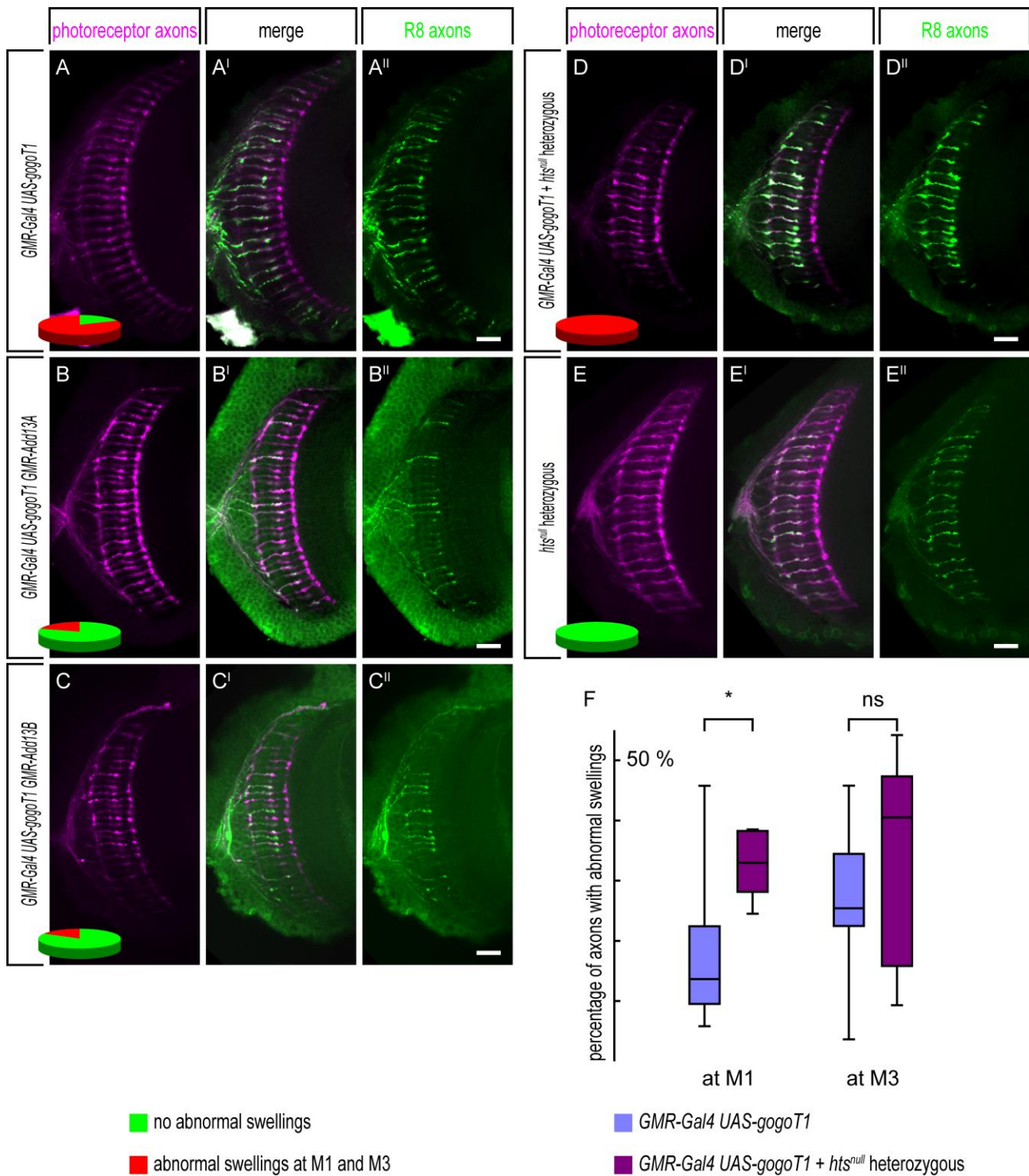


Figure 3.13: *hts* antagonizes *gogo* overexpression

The abnormally thick swellings of R8 axons at M1 and M3 caused by (A) excessive Gogo are suppressed by the co-expression of Add1 under direct control of the *GMR* promoter from either of the two insertions (B) *GMR-Add13A* and (C) *GMR-Add13B*. (D) Removing one copy of *hts* enhances the defects caused by excessive Gogo, leading to even more prominent swellings. (E) Removing one copy of *hts* does not cause defects on its own. (F) Removal of one copy

of *hts* increases the percentage of R8 axons with abnormal swellings caused by excessive Gogo significantly at M1 but only moderately at M3. ns: not significant. *: $P < 0.05$, Mann Whitney test. Anterior up, lateral left. Scale bars: 10 μm .

genotype	no abnormal swellings	swellings at M1	swellings at M1 and M3
<i>GMR-Gal4 UAS-gogoT1</i> (n=11)	2 / 18 %	0	9 / 82 %
<i>GMR-Gal4 UAS-gogoT1</i> <i>GMR-Add13A</i> (n=10)	8 / 80 %	0	2 / 20 %
<i>GMR-Gal4 UAS-gogoT1</i> <i>GMR-Add13B</i> (n=12)	10 / 83 %	0	2 / 17 %
<i>GMR-Gal4 UAS-gogoT1</i> <i>hts^{null}</i> heterozygous (n=5)	0	0	5 / 100 %
<i>hts^{null}</i> heterozygous (n=8)	8 / 100 %	0	0

Table 3.13: *hts* antagonizes the effects of excessive Gogo in photoreceptor axons

Flies with the genotypes listed in the left column were assayed blindly for abnormal swellings of R8 axons. For each genotype, the numbers / percentages of medullae assessed to have no remarkable swellings, abnormal swellings at the M1 or at the M1 and the M3 layer are quoted.

Although the similarities of both their loss-of-function and gain-of-function phenotypes rather suggested a synergistic interaction between *hts* and *gogo*, these data show that the *gogo* overexpression phenotype is antagonized by *hts*.

3.14 Gogo reduces the level of Add1 protein in photoreceptor axons

While exploring the mutual interference between *hts* and *gogo*, it became apparent that the intensity of Hts antibody staining in R7 and R8 axons in the medulla was consistently lower when *gogo* was co-overexpressed compared to axons with an endogenous Gogo level. The endogenous Hts level in photoreceptor axons in the adult medulla is too low to be detected by immunostaining (Figures 3.10A and 3.11E), but Add1 is readily detected when expressed using the Gal4/UAS system (Figures 3.11F-G). However, in photoreceptor axons that co-express Gogo, the protein level of Add1 seems to be strongly reduced as it is hardly detectable by immunostaining (Figures 3.11I-J).

To exclude that the decrease in Add1 protein level is merely an unspecific effect of the change in the Gal4 / UAS ratio, Add1 was expressed under direct control of the *GMR* promoter and again was clearly labeled by the htsF antibody in axons with an endogenous Gogo level (Figure 3.14.1A). When Gogo was co-overexpressed using the Gal4/UAS system, the intensity of Add1 immunofluorescence was significantly reduced (Figures 3.14.1B-C). Therefore, one of the functions of Gogo during axon guidance may be the reduction of the Hts protein level in

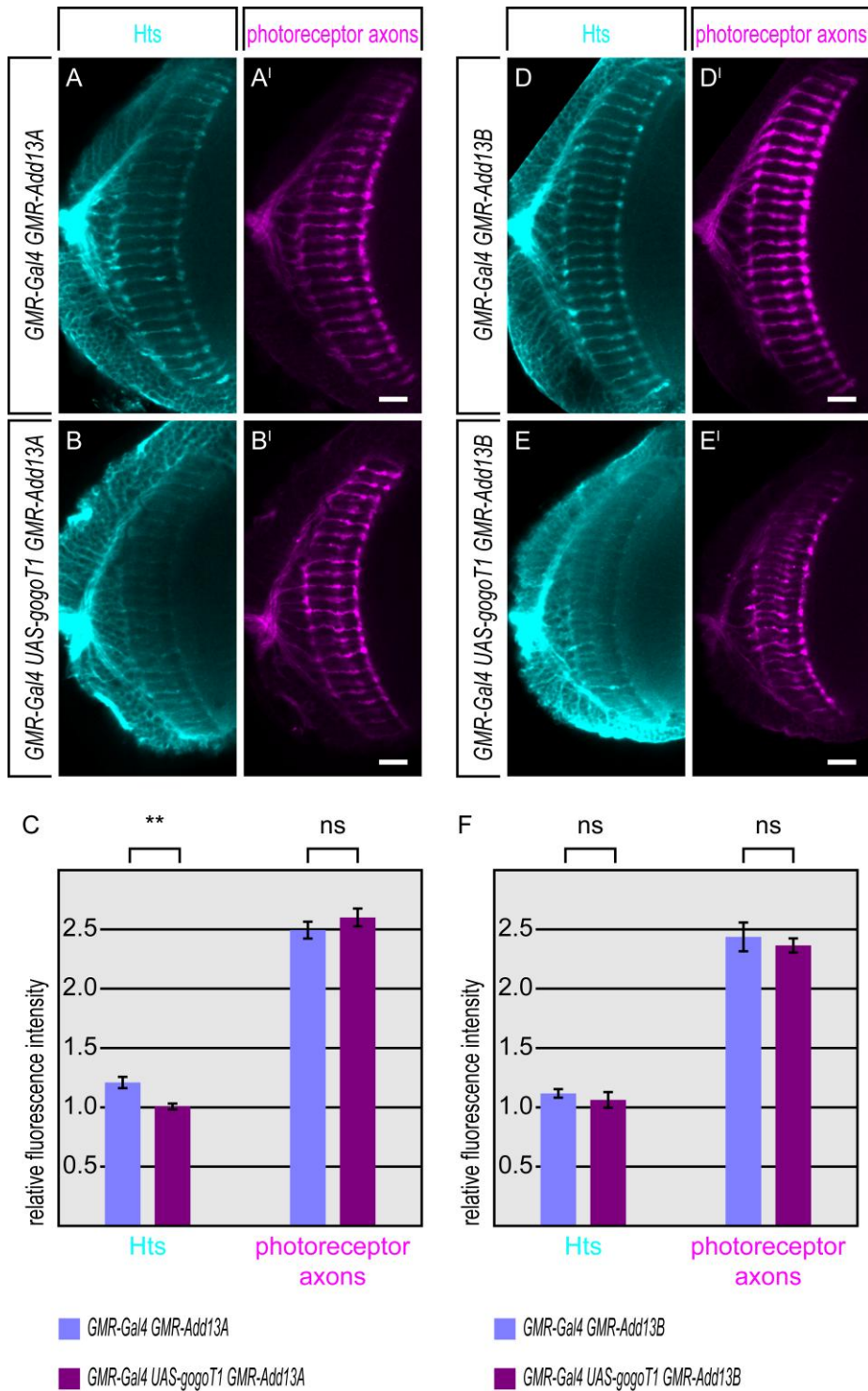


Figure 3.14.1: The axonal Hts protein level is reduced by excessive Gogo

The intensity of Hts immunofluorescence of (A) axons overexpressing Add1 was strongly reduced by (B) excessive Gogo. (C) This difference was statistically significant. Also if (D) Add1 was expressed from another transgenic insertion, (E) excessive Gogo somewhat reduced the relative fluorescence intensity of the axons. (F) However, the difference was not found to be statistically significant in this case. ns: not significant. **: $P < 0.01$, Mann Whitney test. Error bars represent the SEM. All samples were imaged at the same settings. Anterior up, lateral left. Scale bars: 10 μm .

genotype	Gogo immunofluorescence			Hts immunofluorescence		
	low	mid	high	low	mid	high
<i>GMR-Gal4 UAS-gogoT1</i> <i>GMR-Add13B</i> (n=57)	0	35 / 61 %	22 / 39 %	28 / 49 %	29 / 51 %	0
<i>GMR-Gal4 UAS-gogoT3</i> <i>GMR-Add13B</i> (n=28)	0	22 / 79 %	6 / 21 %	4 / 14 %	22 / 79 %	2 / 7 %
<i>GMR-Gal4 UAS-gogo-Myc2B</i> <i>GMR-Add13B</i> (n=28)	0	7 / 25 %	21 / 75 %	2 / 7 %	19 / 68 %	7 / 25 %
<i>GMR-Gal4 UAS-gogo-Myc3B</i> <i>GMR-Add13B</i> (n=28)	0	20 / 71 %	8 / 29 %	4 / 14 %	21 / 75 %	3 / 11%
<i>GMR-Gal4</i> <i>GMR-Add13B</i> (n=46)	46 / 100 %	0	0	0	21 / 46 %	25 / 54 %

Table 3.14: Decrease in Hts caused by different insertions of Gogo constructs

Flies with the genotypes listed in the left column were immunostained with anti-Gogo and anti-Hts antibody. The intensities of the Gogo and the Hts immunostainings were estimated blindly and independently. For each genotype, the numbers / percentages of medullae assessed to show low, mid or high fluorescence intensity of Gogo and Hts are quoted. Data were pooled from three experiments.

photoreceptor axons. This could also explain the absence of Hts labeling from the tips of R7 / R8 axons in the medulla of wild type larvae because they contain a high amount of Gogo protein (Figure 3.3 and Tomasi et al. 2008).

The experiment included also a second transgenic insertion of *GMR-Add1* (Figures 3.14.1D-F). Here, the average fluorescence intensity of the Hts immunostainings was somewhat decreased by excessive Gogo, but the difference was not found to be statistically significant.

Next, the effect of other transgenic insertions encoding full-length Gogo on the Hts protein level in photoreceptor axons was examined. Due to the lack of a counterstaining of the photoreceptor axons, the fluorescence level of each sample was subjectively and blindly estimated to be low, mid or high independently for both the Hts and the Gogo immunostaining. Whereas the Hts protein level in the axons was assessed mid or high in all control samples without a Gogo construct (Figure 3.14.2E), it was on average reduced by each of the four *gogo* constructs tested (Figure 3.14.2A-D, Table 3.14).

As for the induction of the overexpression phenotype, *UAS-gogoT1* was found to be the most potent to reduce the Hts protein level. *UAS-gogoT3*, *UAS-gogo-Myc2B* and *UAS-gogo-Myc3B* reduced Hts to a somewhat lower extent. Therefore, the effectiveness of the different Gogo constructs in reducing Hts did not completely correlate with the severity of their overexpression phenotypes, which was much stronger for *UAS-gogoT1* and *UAS-gogoT3* than for

UAS-gogo-Myc2B and *UAS-gogo-Myc3B* (Figure 3.12.1, Table 3.12). Also, it did not correlate with the estimated level of Gogo protein that they produce, which was higher for *UAS-gogo-Myc2B* than for the other constructs (Figure 3.14.2 and Table 3.14).

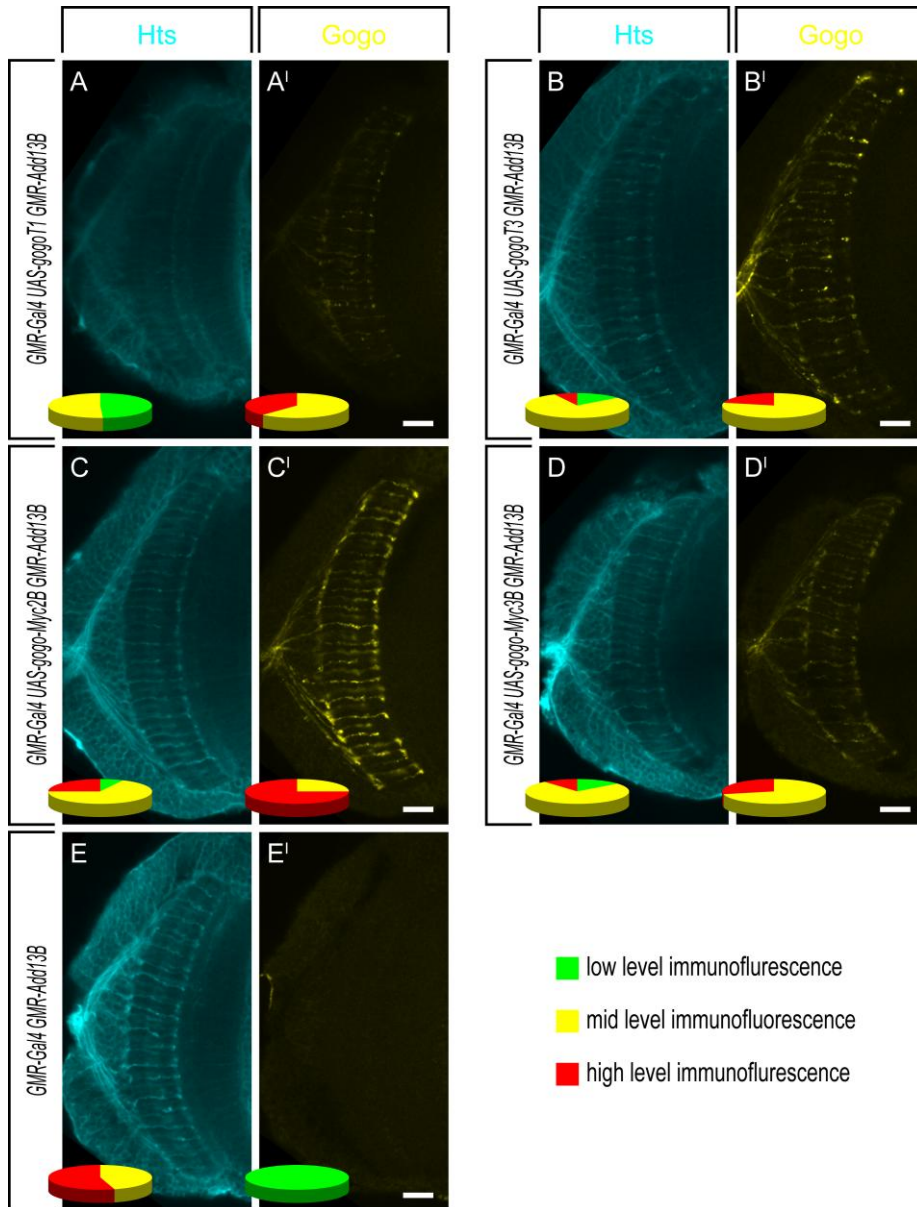


Figure 3.14.2: Decrease in Hts caused by different insertions of Gogo constructs

In flies that had the *GMR-Gal4* driver and expressed *Add1* under direct control of the *GMR* promoter from the transgenic insertion *GMR-Add13B*, the intensity of Hts immunofluorescence of axons overexpressing *Add1* was reduced by excessive Gogo expressed from (A) *UAS-gogoT1*, (B) *UAS-gogoT3*, (C) *UAS-gogo-Myc2B* and (D) *UAS-gogo-Myc3B* when compared to the (E) control without a *UAS-gogo* construct. All samples shown were imaged at the same settings. Anterior up, lateral left. Scale bars: 10 μ m.

Since an excessive amount of Gogo lead to a reduction of the Hts protein level in photoreceptor axons, it appeared possible that a reduction of Gogo would have the opposite effect and lead to an increased amount of Hts. To test this hypothesis, mosaic flies that had clones consisting of either photoreceptors homozygous mutant for *gogo* or heterozygous photoreceptors expressing KO as a marker were examined. Like in the neighboring heterozygous photoreceptors, the Hts protein level in homozygous *gogo* mutant clones that were identified by the absence of KO fluorescence was still too low to be detected by immunostaining (Figure 3.14.3A). Therefore, it could not be decided whether or not the loss of Gogo affected the amount of Hts protein in photoreceptor axons.

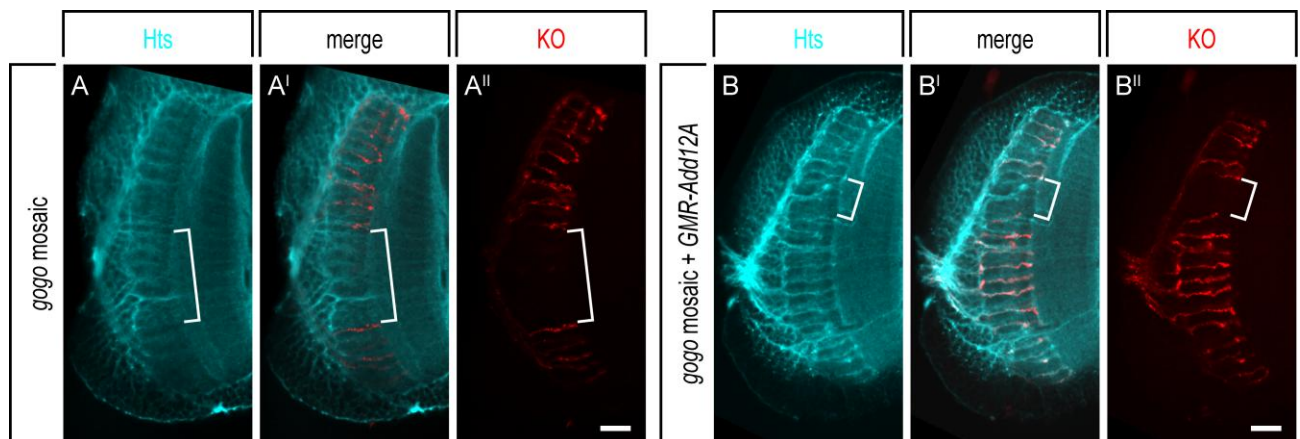


Figure 3.14.3: Loss of Gogo does not detectably increase the axonal Hts level

Mosaic flies with clones consisting of homozygous *gogo* mutant photoreceptors identified by the absence of KO fluorescence (brackets) were immunostained with the anti-Hts antibody 1B1. (A) As in the neighboring heterozygous photoreceptors, Hts can not be detected by immunostaining in homozygous *gogo* mutant photoreceptors. (B) When expressed under direct control of the *GMR* promoter, Add1 can be detected by immunostaining. The intensity of the Hts immunostaining is not noticeably increased in homozygous *gogo* mutant clones (brackets). Anterior up, lateral left. Scale bars: 10 μm .

Next, Add1 was expressed under direct control of the *GMR* promoter to increase its amount to a level at which it could be detected. However, the intensity of Add1 immunofluorescence was not noticeably elevated in *gogo* mutant clones compared to the surrounding heterozygous photoreceptors (Figure 3.14.3B). This does not necessarily contradict the assumption that Gogo reduces the level of Hts protein in photoreceptor axons since the loss of Gogo could lead to an increase in the level of Add1 that may be too marginal to be noticed by antibody staining.

3.15 Hts forms oligomers

To clarify whether Hts was able to form oligomers as mammalian Adducin does (Hughes and Bennett 1995), C-terminally 4xMyc- and 6xHis-tagged versions of Add1 (Add1-Myc and Add1-His)

and HtsPD (HtsPD-Myc and HtsPD-His) were coexpressed in *Drosophila* Schneider cells. Add1-His coimmunoprecipitated with Add1-Myc, and so did HtsPD-His with HtsPD-Myc (Figure 3.15), demonstrating that both Add1 and HtsPD are able to form homooligomers. Moreover, HtsPD-His coimmunoprecipitated with Add1-Myc, indicating that also oligomers consisting of different Hts isoforms are possible.

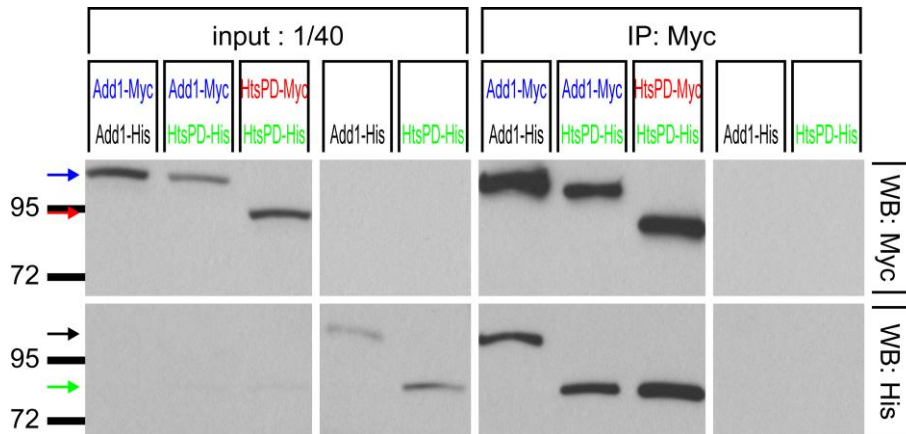


Figure 3.15: Hts forms oligomers

Drosophila Schneider cells expressed the indicated Hts constructs (lanes 1 to 5). The expression levels of Add1-His and HtsPD-His were lower when Add1-Myc or HtsPD-Myc was coexpressed (lanes 1 to 3) than in the negative controls lacking the Myc constructs (lanes 4 and 5). Add1-His coimmunoprecipitated with Add1-Myc (lane 6) but was absent from the negative control (lane 9). HtsPD-His coimmunoprecipitated with both Add1-Myc (lane 7) and HtsPD-Myc (lane 8) but was absent from the negative control (lane 10).

4. DISCUSSION

4.1 Hts and Gogo: collaborators or antagonists?

The results presented in this work show that the axon guidance receptor Gogo physically interacts with the cytoskeletal protein Hts (Figures 3.2.2 and 3.2.3). The loss-of-function phenotypes of *hts* and *gogo* mutants are qualitatively very similar, albeit *gogo* null mutants show a phenotype slightly more severe than the *hts^{null}* mutant (Figures 3.1.2 and 3.4 and Tomasi et al. 2008). This suggests that Gogo and Hts collaborate in a functional complex to guide R7 and R8 axons to their correct targets in the medulla.

However, there is also evidence for an antagonistic interaction between Hts and Gogo. Strong overexpression of Gogo causes abnormally thick swellings of R8 axons at layers M1 and M3 (Figures 3.11, 3.12.1, and 3.13). Strong overexpression of Add1 causes a different, but similar phenotype leading to abnormal swellings that are restricted to layer M1 (Figure 3.11). If both Gogo and Add1 are overexpressed, no abnormally thick swellings occur and R8 axons do not look different from wild type R8 axons. Moreover, in flies lacking one copy of the *hts* locus, the effect of excessive Gogo is enhanced (Figures 3.11 and 3.13). This indicates that Hts and Gogo antagonize each other and need to be in balance for the correct formation of axons.

Direct evidence for an antagonistic interaction between Gogo and Hts comes from the observation that an increase in axonal Gogo protein level reduces the amount of Add1 protein in the axon (Figure 3.14.1). The fact that the Add1 protein level is regulated by Gogo also strongly suggests that *gogo* acts upstream of *hts*.

How can these superficially contradictory results be explained and reconciled? In the following, two mutually not exclusive hypotheses about how the Gogo-Hts complex could function to guide photoreceptor axons will be discussed.

4.2 Hypothesis I: Gogo affects the axonal cytoskeleton via Hts

Axons find their way through the developing embryo to their correct target by means of the growth cone that is equipped with guidance receptors reading guidance cues provided by the growth cone's environment. These guidance cues can be attractive or repulsive, diffusible or tethered to the extracellular matrix or to cell membranes (Chilton 2006). The growth cone translates this guidance information into rearrangements of its cytoskeleton, which leads to a directed growth of the axon (Kalil and Dent 2005; Wen and Zheng 2006; Zhou and Snider 2006).

The two main components of the growth cone cytoskeleton are F-Actin appearing as filopodia and lamellipodia in the peripheral domain of the growth cone and microtubules oriented with their plus-ends pointing distally (reviewed by Dent and Gertler 2003; Rodriguez et al. 2003; Gordon-Weeks

2004; Zhou and Cohan 2004; Kalil and Dent 2005; Conde and Caceres 2009; Lowery and Van Vactor 2009).

The microtubules are tightly crosslinked into bundles within the axon shaft and become looser as they extend through the axonal wrist into the central domain of the growth cone. Single microtubules extend through the transition zone into the peripheral domain and contact the F-Actin within the filopodia. How far the microtubules extend into a filopodium is dependent on the behavior of the filopodial F-Actin (Forscher and Smith 1988; Zhou et al. 2002; Brown and Bridgman 2003; Medeiros et al. 2006; Schaefer et al. 2008).

Within a filopodium, F-Actin is organized as parallel bundles, which requires the action of F-Actin bundling proteins like α -Actinin (Sobue and Kanda 1989) and Fascin (Edwards and Bryan 1995). The barbed ends of these F-Actin bundles point distally, so that F-Actin assembly takes place at the very tip of the filopodium. The assembly of F-Actin at the tip of the filopodium produces a force on the F-Actin bundle that moves the bundle rearwards (retrograde flow) and a force on the plasma membrane that extends the filopodium (Geraldo and Gordon-Weeks 2009). Actin assembly and retrograde flow are regulated independently (Mallavarapu and Mitchison 1999). F-Actin capping proteins influence the rate of Actin assembly (Pollard and Cooper 1986; Mallavarapu and Mitchison 1999), whereas the rate of retrograde F-Actin flow has been suggested to be regulated by a "clutch" that links the cytoskeleton via transmembrane proteins to the substrate and thereby countervails the retrograde F-Actin flow (Mitchison and Kirschner 1988; Suter and Forscher 2000; Bard et al. 2008; Chan and Odde 2008; Geraldo and Gordon-Weeks 2009).

Many lines of evidence attest that the behavior of the filopodial F-Actin determines the organization of microtubules in the growth cone and consequently the directed growth of the axon (reviewed by Geraldo and Gordon-Weeks 2009). When the filopodial F-Actin bundles are stabilized against retraction by attractive guidance cues at a certain site of the growth cone, microtubules will penetrate those filopodia more efficiently, and the growth cone will consequently steer towards that side. Conversely, localized F-Actin disassembly inhibits microtubule extension into the filopodium, and an increased F-Actin flow clears microtubules from the filopodium. The growth cone will turn away from that side.

Adducin bundles Actin filaments (Mische et al. 1987; Taylor and Taylor 1994; Matsuoka et al. 2000) and caps barbed Actin filament ends (Kuhlman et al. 1996; Matsuoka et al. 2000) in vitro. Assuming that its *Drosophila* homolog Hts serves the same molecular functions makes it an attractive candidate for a protein that is involved in the proper organization of the filopodial F-Actin during axon guidance. Due to some analogies to the L1-Ankyrin system, which has been shown to function as a molecular clutch, especially a possible involvement in the regulation of retrograde F-Actin flow immediately comes to mind.

Like Adducin, the peripheral membrane protein Ankyrin is a part of the Actin-Spectrin cytoskeleton (Bennett and Stenbuck 1979). Whereas Adducin binds to the N-terminus of β -Spectrin that interacts with Actin (Bennett and Baines 2001), Ankyrin binds to a different site near the C-terminus of β -Spectrin (Kennedy et al. 1991). Ankyrin also binds to the cell adhesion molecule L1, especially when L1 is homophilically bound to another L1 molecule in trans (Nishimura et al. 2003). The binding of L1 to Ankyrin is regulated by phosphorylation of a Tyrosine in the conserved SFIGQY¹²²⁹ motive in the L1 cytoplasmic region (Garver et al. 1997), and phosphorylation or mutation to Histidine abolishes Ankyrin binding (Jenkins et al. 2001; Needham et al. 2001). Gogo also bears a conserved sequence motif containing Tyrosines in its cytoplasmic tail (Tomasi et al. 2008), but mutating YYD did not affect the interaction between Gogo and Adducin (Figure 3.2.3). The physical link of Ankyrin via L1 to the substrate exerts a pulling force on the filopodial F-Actin during the outgrowth of neurites, which is dependent on the binding of Ankyrin to Spectrin (Nishimura et al. 2003). However, Ankyrin is not required for neurite extension after their initial outgrowth (Nishimura et al. 2003) nor for neurite outgrowth on substrates other than L1 (Ooashi and Kamiguchi 2009), indicating that other, Ankyrin independent molecular clutches exist. It is tempting to speculate that Hts could act as a component of one of these, especially in the growth cones of R8 axons. The extension of *hts*^{null} mutant R8 axons is not inhibited completely (Figure 3.4), so it must be assumed that, if Hts indeed acts as a component of a molecular clutch together with Gogo, it does so in addition to other, maybe more constitutively acting molecules.

One prerequisite for the function of Hts as a component of a molecular clutch is that Hts is physically connected to the cytoskeleton, which is very likely based on its homology to Adducin. Another indication for an intimate link between Adducin and the Actin-Spectrin cytoskeleton, especially during photoreceptor axon guidance, are the similar loss-of-function phenotypes of *hts* and *Spectrin* mutants (Figures 3.4 and 3.5). They furthermore suggest that the hypothetical function of Hts as a component of a molecular clutch is dependent on the binding of Hts to Spectrin, like Ankyrin's function during neuritogenesis is dependent on its binding to Spectrin (Nishimura et al. 2003).

The second prerequisite for this hypothesis is that Hts is physically linked via a transmembrane protein to the substrate. The work presented here shows that Hts binds to the transmembrane protein Gogo (Figures 3.2.2 and 3.2.3). Could Gogo function to link Hts to the substrate? At the first sight, this seems rather unlikely. Excessive Gogo removes Hts from the axon (Figure 3.14.1). Therefore, Gogo should not be able to provide a stable link between Hts and the substrate. Of course, Hts could be linked to the substrate by a transmembrane protein other than Gogo, and the binding of Gogo to Hts may function merely in a regulatory manner. However, it is possible that the binding of Gogo to Hts and the Gogo-mediated removal of Hts from the axon do not happen simultaneously. Possibly, Gogo provides an anchor for Hts to the substrate as long as this is

necessary for filopodial extension, and only later functions to remove Hts from the axon when the Hts-clutch is no longer required. The two functions of Gogo, anchoring Hts to the substrate and removing Hts from the axon, could be separated not only temporally, but also spatially. Gogo could serve as a linker to the substrate at the tip of the growth cone to pull the axon straight forward, but on the sides of the growth cone, it may have another function (possibly due to the binding of a ligand) and clear Hts from the filopodia in order to prevent the axons from steering aside (Figure 4.2A). This fits to the suggested R8-R8 repulsion mediated by Gogo (Tomasi et al. 2008). Additionally to repelling R8 axons from each other to assure their proper spacing in the medulla, Gogo has been shown to have another, adhesive function (Tomasi et al. 2008). Before R8 axons enter the medulla, they are temporarily anchored to the M1 layer (Ting et al. 2005). R8 axons lacking Gogo stray uncoordinatedly at the surface of the medulla, and R8 axons overexpressing Gogo sometimes are stuck to M1 and never leave it to innervate the medulla (Tomasi et al. 2008). This again fits to an adhesive function of Hts mediated by Gogo.

To summarize, this model suggests that, at the distal tip of the growth cone, Hts links the filopodial F-actin via Gogo to the substrate, which inhibits retrograde Actin flow, lets microtubules invade the filopodia and the growth cone steer straight forward. On the lateral filopodia of the growth cone, ligand-bound Gogo acts as a repulsive receptor removing this Hts-clutch, enabling retrograde Actin flow, preventing microtubules from invading the filopodia and thereby assuring the proper spacing of single R8 axons (Figure 4.2A). In addition to this function as a molecular clutch and based on its homology to Adducin, Hts may serve an antipodal function by capping the barbed ends of filopodial Actin filaments, which should inhibit the extension of filopodia. Unlike in the filopodia at the distal tip of the growth cone, this Actin capping function of Hts may predominate in lateral filopodia, assuming that the ligand-bound Gogo removes preferentially those Hts molecules that are incorporated in the molecular clutch but not those capping Actin filaments. There are two reasons for this assumption. First, there is no need to assume that the Actin capping Hts molecules, unlike those that constitute the molecular clutch, are in direct physical contact to (ligand-bound) Gogo molecules, which would protect them from Gogo-mediated removal. Second, Adducin binds much stronger to the barbed ends of Actin filaments ($K_d = 60$ nM) than it does to the sides of the filaments ($K_d = 1500$ nM) (Matsuoka et al. 2000). If the same is true for Hts, than the Hts molecules capping the barbed ends may be less susceptible to Gogo-mediated removal than those at their sides.

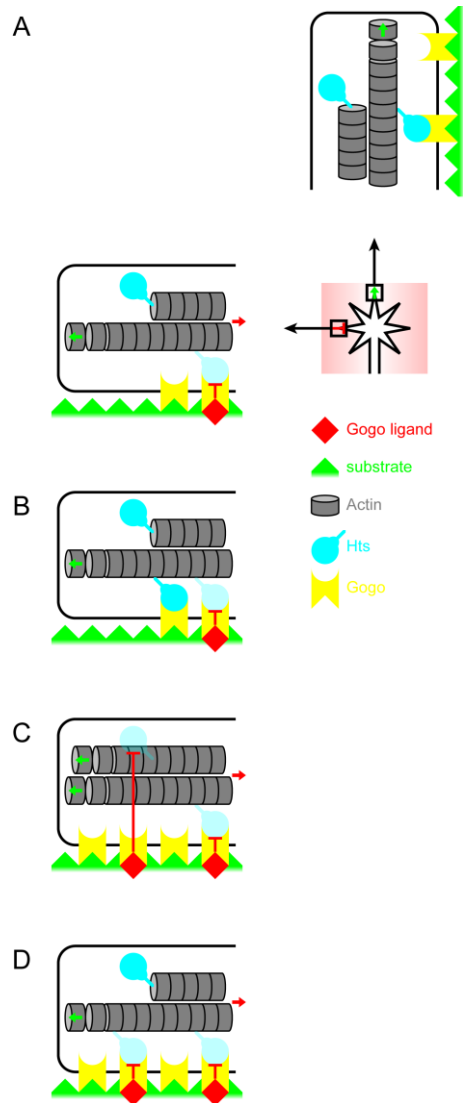


Figure 4.2: A speculative model of the Hts and Gogo functions

(A) At the tip of a wild type axon, Hts could serve as a molecular clutch that links Actin filaments, possibly via Gogo, to the substrate to counteract the retrograde flow driven by Actin polymerization at the barbed end, thus leading to the extension of filopodia. A second function of Hts may be the capping of Actin filaments. At the sides of the growth cone, Gogo may encounter its repulsive ligand from neighboring axons, switch its function and remove Hts from the filopodia to enable the retrograde flow of Actin bundles, thereby counteracting the extension of filopodia. In summary, this would lead to a directed growth of axons and assure their proper spacing. Loss of either Gogo or Hts would impair this directional cue and let the axons grow randomly. (B) Excessive Hts may form ectopic molecular clutches at lateral filopodia, leading to abnormal swellings of the axons. (C) Excessive Gogo could remove additional, Actin capping Hts from the lateral filopodia. The increased Actin polymerization may not completely be compensated by retrograde Actin flow and “blow up” the growth cone. This effect may be even stronger in *hts* heterozygous animals. (D) Excessive Hts may be antagonized by excessive Gogo, leading to morphologically normal axons.

4.3 Experimental evidence supporting hypothesis I

How do the results presented in this work fit the model described above? Assuming that Gogo and Hts act together to pull photoreceptor axons straight forward through the medulla and to assure their proper regular spacing, then the loss of either Hts or Gogo would obviously lead to the uncoordinated growth of axons within the medulla that is indeed observed in *hts* (Figure 3.4) or *gogo* (Figure 3.1.2) mutants.

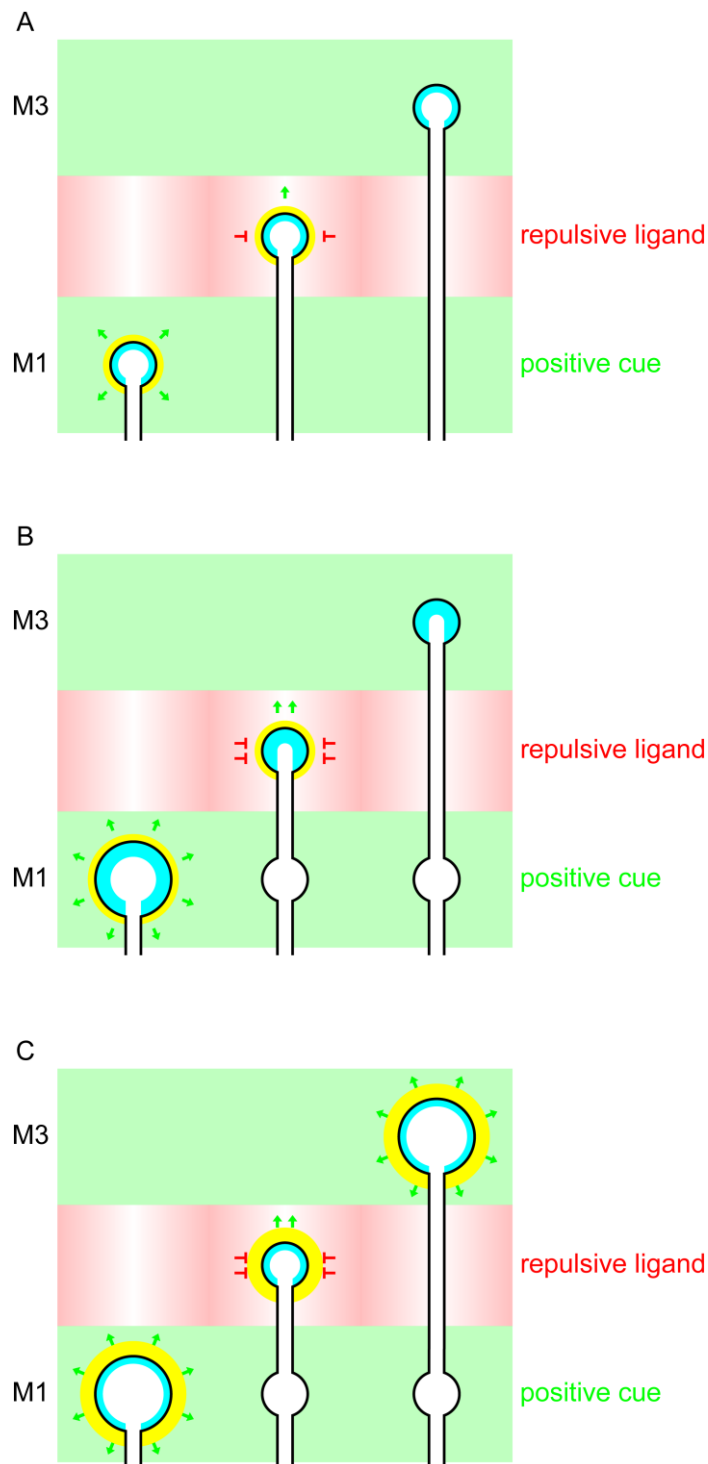


Figure 4.3: A possible explanation of the *hts* and *gogo* overexpression phenotypes

(A) A wild type R8 axon enters the medulla and pauses at the M1 layer in response to an as yet unidentified positive cue, which may be mediated by an attractive function of the Gogo-Hts complex (left). After resuming extension, this attractive function may pull the growth cone towards the M3 layer. Simultaneously, a repulsive function of the Gogo-Hts complex induced by the putative Gogo ligand could assure the correct distance of the emerging axon to its neighbors (middle). After reaching M3, the function of the Gogo-Hts complex ceases as Gogo expression decreases (right). (B) Excessive Hts protein may boost the attractive function of the Gogo-Hts complex at the intermediate R8 target layer (left), which may cause the abnormal swellings observed at M1 (middle). After reaching M3, excessive Hts no longer has any effect due to the lack of Gogo (right). (C) Excessive Gogo protein may increase the attractive function of the Gogo-Hts complex at the intermediate R8 target layer (left) and cause abnormal swellings at M1 (middle). Ectopic Gogo protein is still present after the growth cone has reached its final target layer M3, the function of the Gogo-Hts complex does not cease, and this may cause the additional swellings observed at M3 (right). Cyan represents Hts, yellow represents Gogo.

The thickening of R8 axons at the M1 layer caused by excessive Hts (Figure 3.11) can be explained as the result of an excessive anchoring of the growth cones to M1 where Gogo serves its adhesive function (Figures 4.2B and 4.3B). If the inhibition of retrograde actin flow is increased in the filopodia compared to wild type growth cones by additional Hts, the filopodia would extend radially in all directions and “blow up” the growth cone. This may become evident at the M1 layer, because Gogo serves its adhesive function here. In contrast, excessive Hts does not blow up the growth cones at their terminal layer M3. After the growth cone has reached this final destination, the Gogo-Hts complex is no longer required to guide the axons and therefore might be shut off (Figure 4.3A). In fact, Gogo expression has been shown to decrease in late pupal stages when the process of R8 axon guidance finishes (Tomasi et al. 2008). Without Gogo, excessive Hts no longer functions as an adhesive, F-Actin retraction inhibiting molecular clutch and therefore, no abnormal thickenings arise at this late stage of R8 axon guidance (Figure 4.3B).

In contrast, excessive Gogo causes abnormal thickenings not only at M1, but also at M3 (Figures 3.11, 3.12.1, and 3.13). This is in accordance with the assumption that the excessive expression of Gogo causes abnormally strong adhesion of the growth cone not only at M1, but also in the late steps of final targeting when Gogo expression normally decreases (Figure 4.3C). An alternative explanation for the abnormal thickenings of R8 axons caused by excessive Gogo may be the removal of additional Hts molecules that normally are not susceptible to Gogo-mediated removal and inhibit Actin polymerization at the barbed ends of filopodial F-Actin (Figure 4.2C).

When both Hts and Gogo are overexpressed, no abnormally thick swellings are observed (Figures 3.11 and 3.13). Although the anchoring of R8 growth cones to their temporary target M1 and to their final target M3 should be abnormally strong in this situation, the Hts antagonizing function of Gogo is also increased and may counteract the elevated adhesive force by removing excessive Hts (Figure 4.2D). There is no good formal explanation why excessive Gogo alone

causes abnormally thick swellings presumably due to an enhanced anchoring of the growth cones, whereas its Hts antagonizing function completely outbalances this increased adhesive force when Hts is co-overexpressed. However, not only Gogo and Hts are involved in the function of the Gogo-Hts complex. At least the putative repulsive Gogo ligand should play an important role, and possibly there is another transmembrane protein linking Hts to the substrate. The substrate molecule that mediates the adhesion of the growth cone may be another player. Additionally, Spectrin seems to be involved. Whether the Hts antagonizing or the adhesive function of Gogo prevails in one or the other overexpression situation may depend on which of these factors is the limiting one in a certain context.

4.4 Hypothesis II: Hts recruits Gogo to the Spectrin cytoskeleton

The model presented above nicely explains the findings from this work, but it does not exclude another possible function of the Hts-Gogo interaction. The Spectrin cytoskeleton was suggested to participate in the formation of specialized membrane subdomains by localizing membrane proteins (Bennett 1985; Bennett and Baines 2001), as many membrane proteins are mislocalized when the Spectrin cytoskeleton is disturbed (Zhou et al. 1998; Dubreuil et al. 2000; Jenkins et al. 2001; Komada and Soriano 2002).

β-Spectrin mutants show defects in embryonic midline axon guidance. In *Drosophila*, the embryonic CNS has a ladder-like axon scaffold with longitudinal axon bundles on both sides of the ventral midline that are connected by an anterior and a posterior commissure in each segment. Ipsilateral neurons whose axons do not cross the midline express the axon guidance receptor Robo, which senses the Slit ligand produced by midline glia to prevent midline crossing (Kidd et al. 1998; Kidd et al. 1999). Commissural neurons overcome this Slit mediated repulsion by expressing the Commissureless protein prior to midline crossing, which prevents Robo from reaching the cell surface by sorting it directly from the trans-Golgi network into endosomes (Keleman et al. 2002). In *β-Spectrin* mutant embryos, some Fas2-positive axons that normally do not cross the midline are no longer repelled by Slit and do cross the midline. This defect can be restored by expressing *β-Spectrin* in neurons, but not by expressing it in midline glia. Moreover, mutations in *β-Spectrin* genetically interact with the Slit-Robo pathway, as significantly more Fas2-positive axons cross the midline in *β-Spectrin* mutant, *slit*, *robo* trans-heterozygous embryos than in embryos that are only *β-Spectrin* mutant or only *slit*, *robo* trans-heterozygous. *β-Spectrin* specifically modifies the Slit-Robo pathway, as no genetic interactions were detected with either the Netrin-Frazzled or the Semaphorin-Plexin pathway. Therefore, *β-Spectrin* was considered to modulate the Slit-Robo pathway by regulating the distribution of Robo in *Drosophila* midline CNS axons. However, as no obvious changes in the level or localization of Robo protein were observed when *β-Spectrin* mutant embryos were compared with wild type embryos, *β-Spectrin* may rather affect another component

of the Robo pathway downstream of the receptor itself (Garbe et al. 2007). An alternative explanation could be that the changes in the distribution of Robo protein in *β-Spectrin* mutant axons may be too subtle to be detected by confocal microscopy. The Spectrin cytoskeleton may be required to integrate Robo and some of the downstream components of the Slit-Robo pathway into functional protein complexes, which does not exclude an overall proper localization of these molecules also in *β-Spectrin* mutant axons.

Similarly, the Spectrin cytoskeleton or, more specifically, the Hts-Gogo interaction, may be required for the proper localization of the Gogo receptor or assist in the correct establishment of interactions between Gogo and its downstream effectors. This would easily explain the similar loss-of-function phenotypes observed in *gogo* and *hts* mutants, as both would ultimately cause the loss of functional Gogo protein. However, the axonal Hts protein level is regulated by Gogo (Figure 3.14.1), which strongly suggests that *hts* acts downstream of *gogo* and seems to contradict the assumption that the localization of Gogo is dependent on Hts. Yet, one could imagine that the reduction of axonal Hts protein by excessive Gogo provides a mechanism of self-restriction to prevent excessive Gogo function. In this scenario, the amount of Gogo function is determined by the axonal Hts protein level. The defects caused by excessive Hts must be interpreted as the result of an abnormally high level of functional Gogo. The mutual suppression of *hts* and *gogo* when both are overexpressed can be explained as the additional amount of Hts is simply reduced to a regular level by the excessive Gogo, which, in turn, limits the amount of Gogo function to a regular level. However, the defects caused by excessive Gogo alone can not be explained. The additional amount of Gogo protein should not be functional, as an increase in functional Gogo would require additional Hts. Rather, the increase in the amount of Gogo should cause an abnormally low level of Hts protein and therefore a phenotype that resembles more the *hts* or *gogo* loss-of-function phenotype.

Assuming that the subcellular localization of Gogo is regulated by Hts and taking into account that Hts, like Adducin, is able to oligomerize (Figure 3.15), it could be speculated that at least two Gogo molecules must be in close proximity to function properly (Figure 4.4A). Similarly, receptor tyrosine kinases signal only upon dimerization induced by ligand binding (Li and Hristova 2010). In this scenario, it would be possible that oligomerization is required for Gogo to function properly, but monomeric Gogo protein could exert some ectopic function that leads to abnormal swellings of R8 axon growth cones. An increase in the protein level of either Hts (Figure 4.4B) or Gogo (Figure 4.4C) could cause some monomeric Gogo protein to occur and therefore lead to abnormal swellings of growth cones. However, if both Hts and Gogo are present in excess, the additional Hts molecules could integrate the excessive Gogo molecules into oligomers and therefore prevent the ectopic function of monomeric Gogo leading to abnormal swellings (Figure 4.4D).

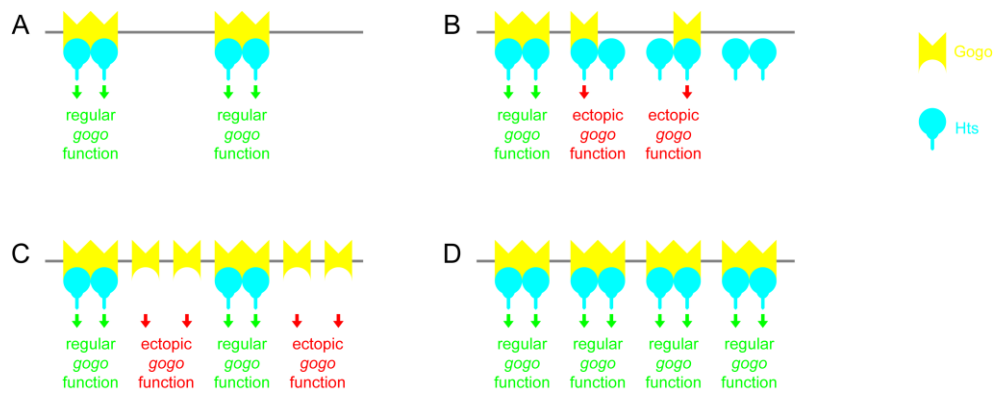


Figure 4.4: Overexpression phenotypes resulting from an ectopic function of monomeric Gogo

(A) Hts forms oligomers and is therefore suitable to bring two or more Gogo molecules into close proximity. This could be required for normal Gogo function. (B) Excessive Hts disturbs the Gogo / Hts stoichiometry and may cause monomeric Gogo to occur. Single Gogo molecules may have an unnatural function that causes the observed defects, swellings of R8 axons. (C) Similarly, excessive Gogo could cause monomeric Gogo molecules to occur and lead to swellings of R8 axons. (D) If both *hts* and *gogo* are overexpressed, the normal ratio of Gogo / Hts molecules is restored. No monomeric Gogo and no ectopic function of monomeric Gogo molecules appear. R8 axons do not suffer defects.

4.5 Hypothesis III: A disordered Spectrin cytoskeleton causes unspecific phenotypes

β-Spectrin mutants show phenotypes that can be explained by defective axon guidance in both worms and flies. *unc-70* is the single *C. elegans* gene encoding β -Spectrin. In *unc-70* mutants, GABA motor neurons exhibit a defective axonal morphology in the ventral nerve cord, the commissures that connect the ventral and the dorsal nerve cord, and the dorsal cord. The ventral cord is discontinuous and defasciculated. Only few commissures are present, and they usually do not reach the dorsal cord. The commissures display a variety of aberrant morphologies and are elaborately branched or prematurely terminated. Some commissures extend anteriorly of the GABA expressing RME neurons, where none are normally present (Hammarlund et al. 2000). In the embryonic CNS of *D. melanogaster*, β -Spectrin is required in neurons for proper midline axon guidance. In *β-Spectrin* mutant embryos, many axons inappropriately cross the CNS midline (Garbe et al. 2007).

Nevertheless, there is no hard proof for a direct, instructional role of the Spectrin cytoskeleton in the process of axon guidance yet. One of the main duties of the Spectrin cytoskeleton is to provide mechanical strength to the plasma membrane (Tchernia et al. 1981; Discher et al. 1993), and it has been demonstrated that β -Spectrin is required for the physical integrity of neuronal processes in *C. elegans*. The defective morphology of axons in *unc-70* mutants is merely a secondary effect of axon breaks. Several types of neurons were shown to initially establish correct axonal projections in *unc-70* mutants. The observed defects in axonal morphology accumulate over time, as the axons break and attempt to regenerate by initiating a new growth cone. This second round

of axon extension is error prone compared with initial outgrowth and produces axons with defective morphology. The guidance errors are indeed the consequence of axon breaks due to the acute strains caused by movement, as they are significantly reduced when axon breaks are prevented by paralyzing the mutant animals (Hammarlund et al. 2007). Could the defects observed in β -Spectrin mutant fly embryos also be explained as secondary effects of axon breaks due to strains caused by movement? On the first sight, this seems indeed likely, as pCC and dMP2 pioneer axons initially make appropriate ipsilateral projections in β -Spectrin mutant embryos and only later show crossing defects, even in a *slit*, *robo* transheterozygous background. Similarly, axons of Ap neurons correctly project toward the midline and make ipsilateral turns from stage 14 to early stage 15, but show midline crossing defects by late stage 16 in β -Spectrin mutant animals. In contrast, they exhibit crossing defects during their initial extension toward the midline and throughout development in *robo* mutants. This suggests that β -Spectrin is required rather for the maintenance of properly established connections on the correct side of the midline than for initial axon guidance (Garbe et al. 2007). On the other hand, β -Spectrin mutant stage 14 embryos already show axonal defects as characteristic loops are formed where commissural axons normally enter the connectives (Hulsmeier et al. 2007). Therefore, the first axonal defects are observed at a stage when the embryo is still completely immobile, several hours before the onset of muscle contractions about 14 hours after egg laying (Crisp et al. 2008), which corresponds to embryonic stage 16 at least (Campos-Ortega and Hartenstein 1985). This seems to contradict the hypothesis that all defects observed in β -Spectrin mutants are the secondary effect of axon breaks due to acute strains caused by movements of the embryo. But then again, one could argue that these early defects are the result of axon breaks that are caused rather by morphogenetic movements than by embryonic movements due to muscle contractions.

Could the defective phenotypes reported in this work also be explained as the mere consequence of axon breaks due to an impaired Spectrin cytoskeleton and reduced mechanical strength of the axons? For the *hts* loss-of-function phenotype, this seems possible. Adducin is well known to be an essential factor in the assembly of the Spectrin cytoskeleton (Gardner and Bennett 1987; Bennett et al. 1988), and based on homology, it can be assumed that the Spectrin cytoskeleton is severely affected in *hts* mutant flies. However, broken axons can be clearly observed in β -Spectrin mutants as a proximal and the corresponding detached distal fragment of an axon belonging to a single neuron can be identified (Hammarlund et al. 2007). This is not obvious in *hts* mutant flies (Figure 3.4). Moreover, it seems unlikely that the defects observed in *gogo* mutants are the consequence of axon breaks, as this would premise that Gogo is an essential component of the Spectrin cytoskeleton. This is unlikely, because the expression of Gogo is restricted to certain tissues, cell types and developmental stages (Tomasi et al. 2008), whereas the Spectrin cytoskeleton is present in almost all cells of metazoan organisms (Bennett 1990; Bennett and

Gilligan 1993). Although it was possible that other proteins take over Gogo's function where it is not expressed, it seems more reasonable to assume that the defects in *gogo* mutants are caused rather by the loss of a more specific function in axon guidance than by the sheer loss of physical strength of the axonal membrane. Assuming that Gogo and Hts fulfill this function together in a protein complex as their physical interaction (Figures 3.2.2 and 3.2.3) and their similar loss-of-function phenotypes (Figures 3.1.2 and 3.4 and Tomasi et al. 2008) imply, this also argues for a specific axon guidance function of Hts.

By contrast, the defects caused by the overexpression of either *hts* or *gogo* indeed may be explained as unspecific consequences of an impaired Spectrin cytoskeleton. In both cases, it causes abnormally thick swellings of R8 axons in the medulla (Figures 3.11, 3.12.1, and 3.13). Interestingly, β -Spectrin mutants have been reported to possess dramatically enlarged growth cones, which are presumably the consequence of an increased fusion of intracellular membrane vesicles with the axonal membrane (Hulsmeier et al. 2007). As the Spectrin cytoskeleton prevents the premature fusion of vesicles with the plasma membrane in secretory cells (Aunis and Bader 1988; Perrin et al. 1992), it may also regulate the fusion of intracellular membrane vesicles with the axonal cell membrane that is required to enlarge and advance the growth cone (Gitler and Spira 1998). Accordingly, the removal of the submembranous Spectrin cytoskeleton by the Ca^{2+} dependent proteolytic activity of the protease Calpain is necessary for the formation of a new growth cone after axotomy and sufficient for the induction of growth cone formation in the axon of an intact neuron (Gitler and Spira 1998). Therefore, the defective phenotypes caused by either excessive Hts or excessive Gogo could be the result of an increased fusion of vesicles with the membrane, assuming that both lead to a destabilized Spectrin cytoskeleton. Excessive Gogo is likely to compromise the Spectrin cytoskeleton, as it reduces the amount of its essential structural component Hts (Figure 3.14.1). It is also reasonable to assume that a strong overexpression of *hts* perturbs the stoichiometry of the molecules setting up the Spectrin cytoskeleton and therefore the integrity of the Spectrin cytoskeleton. In erythrocytes, each junctional complex of the Actin-Spectrin cytoskeleton was supposed to link three Spectrin dimers to each other and to contain one Adducin tetramer (Matsuoka et al. 2000), which corresponds to a stoichiometric ratio of β -Spectrin to Adducin of three to four.

It seems implausible that the same phenotype, the swelling of axons, should be caused once by too much Hts protein and once, in the case of Gogo overexpression, by too little Hts protein. However, the mutual suppression of the *hts* and the *gogo* overexpression phenotype (Figures 3.11 and 3.13) as well as the antagonistic effect of Gogo on the protein level of Hts (Figure 3.14.1) suggests that the overexpression phenotypes of *hts* and *gogo* are indeed the consequences of opponent mechanisms.

4.6 Why is the MARCKS-related domain of Hts not required for axon guidance?

An interesting finding from the work presented here is that the MARCKS-related domain seems not to be required for the functions of Hts during axon guidance. Expression of either Add1, the Hts isoform including the MARCKS-related domain, or HtsPD, an isoform lacking the MARCKS-related domain, in photoreceptors restores the defects caused by the loss of *hts* (Figures 3.7.2 and 3.9). This is consistent with the observation that homozygous *hts*^{1G} mutant flies, which have only truncated Hts protein lacking the MARCKS-related domain, do not show defects in the medulla (Figure 3.4). Both were surprising, since the MARCKS-related domain of Adducin has been shown to be required for the in vitro functions of Adducin including Actin binding, Actin capping, and Spectrin recruiting (Li et al. 1998; Matsuoka et al. 2000).

A possible explanation is that the function of Hts during axon guidance is indeed independent of Actin and Spectrin and that Hts serves a completely novel function here. However, for several reasons it seems more likely that the *Drosophila* Hts can interact with Actin and Spectrin as the mammalian Adducin does, but does not strictly require its MARCKS-related domain for that. There are several reasons for this assumption.

First, in the *Drosophila* germ line exclusively the Hts isoforms ShAdd and Ovhts are expressed, both lacking the MARCKS-related domain (Whittaker et al. 1999; Petrella et al. 2007). Nevertheless, in *hts* mutants, the fusome, a Spectrin based cytoskeletal structure in the germlarium, is disorganized (Lin et al. 1994). This indicates that these MARCKS-related domain lacking proteins are required for the proper assembly of the Spectrin cytoskeleton.

Second, the similar phenotypes of *hts* and *spectrin* mutants in photoreceptor axon guidance (Figures 3.4 and 3.5) suggest that Hts and Spectrin are functionally linked during photoreceptor axon guidance. The *hts* mutant phenotype can be restored by Hts lacking the MARCKS-related domain. This indicates that the interaction with Spectrin does not require the MARCKS-related domain.

Third, it has not been shown directly that mammalian Adducin binds Spectrin via its MARCKS-related domain. The MARCKS-related domain is the target of many regulatory processes. It contains phosphorylation sites for PKA and PKC and it binds calmodulin in a Ca²⁺ dependent manner (Matsuoka et al. 2000). The MARCKS-related domain could function merely in a regulatory manner, regulating the binding of Spectrin to another part of Adducin. Indeed, the neck domain is also required for Adducin binding to Spectrin (Li et al. 1998; Matsuoka et al. 2000) and may therefore contain the actual binding site.

4.7 Outlook

The results presented in this work provide an insight into a mechanism of axon guidance that is largely unexplored yet. Gogo has been described as a novel axon guidance receptor only recently

(Tomasi et al. 2008). Research on Hts so far focused on its function during oogenesis, and a role for Hts in axon guidance has not been reported yet. Also the functions that Adducin and, surprisingly, the Spectrin cytoskeleton in general serve during axon guidance are largely unknown. Are components of the Spectrin cytoskeleton constituents of a clutch module? Does the Spectrin cytoskeleton direct navigating growth cones by organizing the subcellular distribution of axon guidance receptors or other guidance molecules? Does the Spectrin cytoskeleton, as findings on its constituent Ankyrin suggest (Ooashi and Kamiguchi 2009), control growth cone navigation via the modulation of cAMP? Or is its sole duty the supply of mechanical strength to the axonal membrane?

Neither Gogo nor Hts may serve a single, unitary function during axon guidance. Gogo was reported to serve two opposing functions as it is required for the adhesion of R8 growth cones to their intermediate target layer M1 and for the repulsion of R8 axons from each other (Tomasi et al. 2008). Hts is likely to serve diverse molecular functions as its homologue Adducin does. This may also be reflected by the superficial inconsistency of the results shown in this work.

Therefore, it was not possible to sum up the results from this work in a single consistent model that matches the body of literature. Rather, this work raises several new questions and hypotheses that can be tested only by subsequent work.

The first and most important question to answer is whether the Gogo-Hts complex has indeed an instructional role in axon guidance or is required solely for the structural integrity of the axonal cell membrane. Detailed tracking of axons emerging from single labeled neurons could reveal whether the guidance errors observed in *hts* or *gogo* mutants are preceded by axon breaks or occur in the initial navigation of the primary axon.

If an instructive role for the Gogo-Hts complex emerges, it will be crucial to determine if this function involves a direct interaction of Hts with the Actin-Spectrin cytoskeleton. Here, a key experiment will be to determine whether Hts proteins lacking the MARCKS-related domain are able to interact with Actin and Spectrin. A negative result would point to a completely novel molecular function of Hts independent of Actin and Spectrin, because the MARCKS-related domain of Hts seems not to be required for the function of Hts in axon guidance (Figures 3.4, 3.7.2, and 3.9). A positive result would enforce the revision of the assumption that the MARCKS-related domain is the actual interface of Adducin with Actin and Spectrin as its strict requirement for all in vitro activities of Adducin involving Actin and Spectrin suggests (Matsuoka et al. 2000). Moreover, it would raise the question about the precise function of the interaction between Hts and the Spectrin cytoskeleton during axon guidance and provide a promising starting point to determine the role of the Spectrin cytoskeleton in the process of axon guidance in general.

Based on the literature about the Spectrin cytoskeleton, at least three distinct functions of the Spectrin cytoskeleton must be considered. First, the hypothesis that the Gogo-Hts complex acts as

a Spectrin dependent clutch module that inhibits retrograde Actin flow can be tested. For L1 and Ankyrin_B, this has been shown by monitoring the movement of fluorescently labeled Ankyrin_B in transfected cultured neurons, by comparing the rate of the cytochalasin D sensitive retrograde flow of Ankyrin_B with the rate of retrograde Actin flow, and by bead-tracking experiments (Kamiguchi and Yoshihara 2001; Nishimura et al. 2003). Analogous experiments can be performed with Hts and Gogo. Second, a function of the Spectrin cytoskeleton in organizing the subcellular distribution of Gogo can not be ruled out. Ankyrin_C and β -Spectrin were shown to be required for the localization of several proteins to rather large compartments of cell membranes such as axon initial segments, nodes of Ranvier, and the basolateral side of epithelial cells (Zhou et al. 1998; Dubreuil et al. 2000; Jenkins et al. 2001; Komada and Soriano 2002). By contrast, no defects in Gogo localization were observed at the scale of confocal microscopy in homozygous *hts*^{null} mutant clones in the optic lobes of late 3rd instar larvae (Ohler et al. 2011). However, it is still possible that the distribution of Gogo in the plasma membrane depends on Hts at a smaller scale, and this may be tested by electron or STED microscopy. Third, the Spectrin cytoskeleton was implicated in the modulation of the growth cone's response to asymmetric Ca²⁺ signals across the growth cone, as L1 regulates cAMP levels in neurons via Ankyrin_B (Ooashi and Kamiguchi 2009). It is possible that the Gogo-Hts complex functions in a similar way, which can be tested by comparing the levels of cAMP and its distribution in wild type neurons and in neurons that either lack or overexpress *gogo* or *hts*. Genetically encoded cAMP reporters are available (Nikolaev and Lohse 2006).

5. LITERATURE

Allis, C. D., Waring, G. L. and Mahowald, A. P. (1977). Mass isolation of pole cells from *Drosophila melanogaster*. *Dev Biol* 56, 372-81.

Augsburger, A., Schuchardt, A., Hoskins, S., Dodd, J. and Butler, S. (1999). BMPs as mediators of roof plate repulsion of commissural neurons. *Neuron* 24, 127-41.

Aunis, D. and Bader, M. F. (1988). The cytoskeleton as a barrier to exocytosis in secretory cells. *J Exp Biol* 139, 253-66.

Barberis, D., Casazza, A., Sordella, R., Corso, S., Artigiani, S., Settleman, J., Comoglio, P. M. and Tamagnone, L. (2005). p190 Rho-GTPase activating protein associates with plexins and it is required for semaphorin signalling. *J Cell Sci* 118, 4689-700.

Bard, L., Boscher, C., Lambert, M., Mege, R. M., Choquet, D. and Thoumine, O. (2008). A molecular clutch between the actin flow and N-cadherin adhesions drives growth cone migration. *J Neurosci* 28, 5879-90.

Bashirullah, A., Cooperstock, R. L. and Lipshitz, H. D. (1998). RNA localization in development. *Annu Rev Biochem* 67, 335-94.

Beall, E. L. and Rio, D. C. (1997). *Drosophila* P-element transposase is a novel site-specific endonuclease. *Genes Dev* 11, 2137-51.

Bennett, V. (1985). The membrane skeleton of human erythrocytes and its implications for more complex cells. *Annu Rev Biochem* 54, 273-304.

Bennett, V. (1990). Spectrin-based membrane skeleton: a multipotential adaptor between plasma membrane and cytoplasm. *Physiol Rev* 70, 1029-65.

Bennett, V. and Baines, A. J. (2001). Spectrin and ankyrin-based pathways: metazoan inventions for integrating cells into tissues. *Physiol Rev* 81, 1353-92.

Bennett, V., Gardner, K. and Steiner, J. P. (1988). Brain adducin: a protein kinase C substrate that may mediate site-directed assembly at the spectrin-actin junction. *J Biol Chem* 263, 5860-9.

Bennett, V. and Gilligan, D. M. (1993). The spectrin-based membrane skeleton and micron-scale organization of the plasma membrane. *Annu Rev Cell Biol* 9, 27-66.

Bennett, V. and Stenbuck, P. J. (1979). Identification and partial purification of ankyrin, the high affinity membrane attachment site for human erythrocyte spectrin. *J Biol Chem* 254, 2533-41.

Berger, J., Senti, K. A., Senti, G., Newsome, T. P., Asling, B., Dickson, B. J. and Suzuki, T. (2008). Systematic identification of genes that regulate neuronal wiring in the *Drosophila* visual system. *PLoS Genet* 4, e1000085.

Berger, J., Suzuki, T., Senti, K. A., Stubbs, J., Schaffner, G. and Dickson, B. J. (2001). Genetic mapping with SNP markers in *Drosophila*. *Nat Genet* 29, 475-81.

Bernard, P. and Couturier, M. (1992). Cell killing by the F plasmid CcdB protein involves poisoning of DNA-topoisomerase II complexes. *J Mol Biol* 226, 735-45.

- Brand, A. H. and Perrimon, N. (1993). Targeted gene expression as a means of altering cell fates and generating dominant phenotypes. *Development* 118, 401-15.
- Brown, M. E. and Bridgman, P. C. (2003). Retrograde flow rate is increased in growth cones from myosin IIB knockout mice. *J Cell Sci* 116, 1087-94.
- Buck, K. B. and Zheng, J. Q. (2002). Growth cone turning induced by direct local modification of microtubule dynamics. *J Neurosci* 22, 9358-67.
- Buhusi, M., Schlatter, M. C., Demyanenko, G. P., Thresher, R. and Maness, P. F. (2008). L1 interaction with ankyrin regulates mediolateral topography in the retinocollicular projection. *J Neurosci* 28, 177-88.
- Cafferty, P., Yu, L. and Rao, Y. (2004). The receptor tyrosine kinase Off-track is required for layer-specific neuronal connectivity in *Drosophila*. *Development* 131, 5287-95.
- Cagan, R. (2009). Principles of *Drosophila* eye differentiation. *Curr Top Dev Biol* 89, 115-35.
- Cagan, R. L. and Ready, D. F. (1989). The emergence of order in the *Drosophila* pupal retina. *Dev Biol* 136, 346-62.
- Cajal, S. R. (1966). *Recollections of my life*. M.I.T. Press, Cambridge.
- Campbell, D. S. and Holt, C. E. (2001). Chemotropic responses of retinal growth cones mediated by rapid local protein synthesis and degradation. *Neuron* 32, 1013-26.
- Campos-Ortega, J. A. and Hartenstein, V. (1985). *The embryonic development of Drosophila melanogaster*. Springer-Verlag, Berlin, New York.
- Castro, J. P. and Carareto, C. M. A. (2004). *Drosophila melanogaster* transposable elements: mechanisms of transposition and regulation. *Genetica* 121, 107-18.
- Chan, C. E. and Odde, D. J. (2008). Traction dynamics of filopodia on compliant substrates. *Science* 322, 1687-91.
- Charron, F., Stein, E., Jeong, J., McMahon, A. P. and Tessier-Lavigne, M. (2003). The morphogen sonic hedgehog is an axonal chemoattractant that collaborates with netrin-1 in midline axon guidance. *Cell* 113, 11-23.
- Chilton, J. K. (2006). Molecular mechanisms of axon guidance. *Dev Biol* 292, 13-24.
- Choi, K. W. and Benzer, S. (1994). Migration of glia along photoreceptor axons in the developing *Drosophila* eye. *Neuron* 12, 423-31.
- Clandinin, T. R., Lee, C. H., Herman, T., Lee, R. C., Yang, A. Y., Ovasapyan, S. and Zipursky, S. L. (2001). *Drosophila* LAR regulates R1-R6 and R7 target specificity in the visual system. *Neuron* 32, 237-48.
- Conde, C. and Caceres, A. (2009). Microtubule assembly, organization and dynamics in axons and dendrites. *Nat Rev Neurosci* 10, 319-32.
- Crisp, S., Evers, J. F., Fiala, A. and Bate, M. (2008). The development of motor coordination in *Drosophila* embryos. *Development* 135, 3707-17.

- Davis, J. Q. and Bennett, V. (1994). Ankyrin binding activity shared by the neurofascin/L1/NrCAM family of nervous system cell adhesion molecules. *J Biol Chem* 269, 27163-6.
- de Cuevas, M., Lee, J. K. and Spradling, A. C. (1996). α -spectrin is required for germline cell division and differentiation in the *Drosophila* ovary. *Development* 122, 3959-68.
- de Cuevas, M., Lilly, M. A. and Spradling, A. C. (1997). Germline cyst formation in *Drosophila*. *Annu Rev Genet* 31, 405-28.
- Dearborn, R., Jr., He, Q., Kunes, S. and Dai, Y. (2002). Eph receptor tyrosine kinase-mediated formation of a topographic map in the *Drosophila* visual system. *J Neurosci* 22, 1338-49.
- Dearborn, R., Jr. and Kunes, S. (2004). An axon scaffold induced by retinal axons directs glia to destinations in the *Drosophila* optic lobe. *Development* 131, 2291-303.
- Demyanenko, G. P. and Maness, P. F. (2003). The L1 cell adhesion molecule is essential for topographic mapping of retinal axons. *J Neurosci* 23, 530-8.
- Dent, E. W. and Gertler, F. B. (2003). Cytoskeletal dynamics and transport in growth cone motility and axon guidance. *Neuron* 40, 209-27.
- Dickson, B. J. (2002). Molecular mechanisms of axon guidance. *Science* 298, 1959-64.
- Dickson, B. J. and Gilestro, G. F. (2006). Regulation of commissural axon pathfinding by slit and its Robo receptors. *Annu Rev Cell Dev Biol* 22, 651-75.
- Dickson, T. C., Mintz, C. D., Benson, D. L. and Salton, S. R. (2002). Functional binding interaction identified between the axonal CAM L1 and members of the ERM family. *J Cell Biol* 157, 1105-12.
- Dietrich, W. (1909). The facet eyes of dipters. *Z Wiss Zool Abt A* 92, 465-539.
- Ding, D., Parkhurst, S. M. and Lipshitz, H. D. (1993). Different genetic requirements for anterior RNA localization revealed by the distribution of Adducin-like transcripts during *Drosophila* oogenesis. *Proc Natl Acad Sci U S A* 90, 2512-6.
- Discher, D., Parra, M., Conboy, J. G. and Mohandas, N. (1993). Mechanochemistry of the alternatively spliced spectrin-actin binding domain in membrane skeletal protein 4.1. *J Biol Chem* 268, 7186-95.
- Dubreuil, R. R., Wang, P., Dahl, S., Lee, J. and Goldstein, L. S. B. (2000). *Drosophila* β Spectrin functions independently of α Spectrin to polarize the Na,K ATPase in epithelial cells. *J Cell Biol* 149, 647-56.
- Eakin, R. M. (1972). Structure of invertebrate photoreceptors. *Handbook of Sensory Physiology* 7, 625-84.
- Edwards, R. A. and Bryan, J. (1995). Fascins, a family of actin bundling proteins. *Cell Motil Cytoskeleton* 32, 1-9.
- Egea, J. and Klein, R. (2007). Bidirectional Eph-ephrin signaling during axon guidance. *Trends Cell Biol* 17, 230-8.

- Ellis, M. C., O'Neill, E. M. and Rubin, G. M. (1993). Expression of *Drosophila glass* protein and evidence for negative regulation of its activity in non-neuronal cells by another DNA-binding protein. *Development* 119, 855-65.
- Fischbach, K. F. (1983). Neural cell types surviving congenital sensory deprivation in the optic lobes of *Drosophila melanogaster*. *Dev Biol* 95, 1-18.
- Fischbach, K. F. and Technau, G. (1984). Cell degeneration in the developing optic lobes of the sine oculis and small-optic-lobes mutants of *Drosophila melanogaster*. *Dev Biol* 104, 219-39.
- Forscher, P. and Smith, S. J. (1988). Actions of cytochalasins on the organization of actin filaments and microtubules in a neuronal growth cone. *J Cell Biol* 107, 1505-16.
- Fukata, Y., Oshiro, N., Kinoshita, N., Kawano, Y., Matsuoka, Y., Bennett, V., Matsuura, Y. and Kaibuchi, K. (1999). Phosphorylation of adducin by Rho-kinase plays a crucial role in cell motility. *J Cell Biol* 145, 347-61.
- Garbe, D. S., Das, A., Dubreuil, R. R. and Bashaw, G. J. (2007). β -Spectrin functions independently of Ankyrin to regulate the establishment and maintenance of axon connections in the *Drosophila* embryonic CNS. *Development* 134, 273-84.
- Gardner, K. and Bennett, V. (1987). Modulation of spectrin-actin assembly by erythrocyte adducin. *Nature* 328, 359-62.
- Garrity, P. A., Lee, C. H., Salecker, I., Robertson, H. C., Desai, C. J., Zinn, K. and Zipursky, S. L. (1999). Retinal axon target selection in *Drosophila* is regulated by a receptor protein tyrosine phosphatase. *Neuron* 22, 707-17.
- Garrity, P. A., Rao, Y., Salecker, I., McGlade, J., Pawson, T. and Zipursky, S. L. (1996). *Drosophila* photoreceptor axon guidance and targeting requires the dreadlocks SH2/SH3 adapter protein. *Cell* 85, 639-50.
- Garver, T. D., Ren, Q., Tuvia, S. and Bennett, V. (1997). Tyrosine phosphorylation at a site highly conserved in the L1 family of cell adhesion molecules abolishes ankyrin binding and increases lateral mobility of neurofascin. *J Cell Biol* 137, 703-14.
- Geraldo, S. and Gordon-Weeks, P. R. (2009). Cytoskeletal dynamics in growth-cone steering. *J Cell Sci* 122, 3595-604.
- Gitler, D. and Spira, M. E. (1998). Real time imaging of calcium-induced localized proteolytic activity after axotomy and its relation to growth cone formation. *Neuron* 20, 1123-35.
- Golic, K. G. and Lindquist, S. (1989). The FLP recombinase of yeast catalyzes site-specific recombination in the *Drosophila* genome. *Cell* 59, 499-509.
- Gomez, T. M. and Zheng, J. Q. (2006). The molecular basis for calcium-dependent axon pathfinding. *Nat Rev Neurosci* 7, 115-25.
- Gordon-Weeks, P. R. (2004). Microtubules and growth cone function. *J Neurobiol* 58, 70-83.
- Guan, K. L. and Rao, Y. (2003). Signalling mechanisms mediating neuronal responses to guidance cues. *Nat Rev Neurosci* 4, 941-56.
- Gurdon, J. B. and Bourillot, P. Y. (2001). Morphogen gradient interpretation. *Nature* 413, 797-803.

- Hakeda-Suzuki, S., Berger-Muller, S., Tomasi, T., Usui, T., Horiuchi, S. Y., Uemura, T. and Suzuki, T. (2011). Golden goal collaborates with Flamingo in conferring synaptic-layer specificity in the visual system. *Nat Neurosci* *14*, 314-23.
- Hakeda-Suzuki, S., Ng, J., Tzu, J., Dietzl, G., Sun, Y., Harms, M., Nardine, T., Luo, L. and Dickson, B. J. (2002). Rac function and regulation during *Drosophila* development. *Nature* *416*, 438-42.
- Halder, G., Callaerts, P. and Gehring, W. J. (1995). Induction of ectopic eyes by targeted expression of the *eyeless* gene in *Drosophila*. *Science* *267*, 1788-92.
- Hammarlund, M., Davis, W. S. and Jorgensen, E. M. (2000). Mutations in β -Spectrin disrupt axon outgrowth and sarcomere structure. *J Cell Biol* *149*, 931-42.
- Hammarlund, M., Jorgensen, E. M. and Bastiani, M. J. (2007). Axons break in animals lacking β -spectrin. *J Cell Biol* *176*, 269-75.
- Harris, R., Sabatelli, L. M. and Seeger, M. A. (1996). Guidance cues at the *Drosophila* CNS midline: identification and characterization of two *Drosophila* Netrin/UNC-6 homologs. *Neuron* *17*, 217-28.
- Hartley, J. L., Temple, G. F. and Brasch, M. A. (2000). DNA cloning using in vitro site-specific recombination. *Genome Res* *10*, 1788-95.
- Hauck, B., Gehring, W. J. and Walldorf, U. (1999). Functional analysis of an eye specific enhancer of the *eyeless* gene in *Drosophila*. *Proc Natl Acad Sci U S A* *96*, 564-9.
- Hazelett, D. J., Bourouis, M., Walldorf, U. and Treisman, J. E. (1998). *decapentaplegic* and *wingless* are regulated by *eyes absent* and *eyegone* and interact to direct the pattern of retinal differentiation in the eye disc. *Development* *125*, 3741-51.
- Hing, H., Xiao, J., Harden, N., Lim, L. and Zipursky, S. L. (1999). Pak functions downstream of Dock to regulate photoreceptor axon guidance in *Drosophila*. *Cell* *97*, 853-63.
- Holmes, G. P., Negus, K., BurrIDGE, L., Raman, S., Algar, E., Yamada, T. and Little, M. H. (1998). Distinct but overlapping expression patterns of two vertebrate *slit* homologs implies functional roles in CNS development and organogenesis. *Mech Dev* *79*, 57-72.
- Hong, K., Hinck, L., Nishiyama, M., Poo, M. M., Tessier-Lavigne, M. and Stein, E. (1999). A ligand-gated association between cytoplasmic domains of UNC5 and DCC family receptors converts netrin-induced growth cone attraction to repulsion. *Cell* *97*, 927-41.
- Huang, Z. and Kunes, S. (1996). Hedgehog, transmitted along retinal axons, triggers neurogenesis in the developing visual centers of the *Drosophila* brain. *Cell* *86*, 411-22.
- Huang, Z., Shilo, B. Z. and Kunes, S. (1998). A retinal axon fascicle uses spitz, an EGF receptor ligand, to construct a synaptic cartridge in the brain of *Drosophila*. *Cell* *95*, 693-703.
- Huber, A. B., Kolodkin, A. L., Ginty, D. D. and Cloutier, J. F. (2003). Signaling at the growth cone: ligand-receptor complexes and the control of axon growth and guidance. *Annu Rev Neurosci* *26*, 509-63.
- Hughes, C. A. and Bennett, V. (1995). Adducin: a physical model with implications for function in assembly of spectrin-actin complexes. *J Biol Chem* *270*, 18990-6.

- Hulsmeier, J., Pielage, J., Rickert, C., Technau, G. M., Klambt, C. and Stork, T. (2007). Distinct functions of alpha-Spectrin and beta-Spectrin during axonal pathfinding. *Development* 134, 713-22.
- Ishii, N., Wadsworth, W. G., Stern, B. D., Culotti, J. G. and Hedgecock, E. M. (1992). UNC-6, a laminin-related protein, guides cell and pioneer axon migrations in *C. elegans*. *Neuron* 9, 873-81.
- Itoh, A., Miyabayashi, T., Ohno, M. and Sakano, S. (1998). Cloning and expressions of three mammalian homologues of *Drosophila slit* suggest possible roles for *Slit* in the formation and maintenance of the nervous system. *Brain Res Mol Brain Res* 62, 175-86.
- Jarman, A. P., Grau, Y., Jan, L. Y. and Jan, Y. N. (1993). *atonal* is a proneural gene that directs chordotonal organ formation in the *Drosophila* peripheral nervous system. *Cell* 73, 1307-21.
- Jenkins, S. M., Kizhatil, K., Kramarcy, N. R., Sen, A., Sealock, R. and Bennett, V. (2001). FIGQY phosphorylation defines discrete populations of L1 cell adhesion molecules at sites of cell-cell contact and in migrating neurons. *J Cell Sci* 114, 3823-35.
- Joshi, R. and Bennett, V. (1990). Mapping the domain structure of human erythrocyte adducin. *J Biol Chem* 265, 13130-6.
- Joshi, R., Gilligan, D. M., Otto, E., McLaughlin, T. and Bennett, V. (1991). Primary structure and domain organization of human alpha and beta adducin. *J Cell Biol* 115, 665-75.
- Kalil, K. and Dent, E. W. (2005). Touch and go: guidance cues signal to the growth cone cytoskeleton. *Curr Opin Neurobiol* 15, 521-6.
- Kamiguchi, H. and Yoshihara, F. (2001). The role of endocytic L1 trafficking in polarized adhesion and migration of nerve growth cones. *J Neurosci* 21, 9194-203.
- Kaminker, J. S., Canon, J., Salecker, I. and Banerjee, U. (2002). Control of photoreceptor axon target choice by transcriptional repression of Runt. *Nat Neurosci* 5, 746-50.
- Keleman, K., Rajagopalan, S., Cleppien, D., Teis, D., Paiha, K., Huber, L. A., Technau, G. M. and Dickson, B. J. (2002). Comm sorts robo to control axon guidance at the *Drosophila* midline. *Cell* 110, 415-27.
- Kennedy, S. P., Warren, S. L., Forget, B. G. and Morrow, J. S. (1991). Ankyrin binds to the 15th repetitive unit of erythroid and nonerythroid beta-spectrin. *J Cell Biol* 115, 267-77.
- Kidd, T., Bland, K. S. and Goodman, C. S. (1999). Slit is the midline repellent for the Robo receptor in *Drosophila*. *Cell* 96, 785-94.
- Kidd, T., Brose, K., Mitchell, K. J., Fetter, R. D., Tessier-Lavigne, M., Goodman, C. S. and Tear, G. (1998). Roundabout controls axon crossing of the CNS midline and defines a novel subfamily of evolutionarily conserved guidance receptors. *Cell* 92, 205-15.
- Komada, M. and Soriano, P. (2002). β IV-spectrin regulates sodium channel clustering through ankyrin-G at axon initial segments and nodes of Ranvier. *J Cell Biol* 156, 337-48.
- Koundakjian, E. J., Cowan, D. M., Hardy, R. W. and Becker, A. H. (2004). The Zuker collection: a resource for the analysis of autosomal gene function in *Drosophila melanogaster*. *Genetics* 167, 203-6.

- Kuhlman, P. A., Hughes, C. A., Bennett, V. and Fowler, V. M. (1996). A new function for adducin. Calcium/calmodulin-regulated capping of the barbed ends of actin filaments. *J Biol Chem* **271**, 7986-91.
- Landy, A. (1989). Dynamic, structural, and regulatory aspects of lambda site-specific recombination. *Annu Rev Biochem* **58**, 913-49.
- Lee, C. H., Herman, T., Clandinin, T. R., Lee, R. and Zipursky, S. L. (2001). N-cadherin regulates target specificity in the *Drosophila* visual system. *Neuron* **30**, 437-50.
- Leung-Hagesteijn, C., Spence, A. M., Stern, B. D., Zhou, Y., Su, M. W., Hedgecock, E. M. and Culotti, J. G. (1992). UNC-5, a transmembrane protein with immunoglobulin and thrombospondin type 1 domains, guides cell and pioneer axon migrations in *C. elegans*. *Cell* **71**, 289-99.
- Leung, K. M., van Horck, F. P., Lin, A. C., Allison, R., Standart, N. and Holt, C. E. (2006). Asymmetrical beta-actin mRNA translation in growth cones mediates attractive turning to netrin-1. *Nat Neurosci* **9**, 1247-56.
- Li, E. and Hristova, K. (2010). Receptor tyrosine kinase transmembrane domains: function, dimer structure and dimerization energetics. *Cell Adh Migr* **4**, 249-54.
- Li, X., Matsuoka, Y. and Bennett, V. (1998). Adducin preferentially recruits spectrin to the fast growing ends of actin filaments in a complex requiring the MARCKS-related domain and a newly defined oligomerization domain. *J Biol Chem* **273**, 19329-38.
- Lin, C. H., Espreafico, E. M., Mooseker, M. S. and Forscher, P. (1996). Myosin drives retrograde F-actin flow in neuronal growth cones. *Neuron* **16**, 769-82.
- Lin, H., Yue, L. and Spradling, A. C. (1994). The *Drosophila* fusome, a germline-specific organelle, contains membrane skeletal proteins and functions in cyst formation. *Development* **120**, 947-56.
- Ling, E., Gardner, K. and Bennett, V. (1986). Protein kinase C phosphorylates a recently identified membrane skeleton-associated calmodulin-binding protein in human erythrocytes. *J Biol Chem* **261**, 13875-8.
- Long, H., Sabatier, C., Le, M., Plump, A., Yuan, W., Ornitz, D. M., Tamada, A., Murakami, F., Goodman, C. S. and Tessier-Lavigne, M. (2004). Conserved roles for Slit and Robo proteins in midline commissural axon guidance. *Neuron* **42**, 213-23.
- Lowery, L. A. and Van Vactor, D. (2009). The trip of the tip: understanding the growth cone machinery. *Nat Rev Mol Cell Biol* **10**, 332-43.
- Luu, S.-H. (2008). No phosphate, please! Structural and functional analysis of the novel axon guidance receptor Golden goal. Diploma Thesis, Ludwig-Maximilians-Universität, München.
- Mallavarapu, A. and Mitchison, T. (1999). Regulated actin cytoskeleton assembly at filopodium tips controls their extension and retraction. *J Cell Biol* **146**, 1097-106.
- Martin, K. A., Poeck, B., Roth, H., Ebens, A. J., Ballard, L. C. and Zipursky, S. L. (1995). Mutations disrupting neuronal connectivity in the *Drosophila* visual system. *Neuron* **14**, 229-40.
- Mast, J. D., Prakash, S., Chen, P. L. and Clandinin, T. R. (2006). The mechanisms and molecules that connect photoreceptor axons to their targets in *Drosophila*. *Semin Cell Dev Biol* **17**, 42-9.

- Matsuoka, Y., Hughes, C. A. and Bennett, V. (1996). Adducin regulation. Definition of the calmodulin-binding domain and sites of phosphorylation by protein kinases A and C. *J Biol Chem* **271**, 25157-66.
- Matsuoka, Y., Li, X. and Bennett, V. (1998). Adducin is an in vivo substrate for protein kinase C: phosphorylation in the MARCKS-related domain inhibits activity in promoting spectrin-actin complexes and occurs in many cells, including dendritic spines of neurons. *J Cell Biol* **142**, 485-97.
- Matsuoka, Y., Li, X. and Bennett, V. (2000). Adducin: structure, function and regulation. *Cell Mol Life Sci* **57**, 884-95.
- Maurel-Zaffran, C., Suzuki, T., Gahmon, G., Treisman, J. E. and Dickson, B. J. (2001). Cell-autonomous and -nonautonomous functions of LAR in R7 photoreceptor axon targeting. *Neuron* **32**, 225-35.
- Medeiros, N. A., Burnette, D. T. and Forscher, P. (2006). Myosin II functions in actin-bundle turnover in neuronal growth cones. *Nat Cell Biol* **8**, 215-26.
- Meinertzhagen, I. A. and Hanson, T. E. (1993). The development of the optic lobe. In: *The development of Drosophila melanogaster*. Edited by M. Bate and A. Martinez Arias. Cold Spring Harbor Laboratory Press, Cold Spring Harbor.
- Mellott, D. O. and Burke, R. D. (2008). The molecular phylogeny of eph receptors and ephrin ligands. *BMC Cell Biol* **9**, 27.
- Meyerowitz, E. M. and Kankel, D. R. (1978). A genetic analysis of visual system development in *Drosophila melanogaster*. *Dev Biol* **62**, 112-42.
- Mische, S. M., Mooseker, M. S. and Morrow, J. S. (1987). Erythrocyte adducin: a calmodulin-regulated actin-bundling protein that stimulates spectrin-actin binding. *J Cell Biol* **105**, 2837-45.
- Mitchison, T. and Kirschner, M. (1988). Cytoskeletal dynamics and nerve growth. *Neuron* **1**, 761-72.
- Moses, K. and Rubin, G. M. (1991). *glass* encodes a site-specific DNA-binding protein that is regulated in response to positional signals in the developing *Drosophila* eye. *Genes Dev* **5**, 583-93.
- Needham, L. K., Thelen, K. and Maness, P. F. (2001). Cytoplasmic domain mutations of the L1 cell adhesion molecule reduce L1-ankyrin interactions. *J Neurosci* **21**, 1490-500.
- Newsome, T. P., Asling, B. and Dickson, B. J. (2000a). Analysis of *Drosophila* photoreceptor axon guidance in eye-specific mosaics. *Development* **127**, 851-60.
- Newsome, T. P., Schmidt, S., Dietzl, G., Keleman, K., Asling, B., Debant, A. and Dickson, B. J. (2000b). Trio combines with dock to regulate Pak activity during photoreceptor axon pathfinding in *Drosophila*. *Cell* **101**, 283-94.
- Ng, J. and Luo, L. (2004). Rho GTPases regulate axon growth through convergent and divergent signaling pathways. *Neuron* **44**, 779-93.
- Nikolaev, V. O. and Lohse, M. J. (2006). Monitoring of cAMP synthesis and degradation in living cells. *Physiology (Bethesda)* **21**, 86-92.

- Nishimura, K., Yoshihara, F., Tojima, T., Ooashi, N., Yoon, W., Mikoshiba, K., Bennett, V. and Kamiguchi, H. (2003). L1-dependent neuritogenesis involves ankyrin_B that mediates L1-CAM coupling with retrograde actin flow. *J Cell Biol* 163, 1077-88.
- Noren, N. K. and Pasquale, E. B. (2004). Eph receptor-ephrin bidirectional signals that target Ras and Rho proteins. *Cell Signal* 16, 655-66.
- O'Donnell, M., Chance, R. K. and Bashaw, G. J. (2009). Axon growth and guidance: receptor regulation and signal transduction. *Annu Rev Neurosci* 32, 383-412.
- Ohler, S., Hakeda-Suzuki, S. and Suzuki, T. (2011). Hts, the *Drosophila* homologue of Adducin, physically interacts with the transmembrane receptor Golden goal to guide photoreceptor axons. *Dev Dyn* 240, 135-48.
- Oinuma, I., Ishikawa, Y., Katoh, H. and Negishi, M. (2004). The Semaphorin 4D receptor Plexin-B1 is a GTPase activating protein for R-Ras. *Science* 305, 862-5.
- Ooashi, N., Futatsugi, A., Yoshihara, F., Mikoshiba, K. and Kamiguchi, H. (2005). Cell adhesion molecules regulate Ca²⁺-mediated steering of growth cones via cyclic AMP and ryanodine receptor type 3. *J Cell Biol* 170, 1159-67.
- Ooashi, N. and Kamiguchi, H. (2009). The cell adhesion molecule L1 controls growth cone navigation via ankyrin_B-dependent modulation of cyclic AMP. *Neurosci Res* 63, 224-6.
- Osterfield, M., Kirschner, M. W. and Flanagan, J. G. (2003). Graded positional information: interpretation for both fate and guidance. *Cell* 113, 425-8.
- Pasterkamp, R. J. (2005). R-Ras fills another GAP in semaphorin signalling. *Trends Cell Biol* 15, 61-4.
- Perrin, D., Möller, K., Hanke, K. and Söling, H. D. (1992). cAMP and Ca²⁺-mediated secretion in parotid acinar cells is associated with reversible changes in the organization of the cytoskeleton. *J Cell Biol* 116, 127-34.
- Perry, M. M. (1968). Further studies on the development of the eye of *Drosophila melanogaster*. II. The interommatidial bristles. *J Morphol* 124, 249-61.
- Petrella, L. N., Smith-Leiker, T. and Cooley, L. (2007). The Ovhts polyprotein is cleaved to produce fusome and ring canal proteins required for *Drosophila* oogenesis. *Development* 134, 703-12.
- Piper, M., Anderson, R., Dwivedy, A., Weinl, C., van Horck, F., Leung, K. M., Cogill, E. and Holt, C. (2006). Signaling mechanisms underlying Slit2-induced collapse of *Xenopus* retinal growth cones. *Neuron* 49, 215-28.
- Poeck, B., Fischer, S., Gunning, D., Zipursky, S. L. and Salecker, I. (2001). Glial cells mediate target layer selection of retinal axons in the developing visual system of *Drosophila*. *Neuron* 29, 99-113.
- Pokrywka, N. J., Meng, L., Debiec, K. and Stephenson, E. C. (2004). Identification of hypomorphic and null alleles of *swallow* via molecular and phenotypic analyses. *Dev Genes Evol* 214, 185-92.
- Pollard, T. D. and Cooper, J. A. (1986). Actin and actin-binding proteins. A critical evaluation of mechanisms and functions. *Annu Rev Biochem* 55, 987-1035.

- Polleux, F., Ince-Dunn, G. and Ghosh, A. (2007). Transcriptional regulation of vertebrate axon guidance and synapse formation. *Nat Rev Neurosci* 8, 331-40.
- Rajagopalan, S., Vivancos, V., Nicolas, E. and Dickson, B. J. (2000). Selecting a longitudinal pathway: Robo receptors specify the lateral position of axons in the *Drosophila* CNS. *Cell* 103, 1033-45.
- Rajasekharan, S. and Kennedy, T. E. (2009). The netrin protein family. *Genome Biol* 10, 239.
- Rangarajan, R., Gong, Q. and Gaul, U. (1999). Migration and function of glia in the developing *Drosophila* eye. *Development* 126, 3285-92.
- Rao, Y., Pang, P., Ruan, W., Gunning, D. and Zipursky, S. L. (2000). *brakeless* is required for photoreceptor growth-cone targeting in *Drosophila*. *Proc Natl Acad Sci U S A* 97, 5966-71.
- Ready, D. F., Hanson, T. E. and Benzer, S. (1976). Development of the *Drosophila* retina, a neurocrystalline lattice. *Dev Biol* 53, 217-40.
- Robinson, D. N., Cant, K. and Cooley, L. (1994). Morphogenesis of *Drosophila* ovarian ring canals. *Development* 120, 2015-25.
- Robinson, D. N., Smith-Leiker, T. A., Sokol, N. S., Hudson, A. M. and Cooley, L. (1997). Formation of the *Drosophila* ovarian ring canal inner rim depends on *cheerio*. *Genetics* 145, 1063-72.
- Rodriguez, O. C., Schaefer, A. W., Mandato, C. A., Forscher, P., Bement, W. M. and Waterman-Storer, C. M. (2003). Conserved microtubule-actin interactions in cell movement and morphogenesis. *Nat Cell Biol* 5, 599-609.
- Rothberg, J. M., Hartley, D. A., Walther, Z. and Artavanis-Tsakonas, S. (1988). *slit*: An EGF-homologous locus of *D. melanogaster* involved in the development of the embryonic central nervous system. *Cell* 55, 1047-59.
- Rothberg, J. M., Jacobs, J. R., Goodman, C. S. and Artavanis-Tsakonas, S. (1990). *slit*: an extracellular protein necessary for development of midline glia and commissural axon pathways contains both EGF and LRR domains. *Genes Dev* 4, 2169-87.
- Round, J. and Stein, E. (2007). Netrin signaling leading to directed growth cone steering. *Curr Opin Neurobiol* 17, 15-21.
- Ruan, W., Long, H., Vuong, D. H. and Rao, Y. (2002). Bifocal is a downstream target of the Ste20-like serine/threonine kinase misshapen in regulating photoreceptor growth cone targeting in *Drosophila*. *Neuron* 36, 831-42.
- Ruan, W., Pang, P. and Rao, Y. (1999). The SH2/SH3 adaptor protein dock interacts with the Ste20-like kinase misshapen in controlling growth cone motility. *Neuron* 24, 595-605.
- Rutishauser, U. (1993). Adhesion molecules of the nervous system. *Curr Opin Neurobiol* 3, 709-15.
- Sabatier, C., Plump, A. S., Le, M., Brose, K., Tamada, A., Murakami, F., Lee, E. Y. H. P. and Tessier-Lavigne, M. (2004). The divergent Robo family protein Rig-1/Robo3 is a negative regulator of Slit responsiveness required for midline crossing by commissural axons. *Cell* 117, 157-69.

- Sabry, J. H., O'Connor, T. P., Evans, L., Toroian-Raymond, A., Kirschner, M. and Bentley, D. (1991). Microtubule behavior during guidance of pioneer neuron growth cones in situ. *J Cell Biol* *115*, 381-95.
- Samson, M. L., Lisbin, M. J. and White, K. (1995). Two distinct temperature-sensitive alleles at the *elav* locus of *Drosophila* are suppressed nonsense mutations of the same tryptophan codon. *Genetics* *141*, 1101-11.
- Sanchez-Camacho, C. and Bovolenta, P. (2009). Emerging mechanisms in morphogen-mediated axon guidance. *Bioessays* *31*, 1013-25.
- Sato, M., Umetsu, D., Murakami, S., Yasugi, T. and Tabata, T. (2006). DWnt4 regulates the dorsoventral specificity of retinal projections in the *Drosophila melanogaster* visual system. *Nat Neurosci* *9*, 67-75.
- Schaefer, A. W., Kabir, N. and Forscher, P. (2002). Filopodia and actin arcs guide the assembly and transport of two populations of microtubules with unique dynamic parameters in neuronal growth cones. *J Cell Biol* *158*, 139-52.
- Schaefer, A. W., Schoonderwoert, V. T., Ji, L., Mederios, N., Danuser, G. and Forscher, P. (2008). Coordination of actin filament and microtubule dynamics during neurite outgrowth. *Dev Cell* *15*, 146-62.
- Schmucker, D., Clemens, J. C., Shu, H., Worby, C. A., Xiao, J., Muda, M., Dixon, J. E. and Zipursky, S. L. (2000). *Drosophila* Dscam is an axon guidance receptor exhibiting extraordinary molecular diversity. *Cell* *101*, 671-84.
- Schneider, I. (1972). Cell lines derived from late embryonic stages of *Drosophila melanogaster*. *J Embryol Exp Morphol* *27*, 353-65.
- Scicolone, G., Ortalli, A. L. and Carri, N. G. (2009). Key roles of Ephs and ephrins in retinotectal topographic map formation. *Brain Res Bull* *79*, 227-47.
- Senti, K., Keleman, K., Eisenhaber, F. and Dickson, B. J. (2000). *brakeless* is required for lamina targeting of R1-R6 axons in the *Drosophila* visual system. *Development* *127*, 2291-301.
- Senti, K. A., Usui, T., Boucke, K., Greber, U., Uemura, T. and Dickson, B. J. (2003). Flamingo regulates R8 axon-axon and axon-target interactions in the *Drosophila* visual system. *Curr Biol* *13*, 828-32.
- Shinza-Kameda, M., Takasu, E., Sakurai, K., Hayashi, S. and Nose, A. (2006). Regulation of layer-specific targeting by reciprocal expression of a cell adhesion molecule, capricious. *Neuron* *49*, 205-13.
- Simpson, J. H., Bland, K. S., Fetter, R. D. and Goodman, C. S. (2000). Short-range and long-range guidance by Slit and its Robo receptors: a combinatorial code of Robo receptors controls lateral position. *Cell* *103*, 1019-32.
- Snapp, E. L., Iida, T., Frescas, D., Lippincott-Schwartz, J. and Lilly, M. A. (2004). The fusome mediates intercellular endoplasmic reticulum connectivity in *Drosophila* ovarian cysts. *Mol Biol Cell* *15*, 4512-21.
- Sobue, K. and Kanda, K. (1989). Alpha-actinins, caldesmon (brain spectrin or fodrin), and actin participate in adhesion and movement of growth cones. *Neuron* *3*, 311-9.

- Song, J., Wu, L., Chen, Z., Kohanski, R. A. and Pick, L. (2003). Axons guided by insulin receptor in *Drosophila* visual system. *Science* **300**, 502-5.
- Sperry, R. W. (1963). Chemoaffinity in the orderly growth of nerve fiber patterns and connections. *Proc Natl Acad Sci U S A* **50**, 703-10.
- Spradling, A. C., Stern, D., Beaton, A., Rhem, E. J., Lavery, T., Mozden, N., Misra, S. and Rubin, G. M. (1999). The Berkeley *Drosophila* Genome Project gene disruption project: Single P-element insertions mutating 25% of vital *Drosophila* genes. *Genetics* **153**, 135-77.
- Stein, E., Zou, Y., Poo, M. and Tessier-Lavigne, M. (2001). Binding of DCC by netrin-1 to mediate axon guidance independent of adenosine A2B receptor activation. *Science* **291**, 1976-82.
- Steller, H., Fischbach, K. F. and Rubin, G. M. (1987). *disconnected*: a locus required for neuronal pathway formation in the visual system of *Drosophila*. *Cell* **50**, 1139-53.
- Steven, R., Kubiseski, T. J., Zheng, H., Kulkarni, S., Mancillas, J., Ruiz Morales, A., Hogue, C. W., Pawson, T. and Culotti, J. (1998). UNC-73 activates the Rac GTPase and is required for cell and growth cone migrations in *C. elegans*. *Cell* **92**, 785-95.
- Suh, G. S., Poeck, B., Chouard, T., Oron, E., Segal, D., Chamovitz, D. A. and Zipursky, S. L. (2002). *Drosophila* JAB1/CSN5 acts in photoreceptor cells to induce glial cells. *Neuron* **33**, 35-46.
- Suter, D. M. and Forscher, P. (2000). Substrate-cytoskeletal coupling as a mechanism for the regulation of growth cone motility and guidance. *J Neurobiol* **44**, 97-113.
- Taylor, T. D. and Garrity, P. A. (2003). Axon targeting in the *Drosophila* visual system. *Curr Opin Neurobiol* **13**, 90-5.
- Taylor, K. A. and Taylor, D. W. (1994). Formation of two-dimensional complexes of F-actin and crosslinking proteins on lipid monolayers: demonstration of unipolar alpha-actinin-F-actin crosslinking. *Biophys J* **67**, 1976-83.
- Tchernia, G., Mohandas, N. and Shohet, S. B. (1981). Deficiency of skeletal membrane protein band 4.1 in homozygous hereditary elliptocytosis. Implications for erythrocyte membrane stability. *J Clin Invest* **68**, 454-60.
- Telonis-Scott, M., Kopp, A., Wayne, M. L., Nuzhdin, S. V. and McIntyre, L. M. (2009). Sex-specific splicing in *Drosophila*: widespread occurrence, tissue specificity and evolutionary conservation. *Genetics* **181**, 421-34.
- Tessier-Lavigne, M. and Goodman, C. S. (1996). The molecular biology of axon guidance. *Science* **274**, 1123-33.
- Thomas, W. G., Motel, T. J., Kule, C. E., Karoor, V. and Baker, K. M. (1998). Phosphorylation of the angiotensin II (AT1A) receptor carboxyl terminus: a role in receptor endocytosis. *Mol Endocrinol* **12**, 1513-24.
- Ting, C. Y. and Lee, C. H. (2007). Visual circuit development in *Drosophila*. *Curr Opin Neurobiol* **17**, 65-72.
- Ting, C. Y., Yonekura, S., Chung, P., Hsu, S. N., Robertson, H. M., Chiba, A. and Lee, C. H. (2005). *Drosophila* N-cadherin functions in the first stage of the two-stage layer-selection process of R7 photoreceptor afferents. *Development* **132**, 953-63.

- Tomasi, T. (2008). The transmembrane protein Golden goal regulates retinal axon guidance in *Drosophila*. Dissertation, Ludwig-Maximilians-Universität, München.
- Tomasi, T., Hakeda-Suzuki, S., Ohler, S., Schleiffer, A. and Suzuki, T. (2008). The transmembrane protein Golden goal regulates R8 photoreceptor axon-axon and axon-target interactions. *Neuron* 57, 691-704.
- Tomlinson, A. and Ready, D. F. (1987). Neuronal differentiation in *Drosophila* ommatidium. *Dev Biol* 120, 366-76.
- Toyofuku, T., Yoshida, J., Sugimoto, T., Zhang, H., Kumanogoh, A., Hori, M. and Kikutani, H. (2005). FARP2 triggers signals for Sema3A-mediated axonal repulsion. *Nat Neurosci* 8, 1712-9.
- Voas, M. G. and Rebay, I. (2004). Signal integration during development: insights from the *Drosophila* eye. *Dev Dyn* 229, 162-75.
- Warn, R. M., Gutzeit, H. O., Smith, L. and Warn, A. (1985). F-actin rings are associated with the ring canals of the *Drosophila* egg chamber. *Exp Cell Res* 157, 355-63.
- Washburn, T. and O'Tousa, J. E. (1992). Nonsense suppression of the major rhodopsin gene of *Drosophila*. *Genetics* 130, 585-95.
- Wen, Z. and Zheng, J. Q. (2006). Directional guidance of nerve growth cones. *Curr Opin Neurobiol* 16, 52-8.
- Whittaker, K. L., Ding, D., Fisher, W. W. and Lipshitz, H. D. (1999). Different 3' untranslated regions target alternatively processed *hu-li tai shao* (*hts*) transcripts to distinct cytoplasmic locations during *Drosophila* oogenesis. *J Cell Sci* 112 (Pt 19), 3385-98.
- Williams, R. W. and Herrup, K. (1988). The control of neuron number. *Annu Rev Neurosci* 11, 423-53.
- Wilson, P. G. (2005). Centrosome inheritance in the male germ line of *Drosophila* requires *hu-li tai-shao* function. *Cell Biol Int* 29, 360-9.
- Wolff, T. and Ready, D. F. (1991). Cell death in normal and rough eye mutants of *Drosophila*. *Development* 113, 825-39.
- Wolff, T. and Ready, D. F. (1993). Pattern formation in the *Drosophila* retina. In: The development of *Drosophila melanogaster*. Edited by M. Bate and A. Martinez Arias. Cold Spring Harbor Laboratory Press, Cold Spring Harbor.
- Xu, T. and Rubin, G. M. (1993). Analysis of genetic mosaics in developing and adult *Drosophila* tissues. *Development* 117, 1223-37.
- Yazdani, U. and Terman, J. R. (2006). The semaphorins. *Genome Biol* 7, 211.
- Yoon, B. C., Zivraj, K. H. and Holt, C. E. (2009). Local translation and mRNA trafficking in axon pathfinding. *Results Probl Cell Differ* 48, 269-88.
- Yuan, S.-S. F., Cox, L. A., Dasika, G. K. and Lee, E. Y. H. P. (1999a). Cloning and functional studies of a novel gene aberrantly expressed in RB-deficient embryos. *Dev Biol* 207, 62-75.

- Yuan, W., Zhou, L., Chen, J. H., Wu, J. Y., Rao, Y. and Ornitz, D. M. (1999b). The mouse SLIT family: secreted ligands for ROBO expressed in patterns that suggest a role in morphogenesis and axon guidance. *Dev Biol* 212, 290-306.
- Yue, L. and Spradling, A. C. (1992). *hu-li tai shao*, a gene required for ring canal formation during *Drosophila* oogenesis, encodes a homolog of adducin. *Genes Dev* 6, 2443-54.
- Zaccai, M. and Lipshitz, H. D. (1996a). Differential distributions of two adducin-like protein isoforms in the *Drosophila* ovary and early embryo. *Zygote* 4, 159-66.
- Zaccai, M. and Lipshitz, H. D. (1996b). Role of Adducin-like (*hu-li tai shao*) mRNA and protein localization in regulating cytoskeletal structure and function during *Drosophila* Oogenesis and early embryogenesis. *Dev Genet* 19, 249-57.
- Zhou, D., Lambert, S., Malen, P. L., Carpenter, S., Boland, L. M. and Bennett, V. (1998). AnkyrinG is required for clustering of voltage-gated Na channels at axon initial segments and for normal action potential firing. *J Cell Biol* 143, 1295-304.
- Zhou, F. Q. and Cohan, C. S. (2004). How actin filaments and microtubules steer growth cones to their targets. *J Neurobiol* 58, 84-91.
- Zhou, F. Q. and Snider, W. D. (2006). Intracellular control of developmental and regenerative axon growth. *Philos Trans R Soc Lond B Biol Sci* 361, 1575-92.
- Zhou, F. Q., Waterman-Storer, C. M. and Cohan, C. S. (2002). Focal loss of actin bundles causes microtubule redistribution and growth cone turning. *J Cell Biol* 157, 839-49.
- Zhou, Y., Gunput, R. A. and Pasterkamp, R. J. (2008). Semaphorin signaling: progress made and promises ahead. *Trends Biochem Sci* 33, 161-70.
- Zou, Y. and Lyuksyutova, A. I. (2007). Morphogens as conserved axon guidance cues. *Curr Opin Neurobiol* 17, 22-8.

Acknowledgements

I want to thank Dr. Takashi Suzuki, who gave me the opportunity to run the experiments in his lab and always gave me the right balance between support and independence.

I am grateful to my Doktorvater Prof. Dr. Rüdiger Klein and the members of my thesis committee, Dr. Gaia Tavosanis and Prof. Dr. Dr. h.c. mult. Hans Thoenen, for invaluable intellectual support.

Thanks to my colleague Dr. Satoko Hakeda-Suzuki, who collaborated on my project and taught me much about flies.

Thanks to all colleagues from the Suzuki lab, Ana-Maria Malenica, Irina Hein, Jing Shi, Sandra Müller-Berger, Klaudiusz Mann, and Si-Hong Luu for the many pleasant hours that we spent together in the lab and the even more pleasant hours that we spent outside the lab. Thanks also to all other colleagues from the MPI, especially those who became friends over the years and never let me fall (except from the Kopfriss).

Special thanks to Dr. Tatiana Tomasi for too much to list it here.

Last but not least, I thank Prof. Dr. Lynn Cooley, Prof. Dr. Christian Klämbt, Dr. Gaia Tavosanis, Dr. Frederik Wirtz-Peitz and Prof. Dr. Alfonso Martinez Arias, Dr. Satoko Hakeda-Suzuki, Klaudiusz Mann, Si-Hong Luu, the Bloomington Stock Center, and the Developmental Studies Hybridoma Bank for donating reagents.

Curriculum vitae



Stephan Ohler

Greppenweg 12
94036 Passau
Germany

Date of birth: September 16th, 1978
Place of birth: Passau, Germany
Nationality: German

Email: stephan.ohler@web.de

PhD THESIS

February 2005 – current

Max Planck Institute of Neurobiology, Martinsried, Germany
Supervisor: Dr. Takashi Suzuki
Topic: “Biochemical analysis of molecular determinants in axon guidance of the *Drosophila* visual system.”
Degree aspired: Dr. rer. nat.

PUBLICATIONS

Tatiana Tomasi, Satoko Hakeda-Suzuki, Stephan Ohler, Alexander Schleiffer, and Takashi Suzuki (2008)
The transmembrane protein Golden goal regulates R8 photoreceptor axon-axon and axon-target interactions.
Neuron, 57, 691-704.

Stephan Ohler, Satoko Hakeda-Suzuki, Takashi Suzuki (2011)
Hts, the *Drosophila* homologue of Adducin, physically interacts with the transmembrane receptor Golden goal.
Developmental Dynamics, 240, 135.48.

DIPLOMA THESIS

July 2003 – January 2005

Research Institute of Molecular Pathology, Vienna, Austria
Supervisor: Dr. Jürgen A. Knoblich
Topic: “The role of *lethal (2) giant larvae* in asymmetric cell divisions of neuroblasts in *Drosophila melanogaster*.”
Grade: “sehr gut”

STUDIES

October 1999 – February 2008

University of Vienna, Austria
Main field of study: genetics - microbiology
Degree obtained: Magister der Naturwissenschaften (Mag. rer. nat.)
Grade: “bestanden”

ZIVILDienst (National Service - non-military option)

October 1998 – November 1999

Caritas-Altenheim Mariahilf, Passau, Germany

SCHOOL

September 1989 – June 1998

Maristengymnasium Fürstzell, Germany